Nonlinear optical imaging at the nanoscale
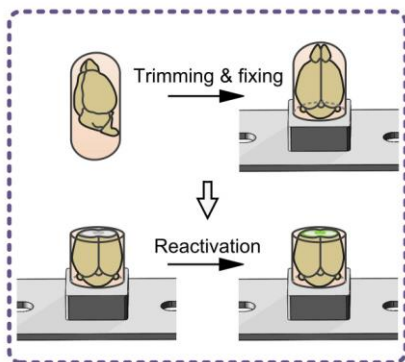
Sophie Brasselet
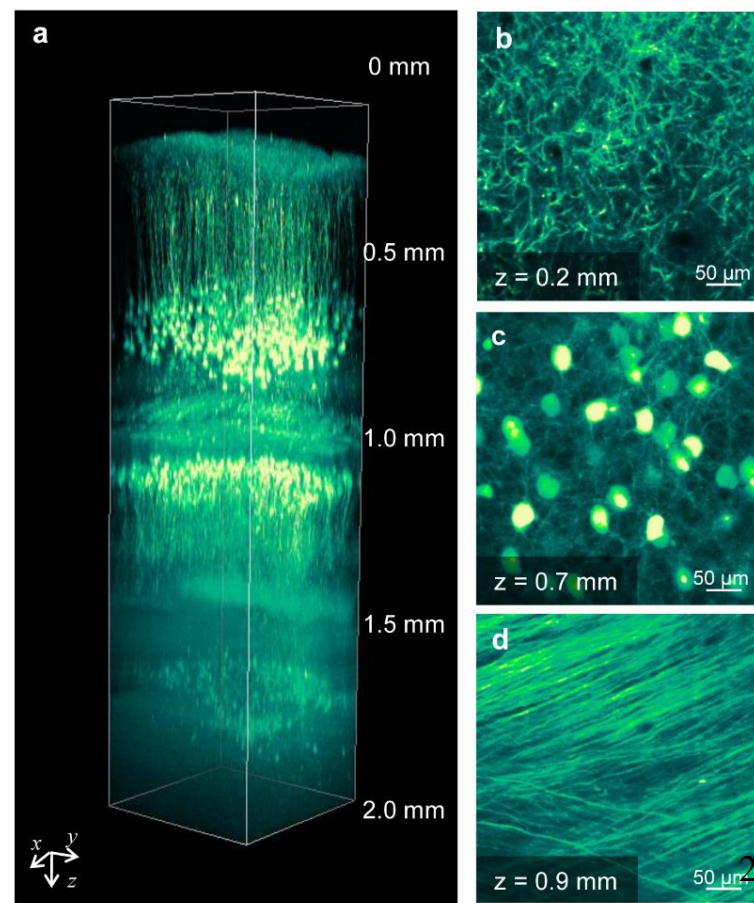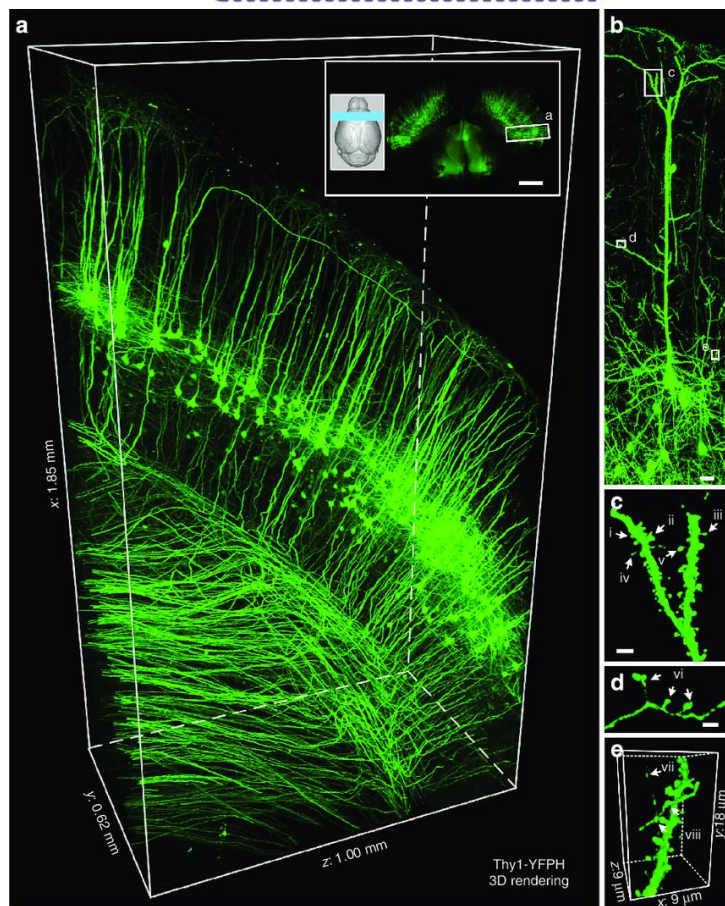
MOSAIC, Institut Fresnel, Marseille

CNRS – Aix Marseille Université – Ecole Centrale de Marseille
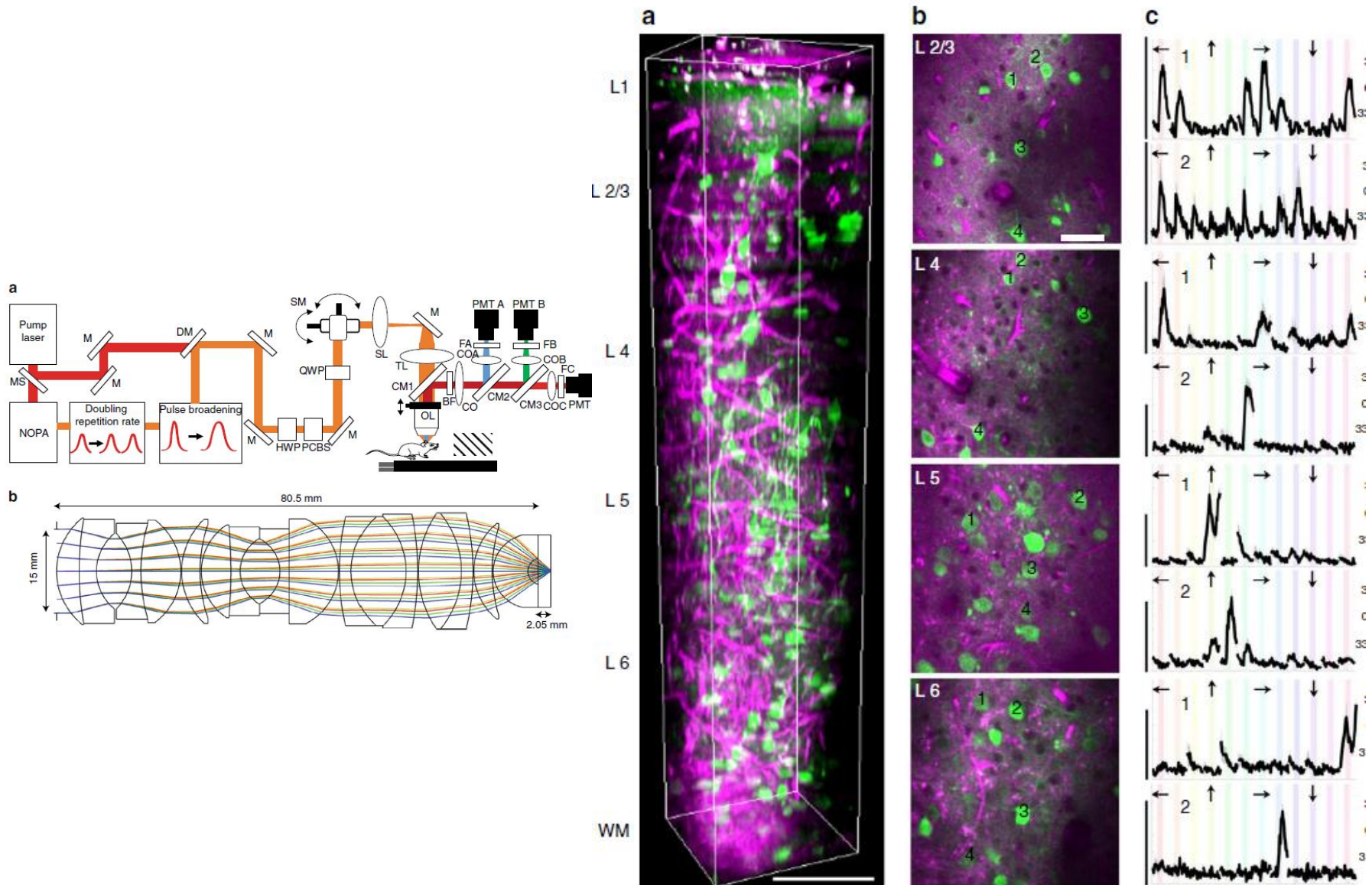
sophie.brasselet@fresnel.fr
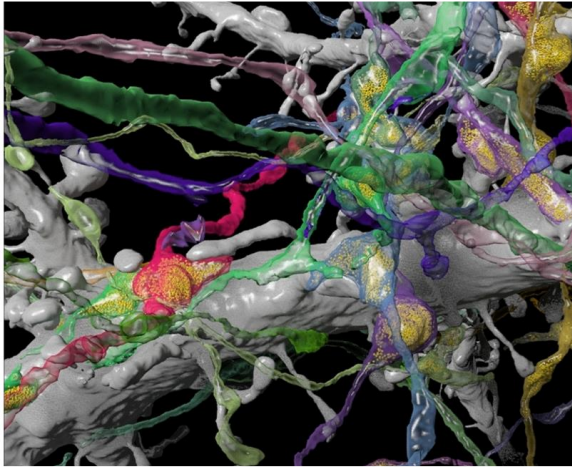
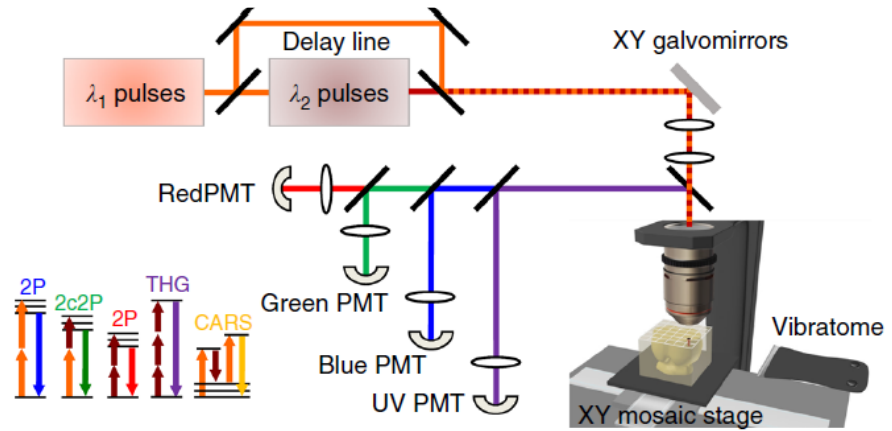# Neurons imaged **in 3D with sub-micrometric resolution**

30% TDE

Neuronal responses imaged **in real time** and in 3D

Neuronal circuitry imaged in real time and in 3D

Electron Microscopy, Mathematics and Visualization
DOI: 10.1007/978-1-4471-6497-5_21

Chromatic multiphoton serial microscopy

fMRI, IEEE Transactions on Visualization and Computer Graphics 9(4), 454– 462 (2003)
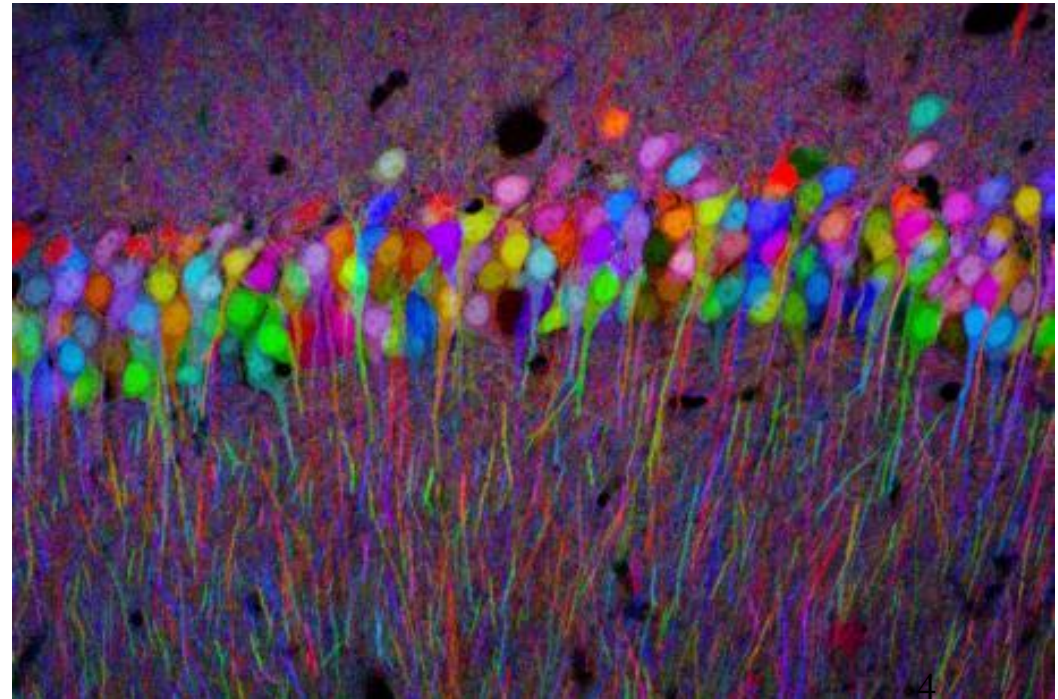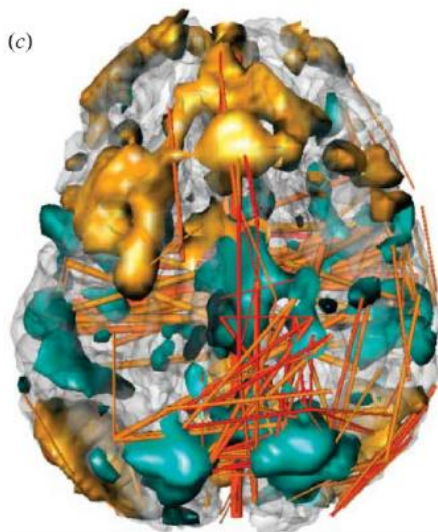
Brain Bow 2 photon image, Jean Livet I. de la vision

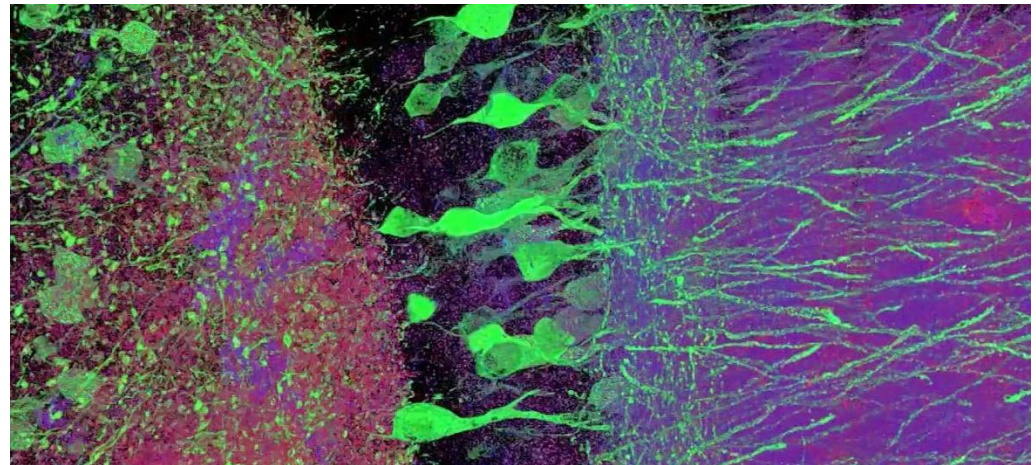# Nonlinear optical imaging at the nanoscale

Introduction : motivation

Principles of nonlinear optical microscopy

Polarized nonlinear microscopy

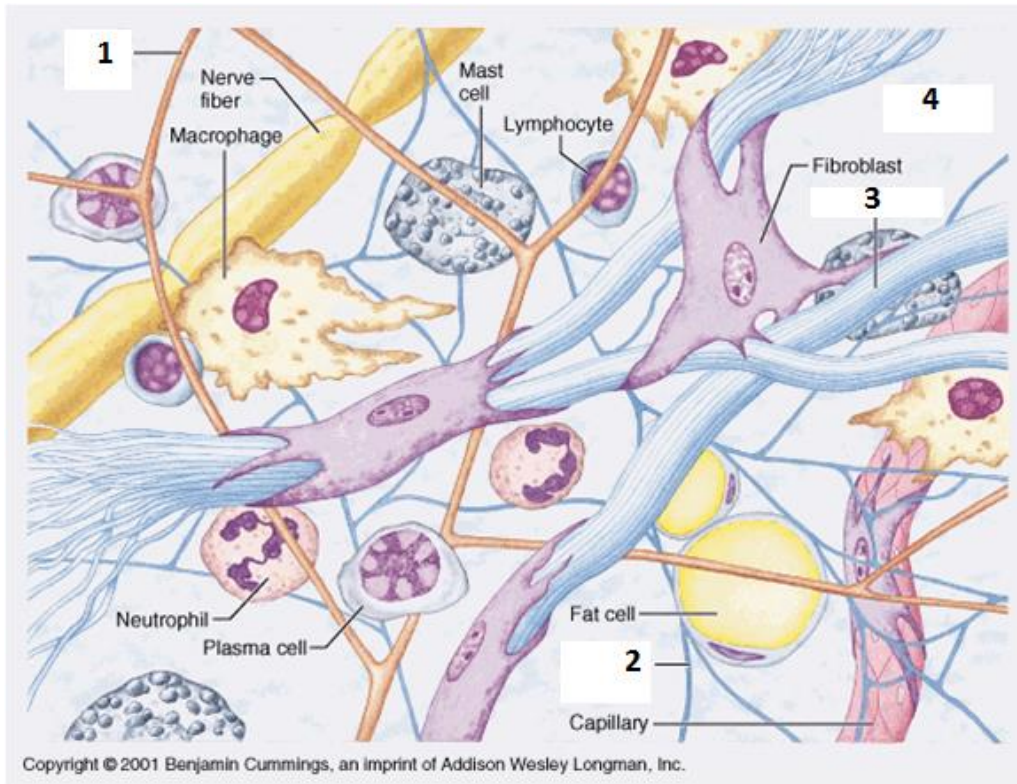Nonlinear microscopy in depth in complex media

Introduction : motivation

Optical waves in microscopy:
Low depth (~100's μm – 1mm)
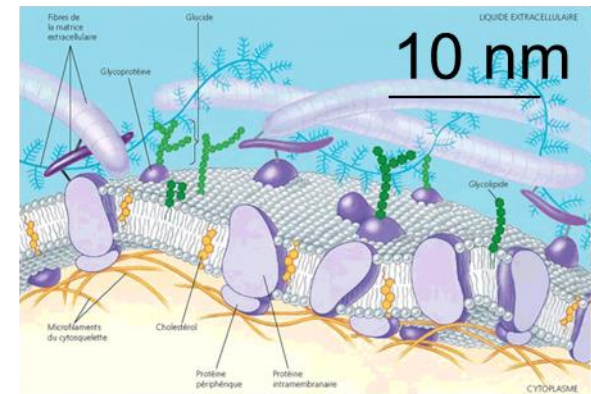High resolution (~ 200 - 300 nm)
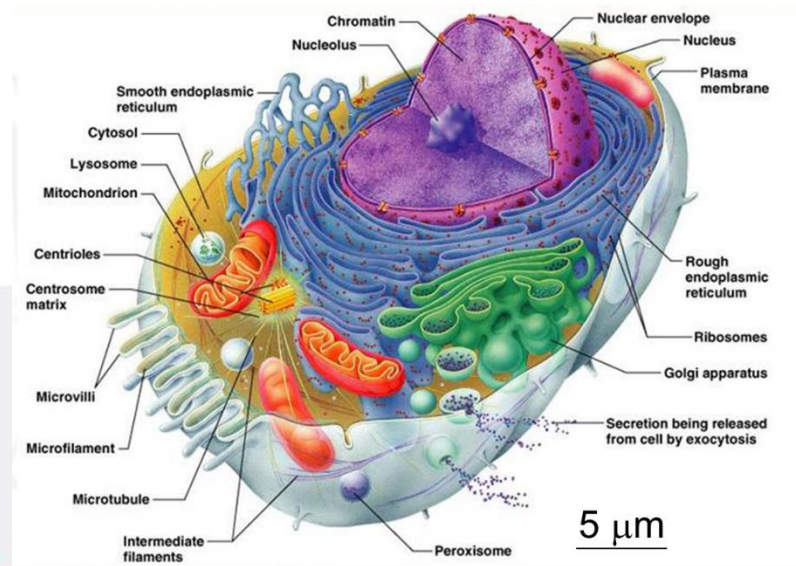
Ed Boyden, Fei Chen, Paul Tillberg/MIT

The tissue scale

The cell scale

The extra-cellular matrix is made of proteins and fibers (collagen, elastin, ..)

Copyright © 2001 Benjamin Cummings, an imprint of Addison Wesley Longman, Inc.

5 μm

10 nm

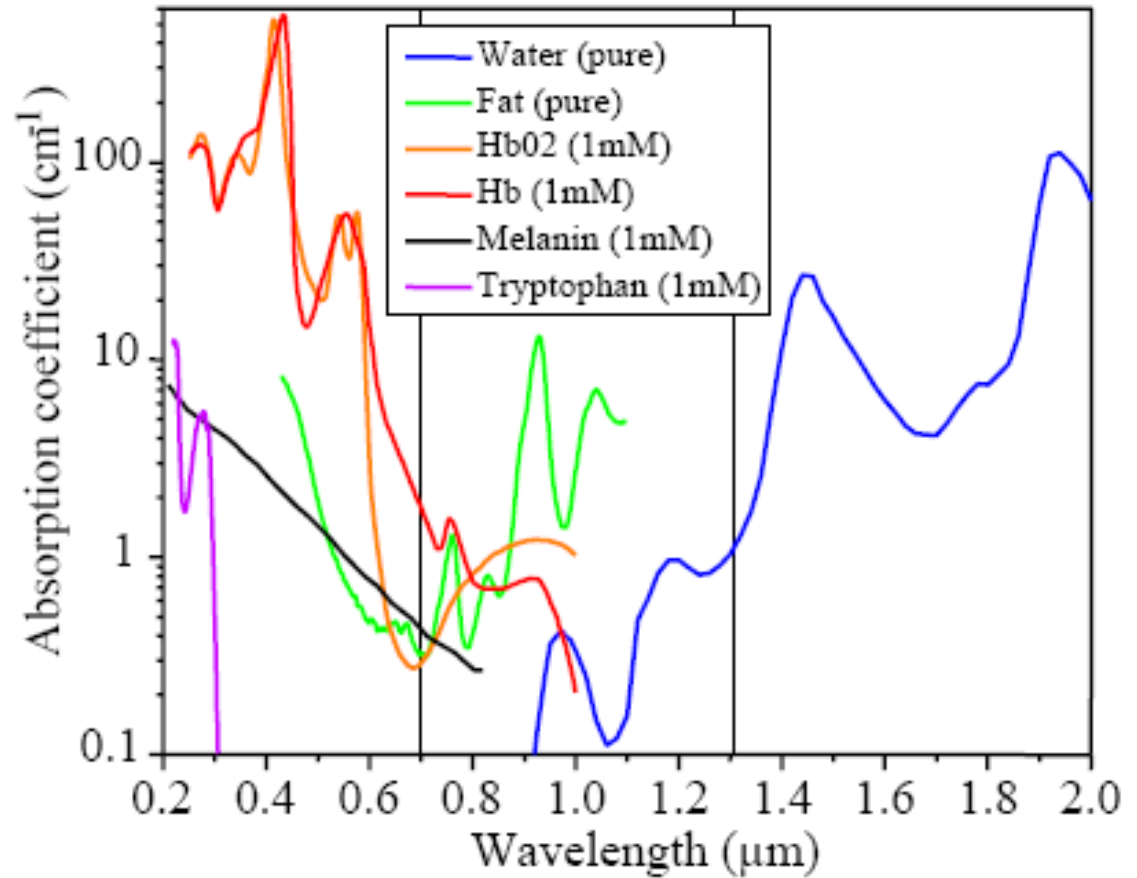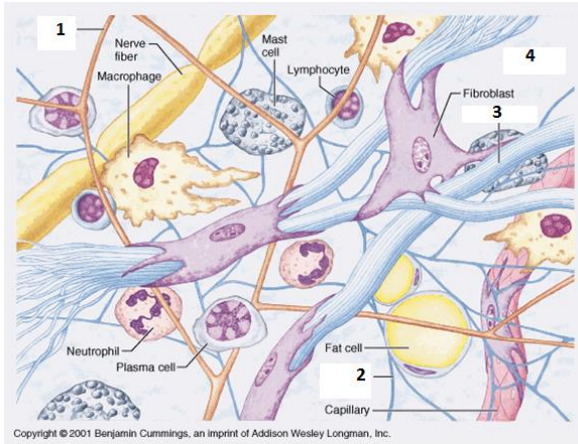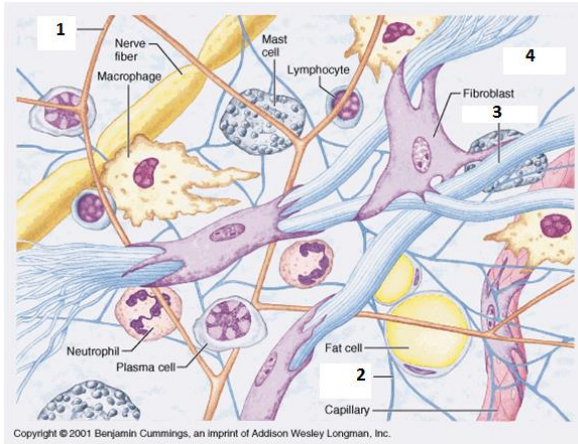Cell membrane

Fundamental limit of optics: absorption in tissues

0.7 – 1.2 μm : reduced absorption compared to VIS light

Fundamental limit of optics: scattering in tissues

0.7 – 1.2 μm : reduced Rayleigh scattering compared to VIS light

$< \lambda$ Rayleigh Regime
- E.g. particles in the sky
- Strongly wavelength dependent
- Mostly isotropic

Fundamental limit of optics: scattering in tissues

0.7 – 1.2 μm : reduced Rayleigh scattering compared to VIS light
But strong Mie scattering at a few 100's um depth !
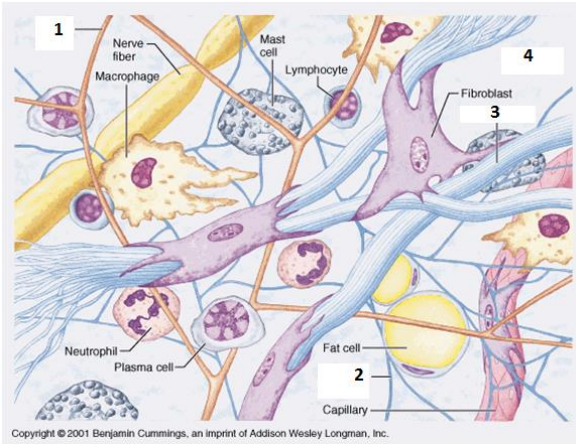

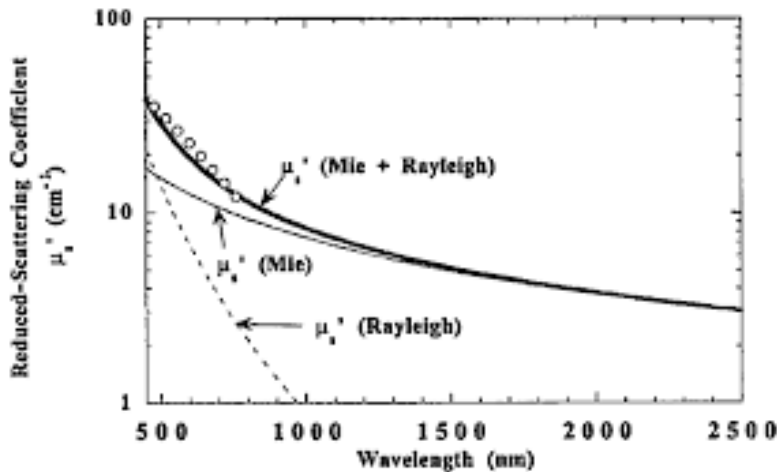$< \lambda$ **Rayleigh Regime**
- E.g. particles in the sky
- Strongly wavelength dependent
- Mostly isotropic

$\geq \lambda$ **Mie Regime**
- Cells, water droplets (fog)
- Anisotropic: mostly forward scattering

10
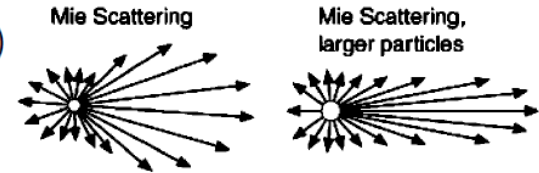
Fundamental limit of optics: depth in scattering media

Propagation distance (mm)

0   0.1   0.2   0.3   0.4   0.5   0.6   0.7   0.8   0.9   1

Ntziachristos Nature 2010

Ballistic regime

Increasing photon scattering

Random walk

Biological tissue :

$l_t \sim$ 1mm

$l_s \sim$ 100μm

11

Fluorescence

10 μm

https://www.aatbio.com

13

Minus end

Plus end

Actin Filament

3 nm

10 μm

https://www.aatbio.com

14

Minus end
Plus end
Actin Filament

3 nm

1 nm

$(CH_3)_2N$ — O — $N(CH_3)_2$ ClO_4^-

C—OCH_2CH_3
O

3 Angst.

10 μm

https://www.aatbio.com

15
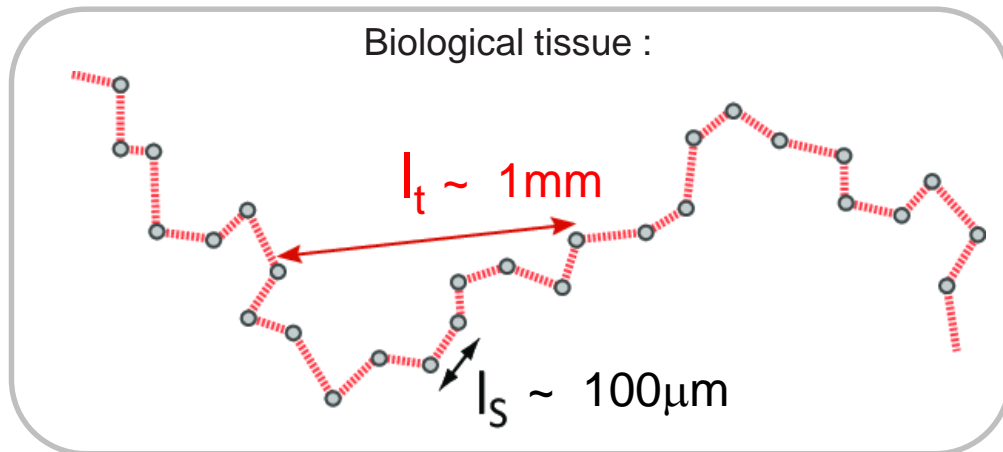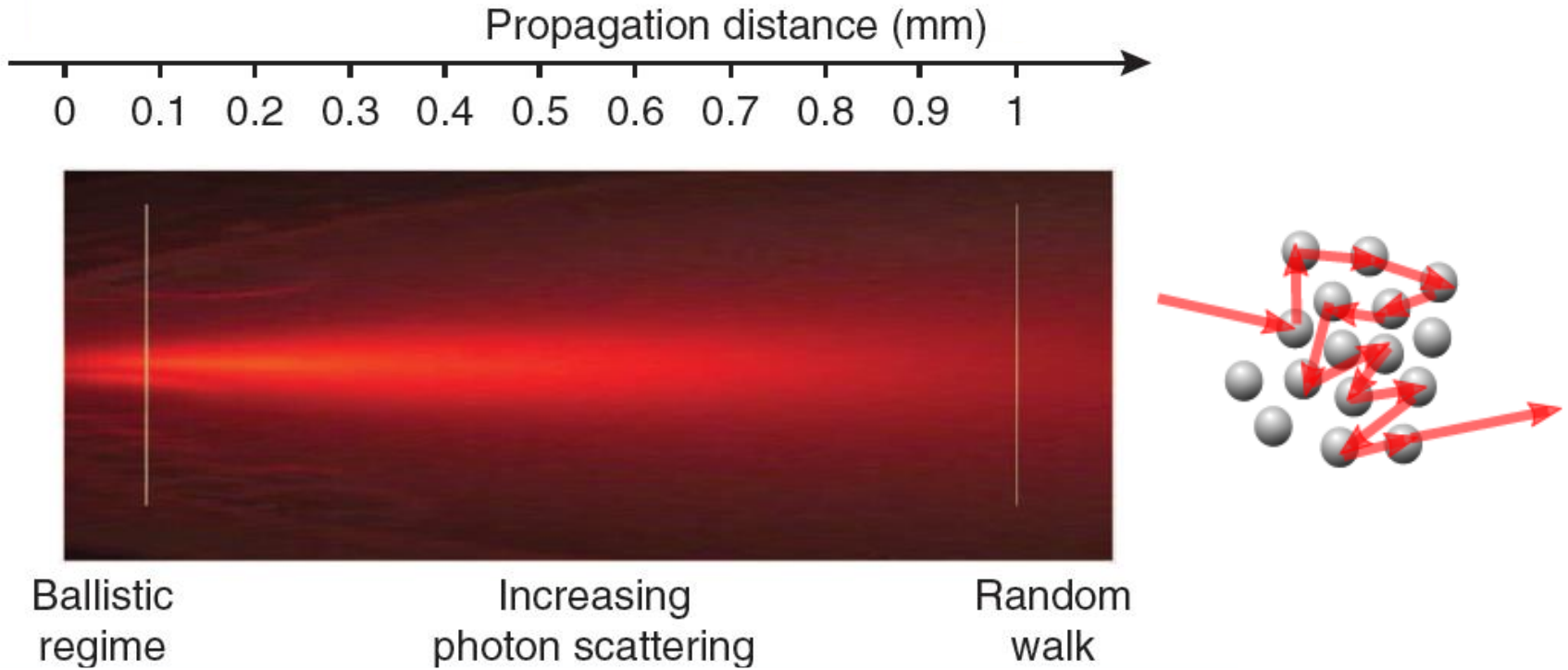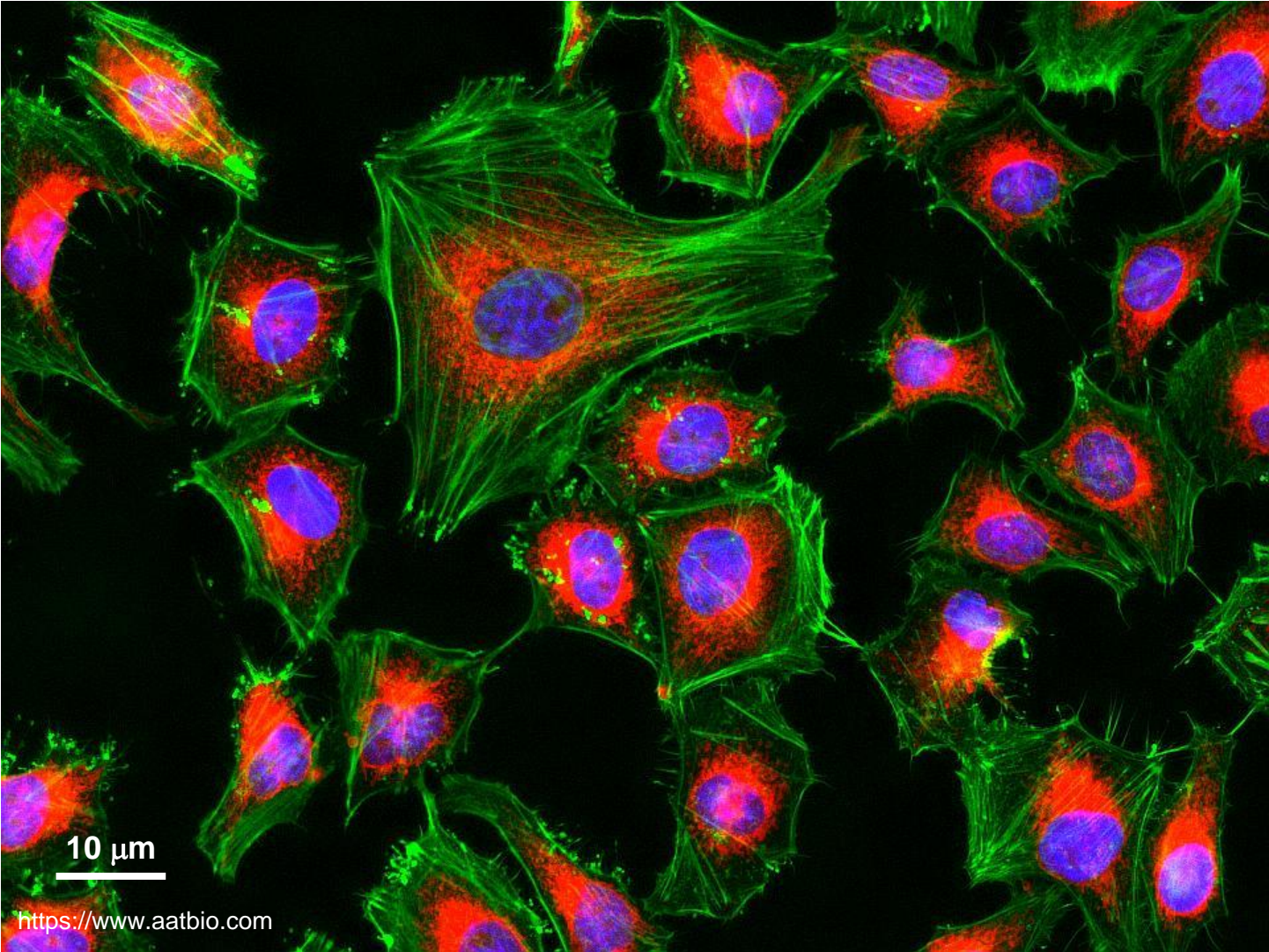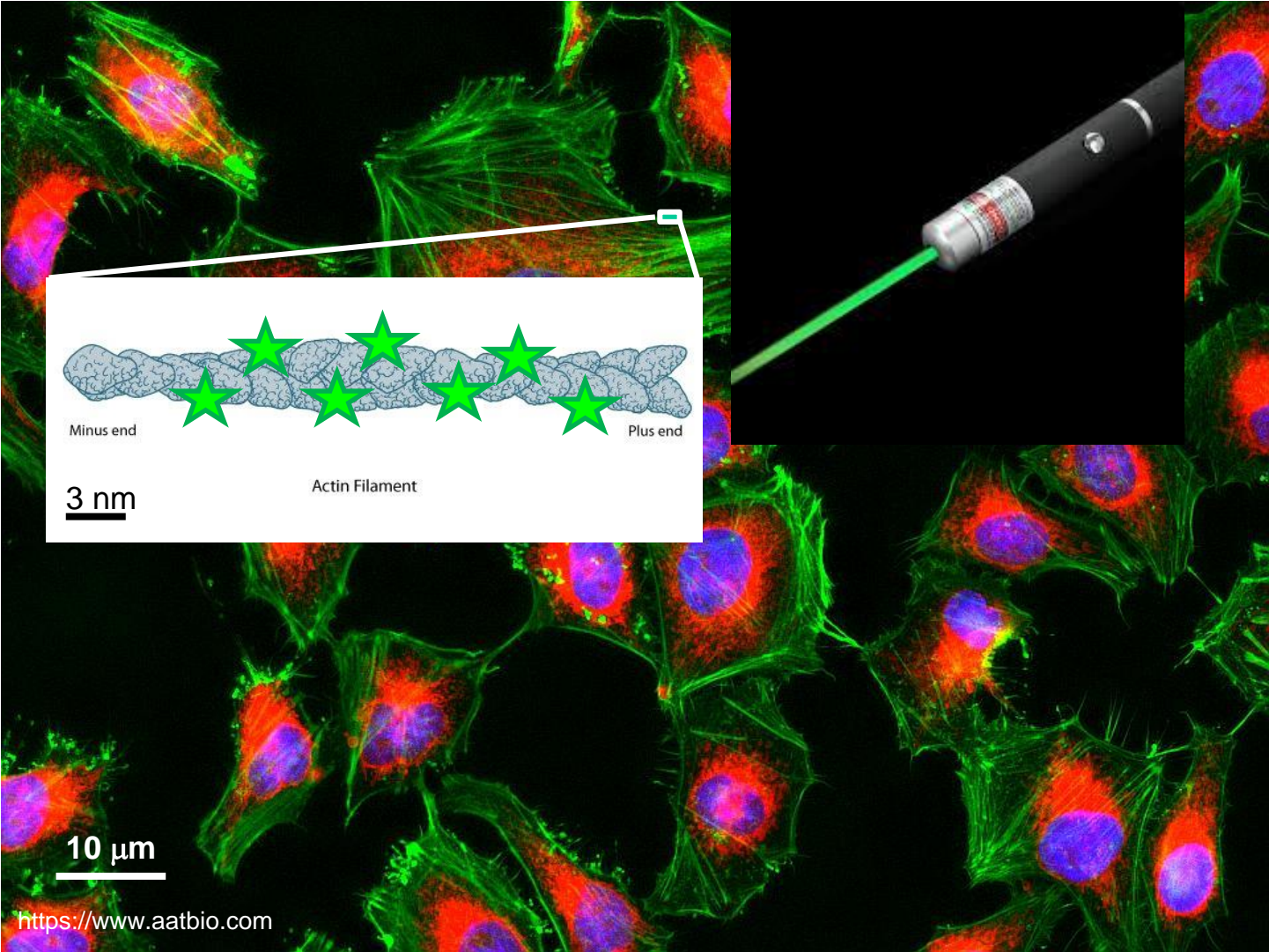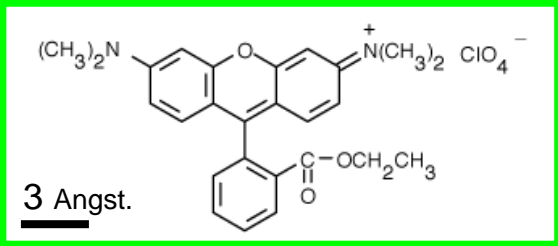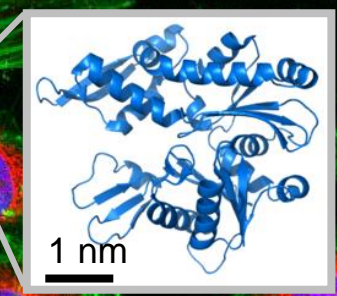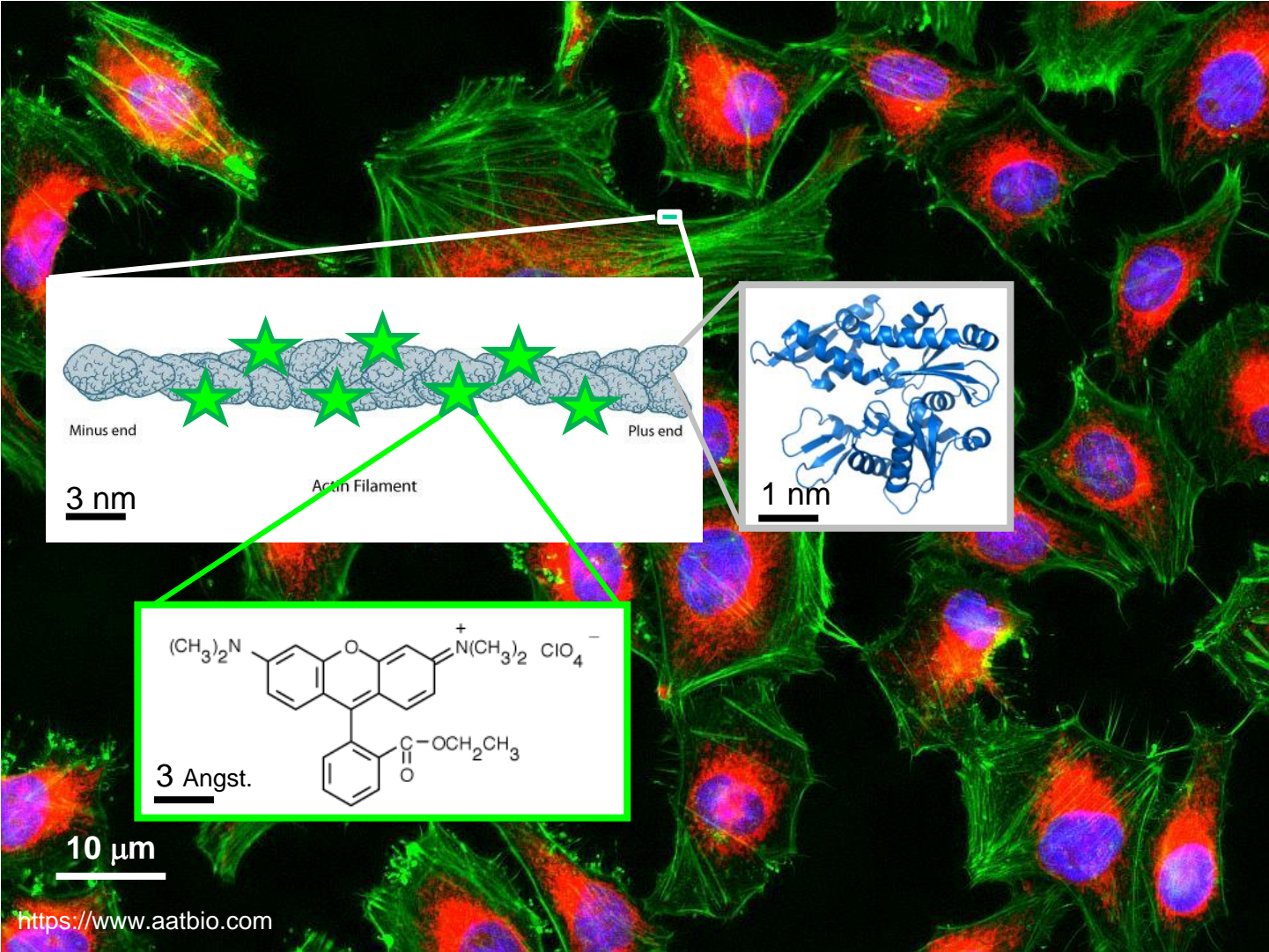
Fluorescence labels for biology: examples

Chromophores:

Cy5

TMR

Lipid probes :

Chaînes carbonées
(hydrophobe)

Tête polaire
(hydrophilie)

Protein GFP:

10Å
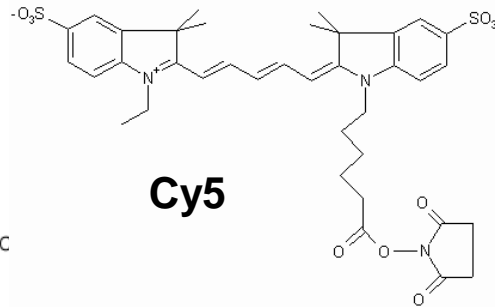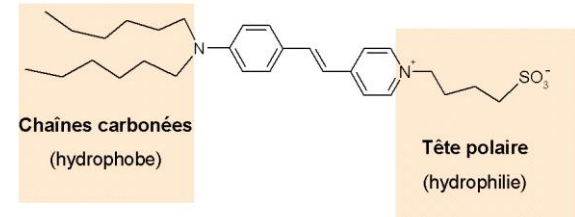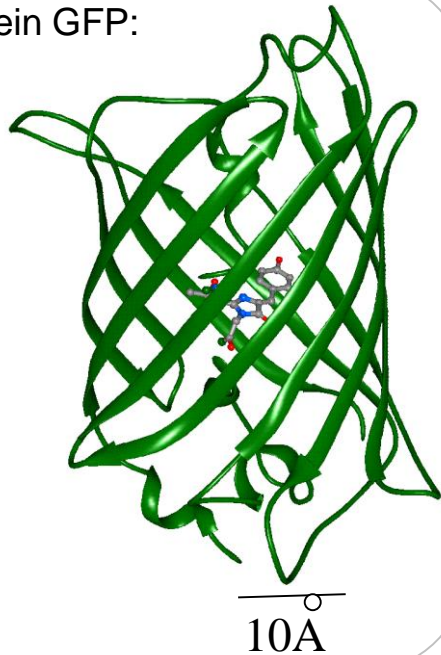
"Quantum Dots" (CdSe/ZnS):
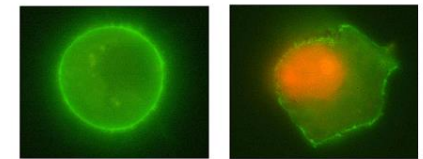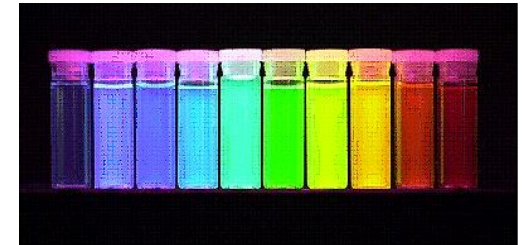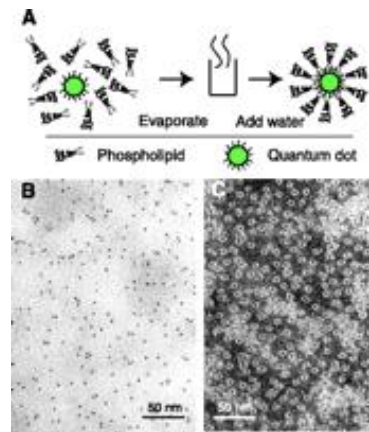
Dubertret et al., ESPCI
Alivisatos et al., Berkeley U., USA

16

Fluorescence labels for biology: genetically modified organisms

http://wondreal.blogspot.com

http://wondreal.blogspot.com

2008 Nobel Prize in Chemistry
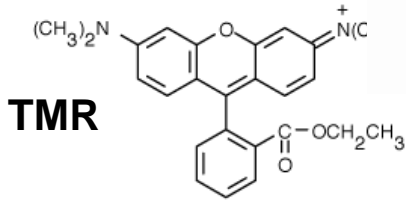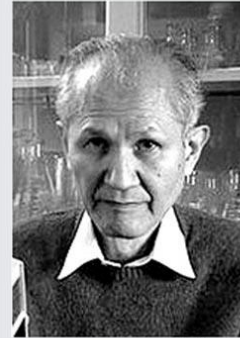

Photo: J. Henriksson/SCANPIX

Photo: J. Henriksson/SCANPIX

Photo: UCSD

Osamu Shimomura   **Martin Chalfie**   **Roger Y. Tsien**

"For the discovery and development of the **Green Fluorescent Protein GFP**"

Mature GFP Chromophore

1 nm
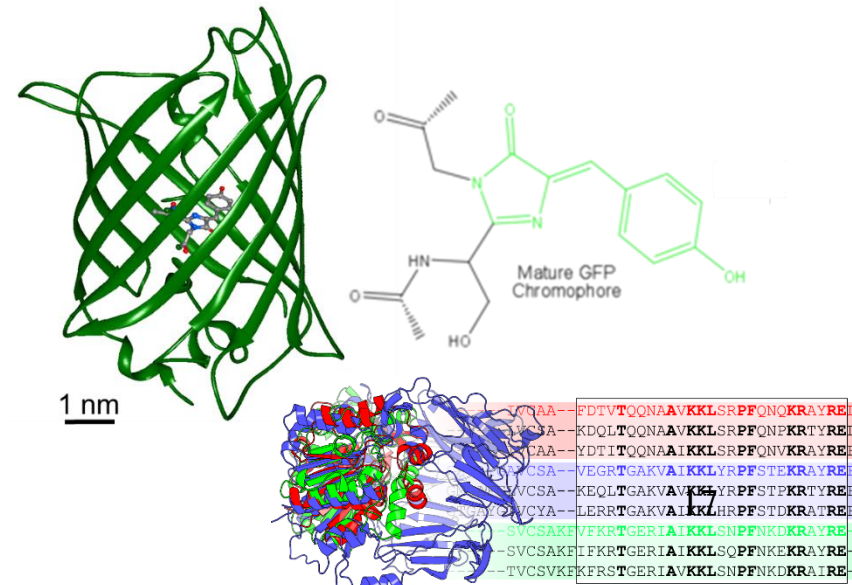
Fluorescence
How many photons can we get out of one molecule ?

Fluorescence = Absorption x Emission
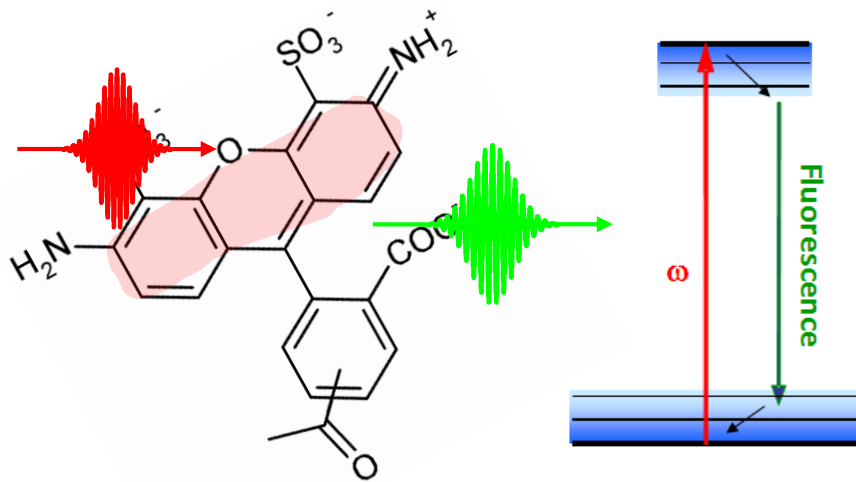
1 photon Fluorescence : 1PF

Absorption probability :

$$P_{abs} = \sigma_{abs}.I$$

Singlet excited states

Internal conversion

Vibrational relaxation

Triplet excited state

Intersystem crossing

S_2

S_1

T_1

Energy

Absorption

Fluorescence

Internal and external conversion

Phosphorescence

S_0

Ground state

Vibrational relaxation

λ_2 λ_1 λ'_r λ_r λ_3 λ_4
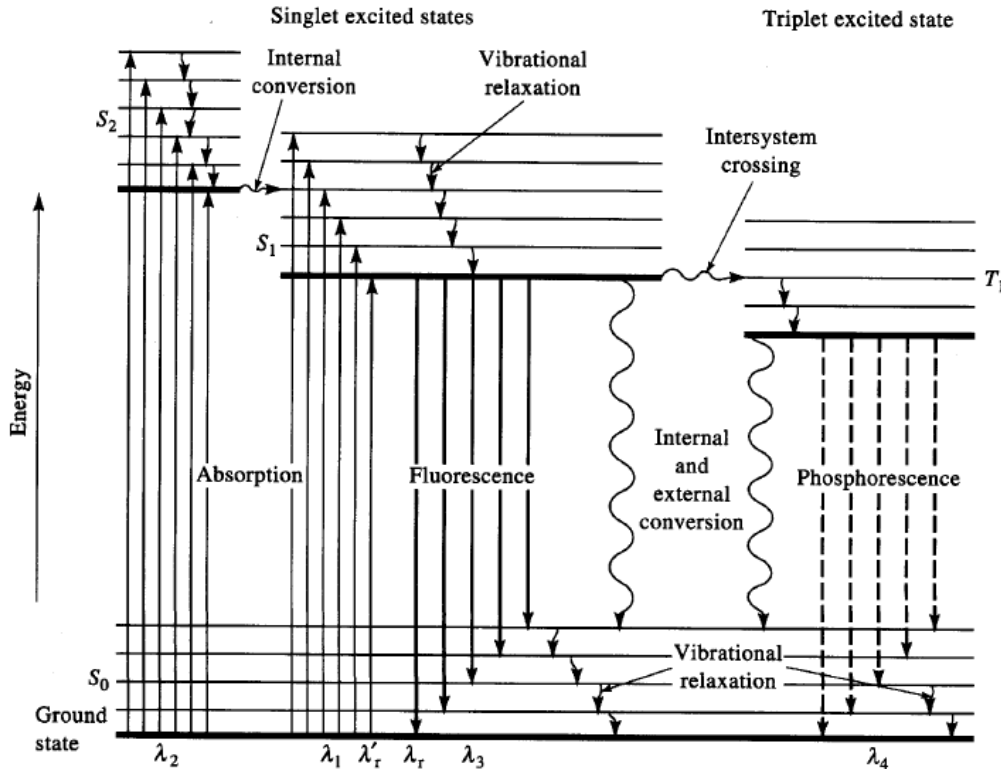
Fluorescence quantum yield:

$$\Phi_f = \frac{k_r}{k_r + k_{nr}}$$

$$P_{abs}^{(1\,photon)} \propto \left| \vec{\mu}_{01}.\vec{E} \right|^2 = \sigma_{abs}.I$$

$$\mu_{01} = \int \psi^*_1\!\left(\vec{r}\right).\left(-e\vec{r}\right).\psi_0\!\left(\vec{r}\right)d\vec{r}$$ Transition dipole moment
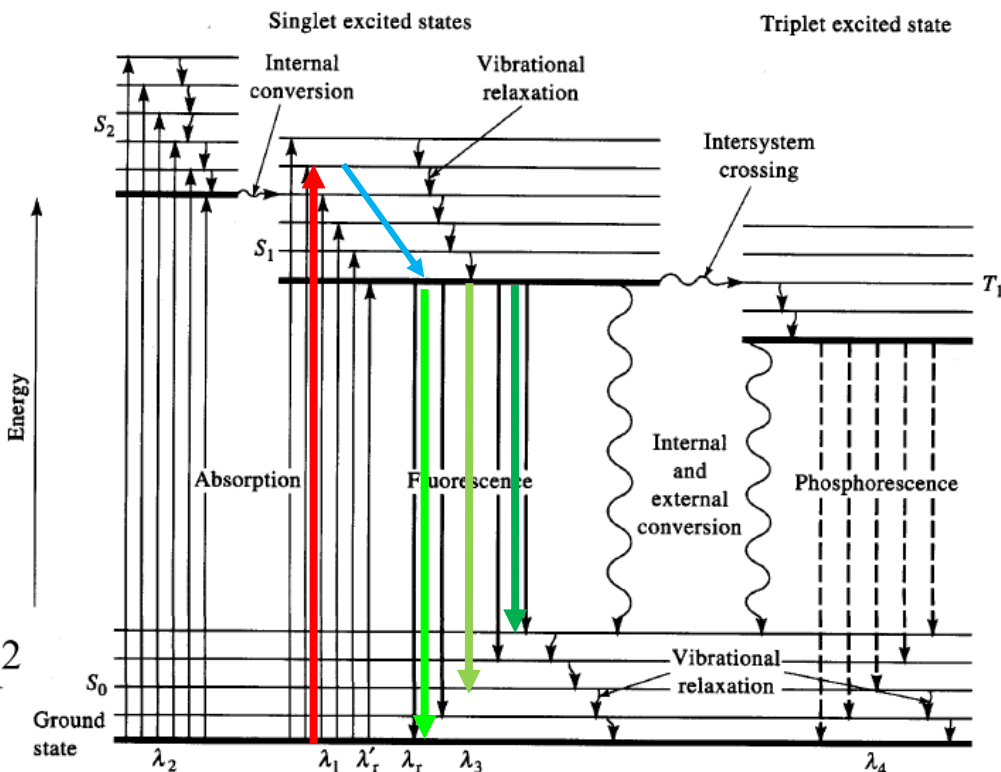
1 photon Fluorescence : 1PF
Fluorescence = Absorption x Emission

Absorption probability :

$$P_{abs} = \sigma_{abs} \cdot I$$

$$\sigma_{abs} \sim 10^{-16} \text{ cm}^2$$

Fluorescence quantum yield:

$$\Phi_f = \frac{k_r}{k_r + k_{nr}}$$

$$\Phi_f \approx 0.5 - 0.9$$

$$I_{1PF}(t, t') \propto P_{abs}(t) \cdot P_{em}(t') \cdot e^{-(t-t')/\tau_f}$$

Absorption probability   Emission probability

1P absorption rate from a single molecule

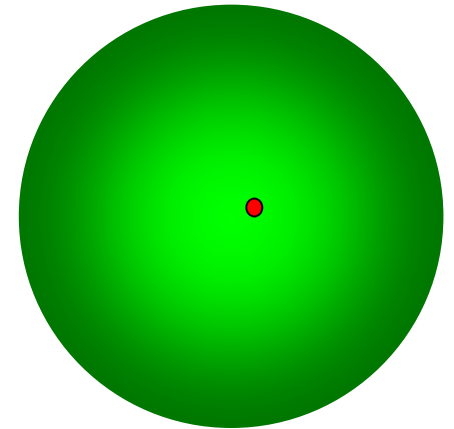Molecule : absorption cross section σ

Excitation surface: A

~ 300nm

Laser ~10^{24} ph/s/μm^2 $\langle P(t) \rangle$
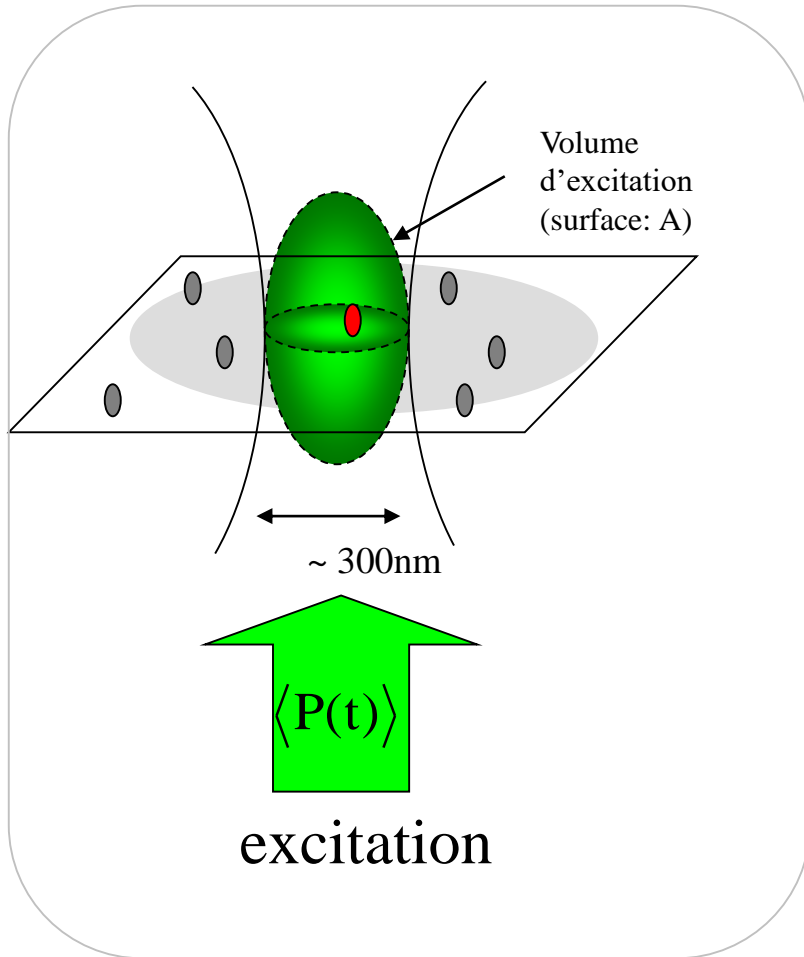
excitation

Absorption rate :

$$\mathrm{Pabs} = \frac{\langle P(t) \rangle}{h\nu} \cdot \frac{\sigma}{A}$$

Typ. ~10^6 ph/s

Focal spot

21

1 photon fluorescence signal from a single molecule

Volume d'excitation (surface: A)

~ 300nm

$\langle P(t) \rangle$

excitation

$$\langle I(t) \rangle = C \cdot \Phi_f \cdot \frac{\langle P(t) \rangle}{h\nu} \cdot \frac{\sigma}{A} \qquad \text{ph/s}$$

Fluorescence quantum yield:

$$\Phi_f \approx 0.5 - 0.9$$

Collection factor:

$$C \approx 2 - 10\%$$
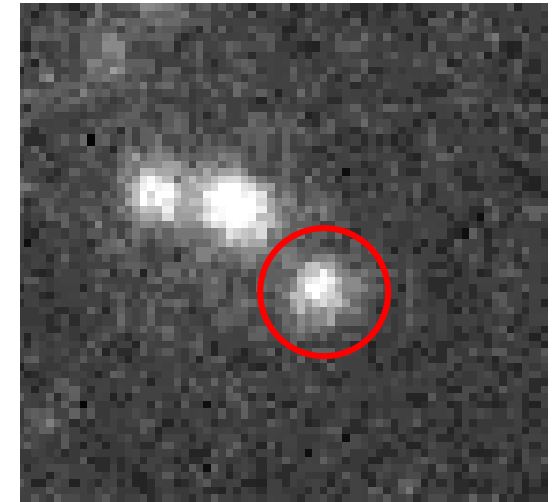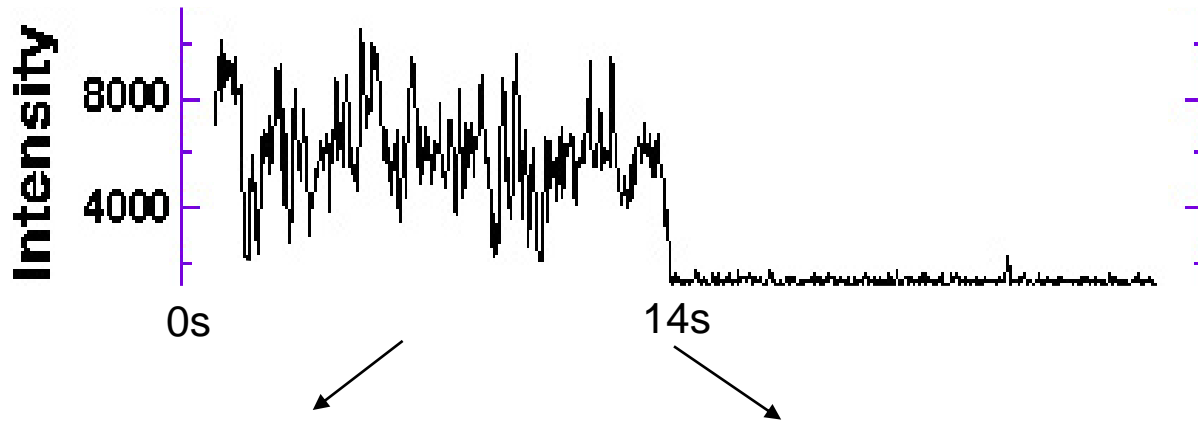
Molecule absorption cross section:

$$\sigma \approx 3 \times 10^{-16} \, cm^2$$

$$\sigma_{Raman} \approx 10^{-28} \, cm^2$$

$$\langle P(t) \rangle = 10 \mu W$$
$$A \approx 1 \mu m^2$$

$\Rightarrow$

$$\langle I(t) \rangle = 6300 \, ph/s \quad \text{signal}$$
$$\langle I \rangle_{Raman} \approx 10 ph/s \quad \text{noise}$$

1 photon fluorescence signal from a single molecule

ex. Cy3 (cyanine) exc. 633nm, em. 670nm

Photophysics : fluctuations due to interaction with environment, orientation changes,

Photobleaching event : reaction with oxygen singulet leads to non fluorescent radical
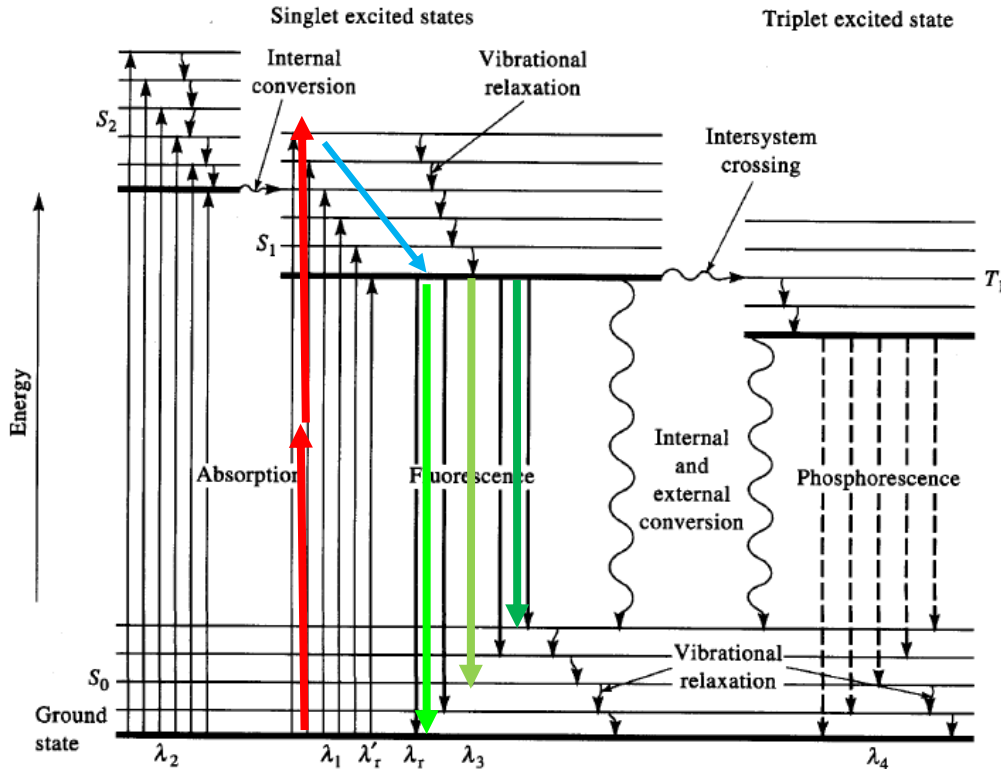
Molecules interdistance > optical resolution

Local analysis
Spatial localization
Super resolution microscopy

2 photon Fluorescence : 2PF

Fluorescence = 2P Absorption x Emission

Singlet excited states

Triplet excited state

2PF Absorption probability

Energy

S_2

S_1

Internal conversion

Vibrational relaxation

Intersystem crossing

T_1

Absorption

Fluorescence

Internal and external conversion

Phosphorescence

Vibrational relaxation

S_0

Ground state

λ_2 λ_1 λ'_r λ_r λ_3 λ_4

Fluorescence quantum yield:

$$\Phi_f = \frac{k_r}{k_r + k_{nr}}$$

$$\Phi_f \approx 0.5 - 0.9$$

$$I_{2\mathrm{PF}}(t, t') \propto P_{\mathrm{abs}}^{(2P)}(t) \cdot P_{\mathrm{em}}(t') \cdot e^{-(t-t')/\tau_f}$$
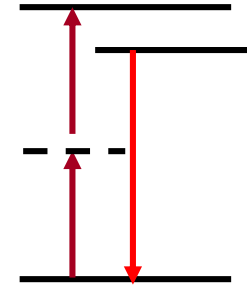
2P Absorption probability   Emission probability

24

Two photon excited fluorescence (2PF) efficiency

1-photon excitation

A

σ
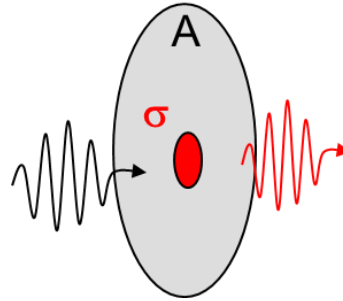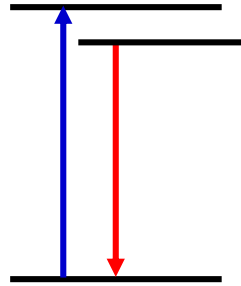
2-photon excitation :
virtual ultra-short lived (<1fs)
intermediate state

1molecule in
bright day
light :
1 event /s

1molecule in
bright day
light :
1 event / 10
million years

Absorption probabilities :

$$P_{abs}^{(1\,photon)} = \left|\vec{\mu}_{01}.\vec{E}\right|^2$$

$$P_{abs}^{(2\,photon)} \approx \left|\left(\vec{\mu}_{0n}.\vec{E}\right)\left(\vec{\mu}_{n1}.\vec{E}\right)\right|^2$$

$$P_{abs}^{(1\,photon)} = \sigma^{(1)}.E^2$$

$$P_{abs}^{(2\,photon)} = \sigma^{(2)}.E^4$$

Absorption cross sections :

$$\sigma^{(1)} \approx (1-10)\cdot 10^{-16}\,cm^2$$

$$\sigma^{(2)} \approx (10-1000)\cdot 10^{-50}\,cm^4 s/ph$$

25

Usual unit : Göppert-Mayer 1 GM = 10^{-50} cm^{4}s/ph

Two photon absorption cross section

Intrinsic

Fluorescent proteins (GFP, etc)   10-100 GM

Zipfel, Webb (Cornell Univ.)

elastin
(rat artery wall, fresh)
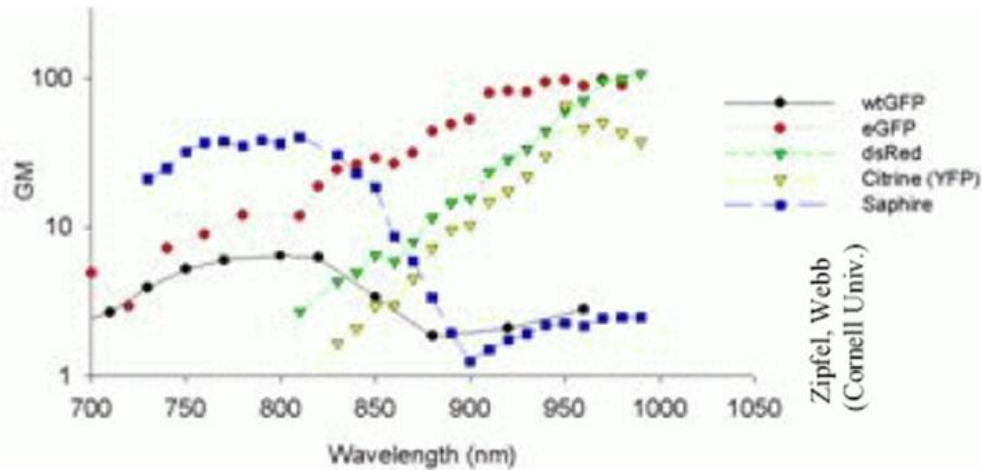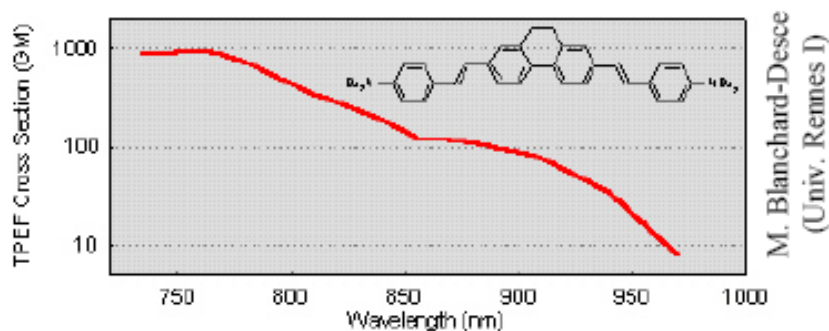
2PEF

Boulesteix et al. (2006) Cytometry **69A**

Engineered

Engineered fluorophores with enhanced 2PEF
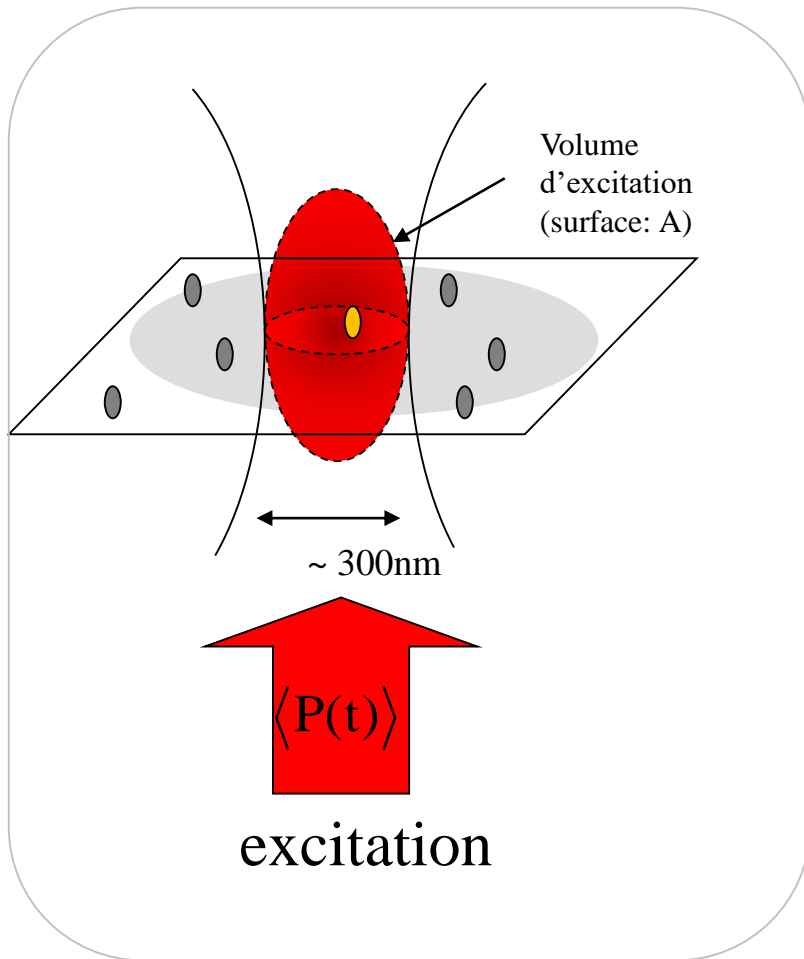100-1000 GM

M. Blanchard-Desce (Univ. Rennes I)

Endogenous fluorophores (NADH, etc)
$10^{-3} - 10^{-1}$ GM

Standard fluorophores (Rhodamine…)
0.1-10 GM

26

2 photon fluorescence signal from a single molecule

Volume
d'excitation
(surface: A)

~ 300nm

$\langle P(t) \rangle$

excitation

$$\left\langle I^{2ph}(t) \right\rangle = C . \Phi_f . \left(\frac{\langle P(t) \rangle}{h \nu_{2ph}} \frac{1}{A} \right)^2 . \sigma^{(2)} \ \text{ph/s}$$

Fluorescence
quantum yield:

$$\Phi_f \approx 0.5 - 0.9$$

Collection
factor:

$$C \approx 2 - 10\%$$

Molecule 2 photon
absorption cross
section:

$$\sigma^{(2)} = 100.10^{-50} cm^4 s / ph$$

In the continuous (CW) excitation regime :

$$\langle P(t) \rangle = 10 mW$$

$$A \approx 1 \mu m^2$$

$$\Rightarrow \left\langle I^{2ph}(t) \right\rangle = 0.6 \, ph / s \quad \text{Signal << noise!}$$

Short laser pulses are required for two-photon imaging:

Optimal excitation with minimum average power

$$I^{2PF} = \sigma_{abs}^{(2)} \cdot |\langle E(t)^2 \rangle|^2$$

Continuous laser : $\quad P(t) = P_0 = \overline{P}$ $\qquad \longrightarrow \qquad$ $I^{(TPEF)} \propto \overline{P}^2 = P_0^2$

Pulsed laser : $\qquad P(t) = P_{peak} \cdot f(t)$

Rectangle shape
Width τ, frequency f : $\quad P_{peak} = \dfrac{1}{\tau \cdot f} \overline{P}$
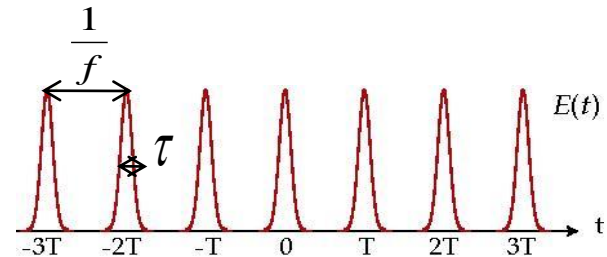
$$\longrightarrow \qquad I^{(TPEF)} \propto \overline{P}^2 = \frac{P_0^2}{\tau \cdot f}$$

« enhancement »

Typically : f = 76MHz, τ = 220fs, for same average power:
$$I^{(pulsed)} = 6 \times 10^4 \, I^{(CW)}$$

Hell et al. 1994

28

Two-photon fluorescence (2PF) from ensemble of molecules

1 molecule :
$$I_I^{2-ph} \propto |\mu^{abs}(\Omega) \cdot \mathbf{E}^\omega|^4 |\mu^{em}(\Omega) \cdot \mathbf{I}|^2$$
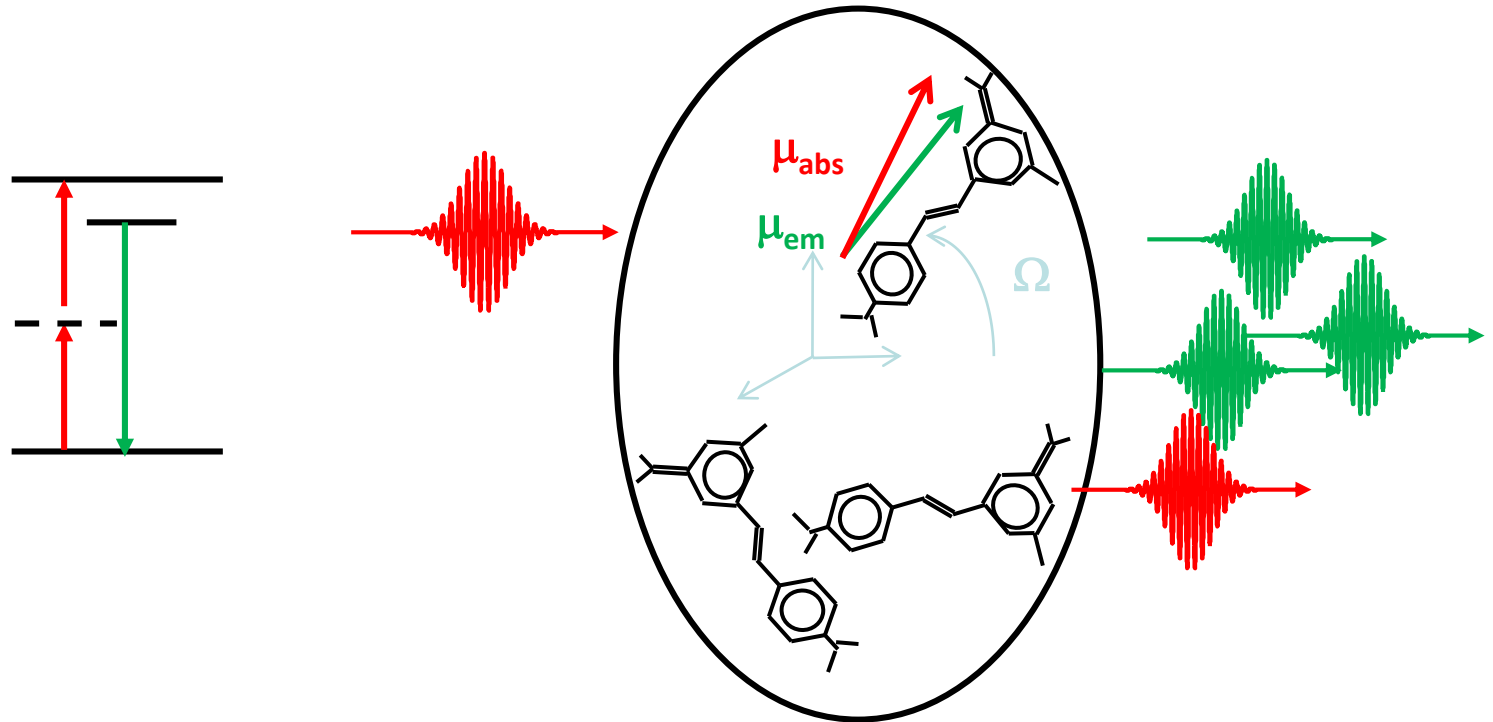
N molecules : sum of intensities (incoherent process)

$$I_I^{2-ph} = N \int_\Omega |\mu(\Omega) \cdot \mathbf{E}|^4 |\mu^{em}(\Omega) \cdot \mathbf{I}|^2 \, f(\Omega) \, d\Omega$$

$$\boxed{I_I^{2-ph} = N \cdot \Phi_f \cdot C \cdot \sigma^{(2)} \cdot (I^\omega)^2}$$

Microscopy

Optical resolution of a microscope objective

Real illumination/image Point Spread Function (PSF)
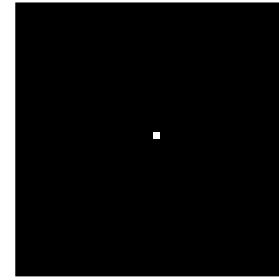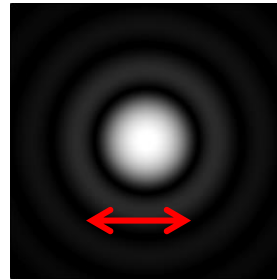
« Ideal » illumination/object

$\lambda/(2NA)$ ~200nm

- Minimize aberrations (chromatic / spherical..) and therefore optimize the quality of an image

- Provide a high numerical aperture to gain in optical resolution

Immersion medium

$$NA = n. \sin\alpha$$

In a medium of index n

NA ~ 0.5 – 1.49

α

Optical resolution of a microscope objective

Real illumination/image Point Spread Function (PSF)

$\lambda/(2NA)$ ~200nm

« **Ideal** » **illumination/object**

5μm

Fluorescence

300 nm
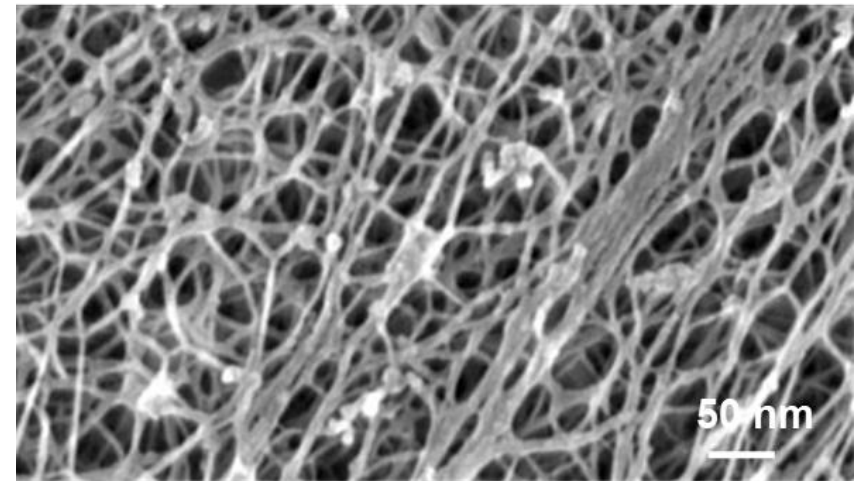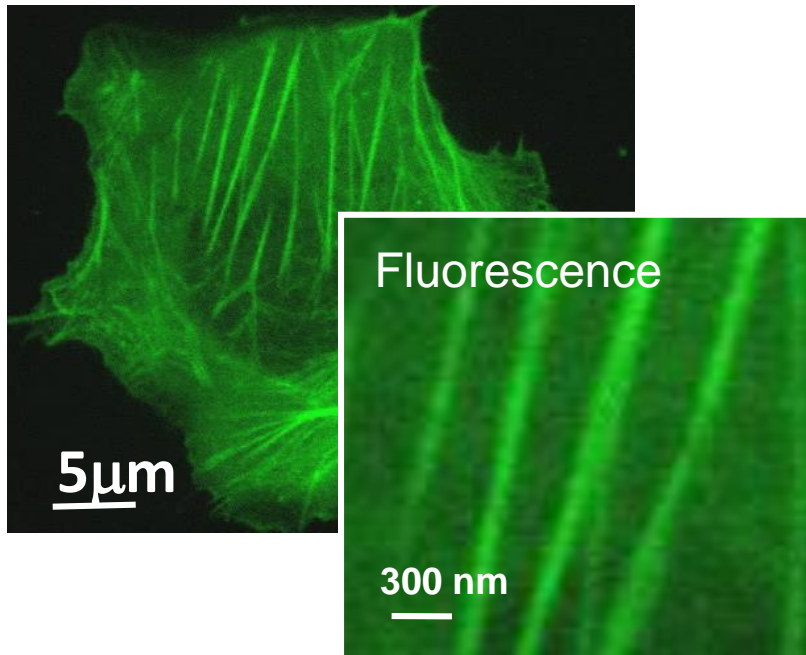
50 nm

Detergent extracted actin cytoskeleton SEM- Ian Wells, DB Stolz

Two photon excited fluorescence (2PF) imaging

$$P_{abs}^{(1\,photon)} \propto I$$

$$V^{(1\,photon)} = \frac{0.7\pi n\lambda^3}{NA^3}$$
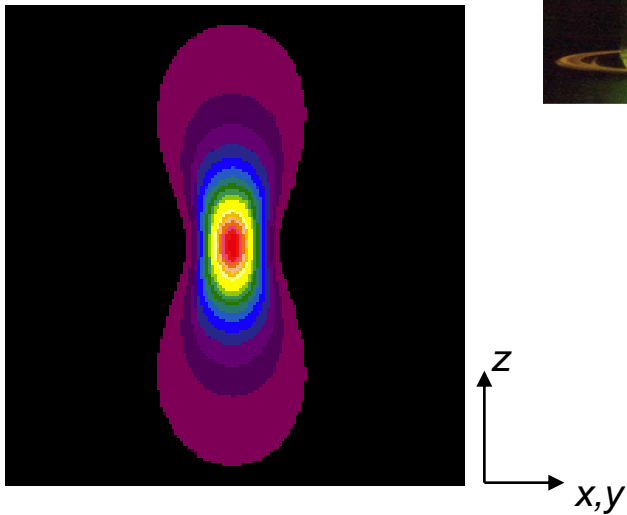
1-photon   2-photon
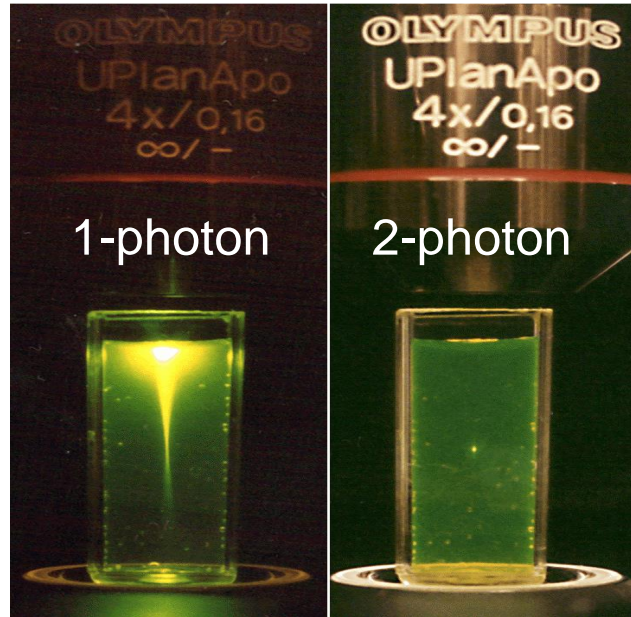
1 and 2 photon fluorescence
in a solution

$$P_{abs}^{(2\,photon)} \propto I^2$$

$$V^{(2\,photon)} = \frac{8n\lambda^3}{\pi^3 NA^4}$$

Reduced volume by about
$$\div \sqrt{2}$$

λ = 750nm, NA 1.2

z

x,y

1-photon
0.81 μmx0.37 μm
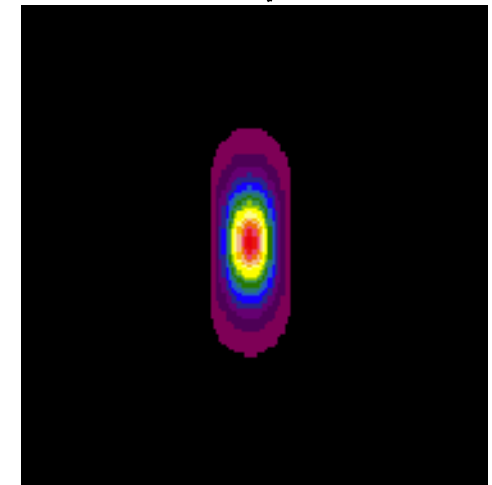
2-photon
0.52 μmx0.26 μm

Two photon excited fluorescence (2PF) Scanning microscopy

Emission spectrum

Absorption spectrum

1 photon exc. (λ)

2 photon exc. (2λ)

λ

Pump Laser

Mode Locked Ti:Sapphire Laser

Eyepiece

P.M.T.

z

Objective

Specimen Plane

34
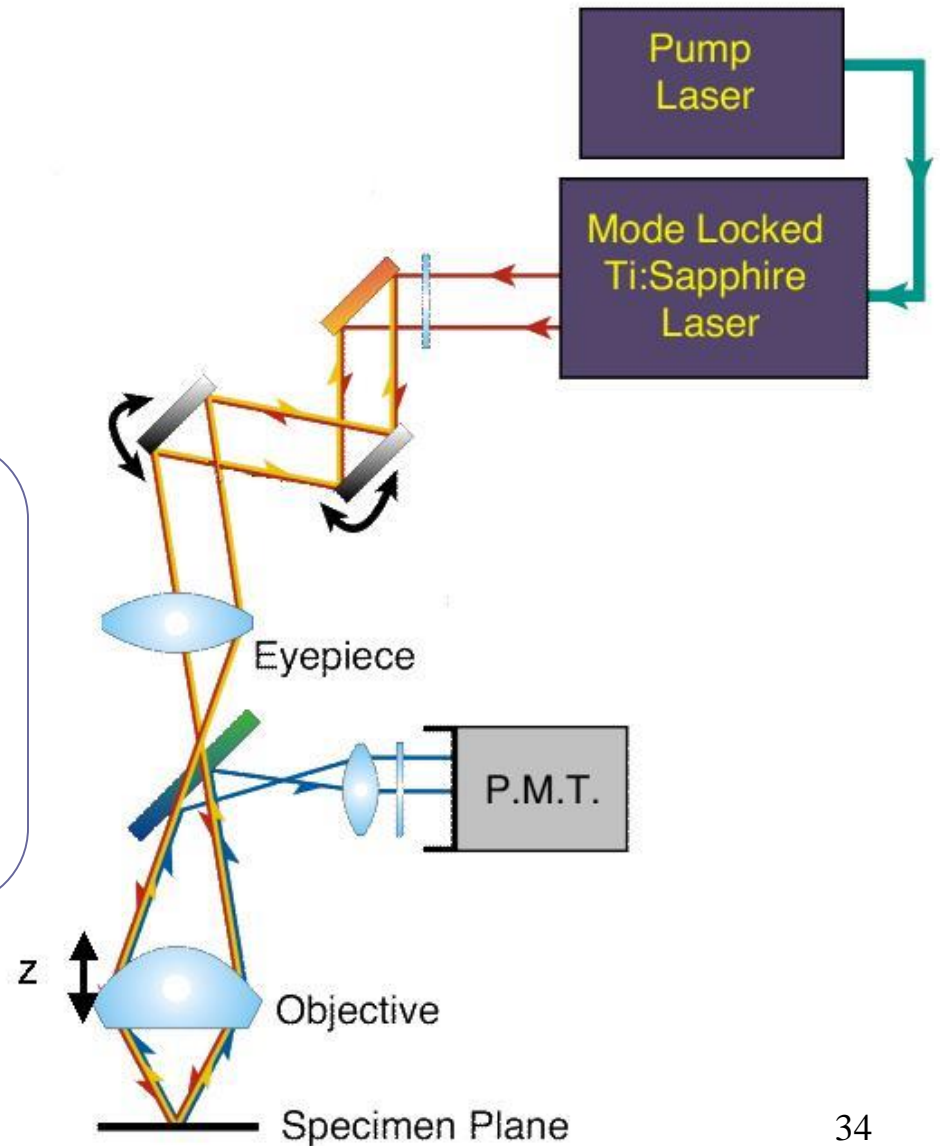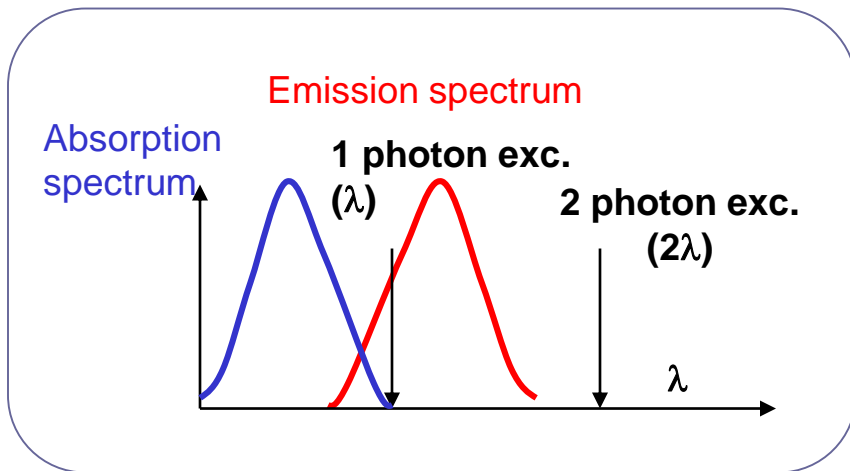
2PF excitation / radiation in a microscope
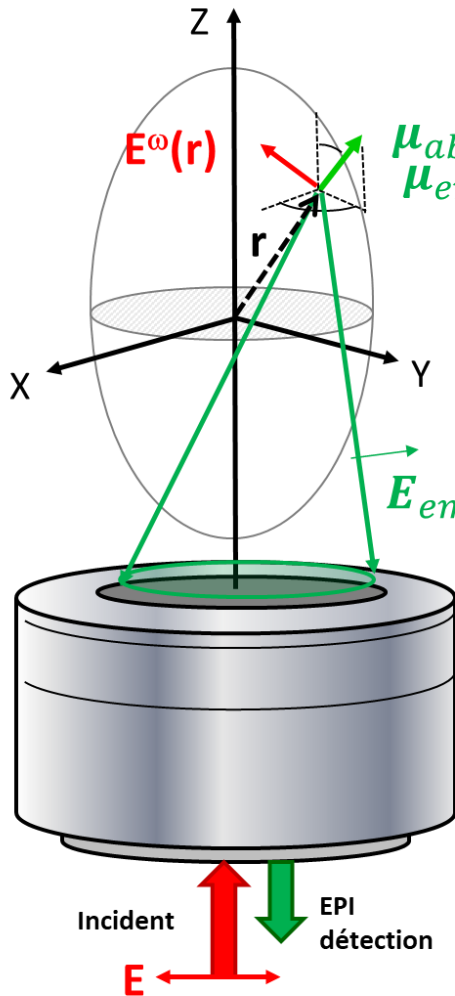
$$\boldsymbol{E}_{em}(\Omega, \boldsymbol{k}) \propto (\boldsymbol{k} \times \boldsymbol{\mu}_{em}) \times \boldsymbol{k}$$
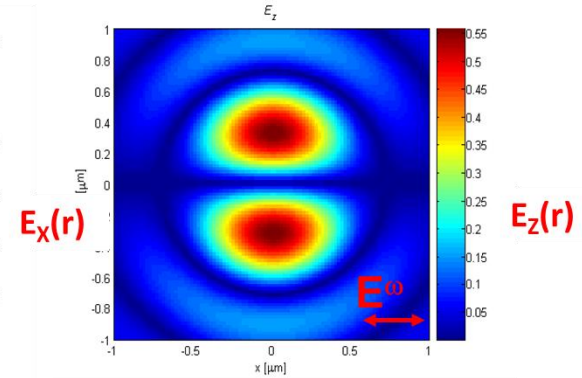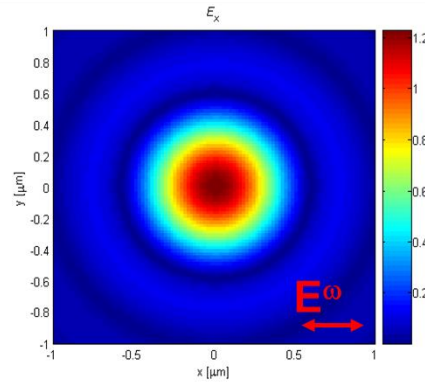
Incoherent addition:

$$I_u^{2PF} =$$

$$N \left\langle \int_{NA} \int_V \int_\Omega \; | \; |\boldsymbol{\mu}_{abs}(\Omega, \boldsymbol{r}) \cdot \boldsymbol{E}(\boldsymbol{r})^4 \, |\boldsymbol{E}_{em}(\Omega, \boldsymbol{k}, \boldsymbol{r}) \cdot \boldsymbol{u}|^2 \, f(\Omega) \, d\Omega \, \mathrm{d}\boldsymbol{r} \, \mathrm{d}\boldsymbol{k} \right\rangle$$

From incoherent 2PF to coherent NLO
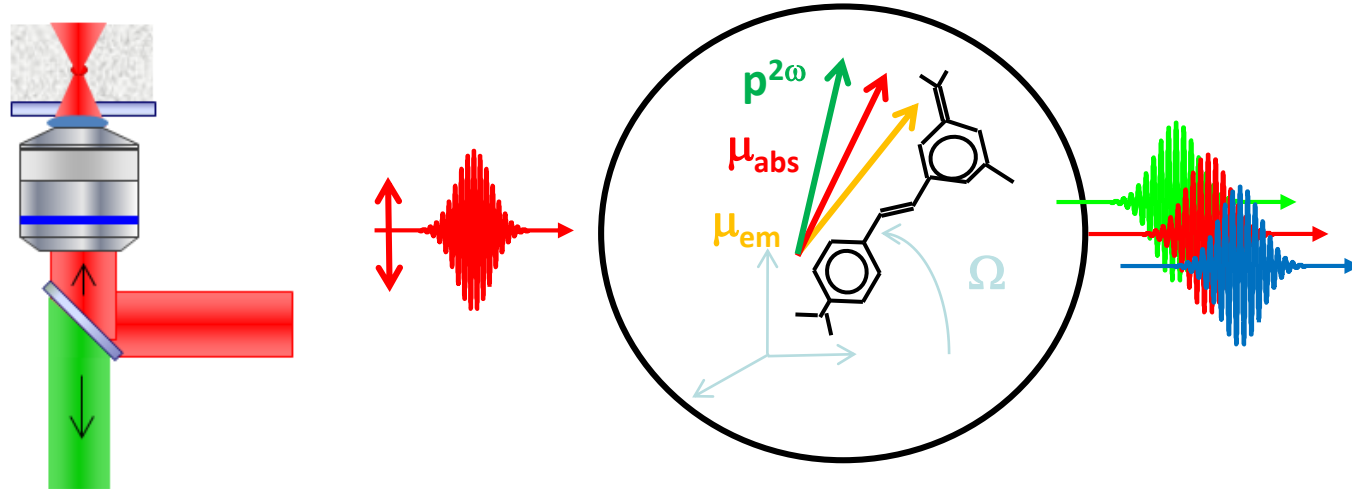
Incoherent process:
2PF

Coherent nonlinear processes :
SHG-THG, FWM, CARS
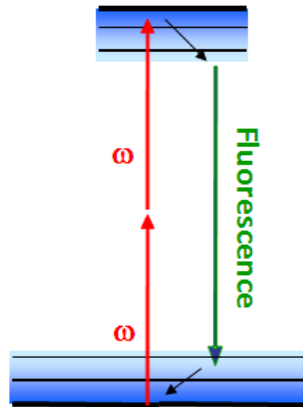
- Single molecule detection
- Biological systems are labelled
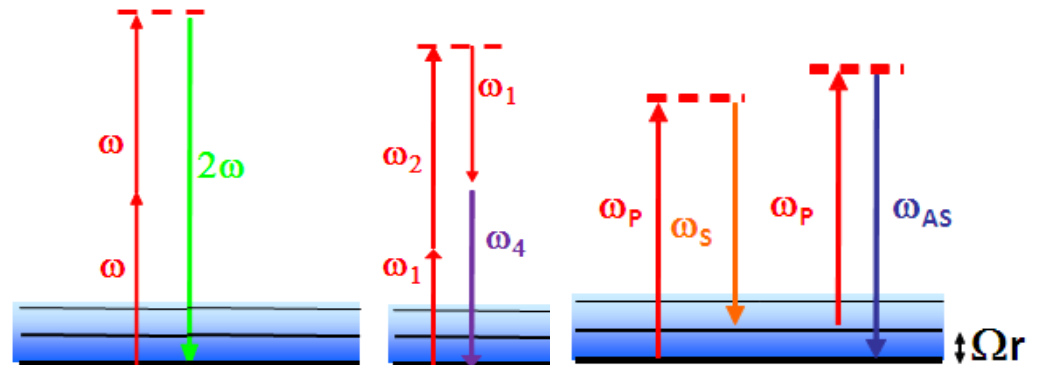
- In-depth detection in tissues
- No labelling

Nonlinear optics regime
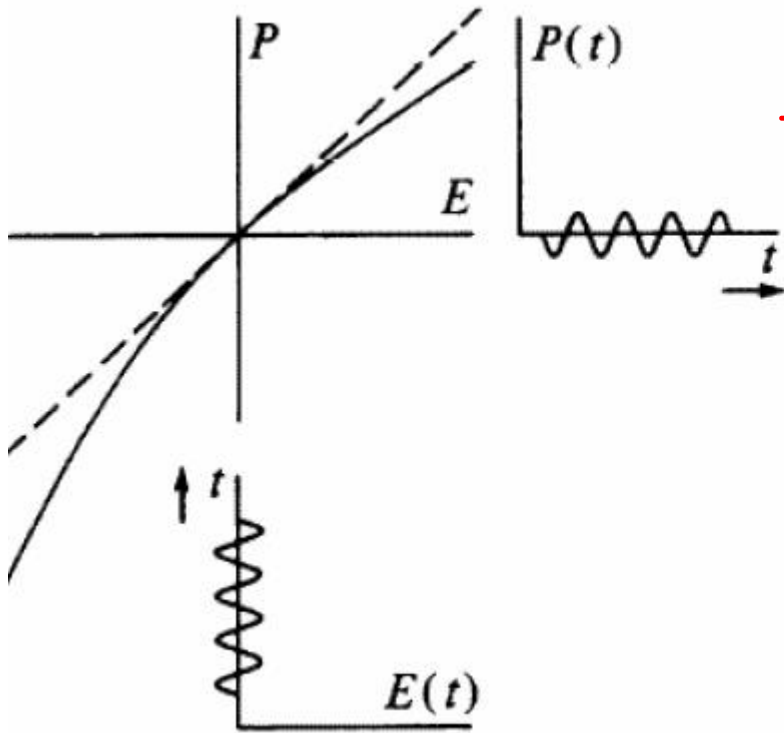
Linear regime

Non Linear regime

$$x(\omega) = x^{(1)}(\omega)$$
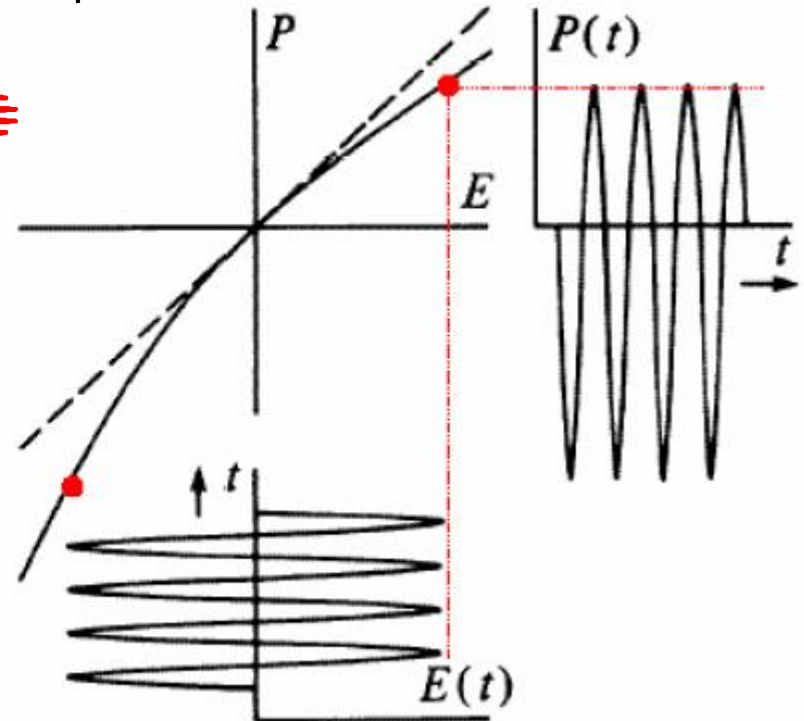
$$\mathbf{P}(\omega) = \varepsilon_0 \chi^{(1)} \mathbf{E}$$

$$x(\omega) = x^{(1)}(\omega) + x^{(2)}(\omega) + ...$$

$$\mathbf{P}(\omega) = \varepsilon_0 (\chi^{(1)} \mathbf{E} + \chi^{(2)} \mathbf{E} : \mathbf{E} + \chi^{(3)} \mathbf{E} : \mathbf{E} : \mathbf{E} + ...)$$

$\chi^{(n)}$ non linear suceptibility tensors

37

SHG and THG Microscopy imaging
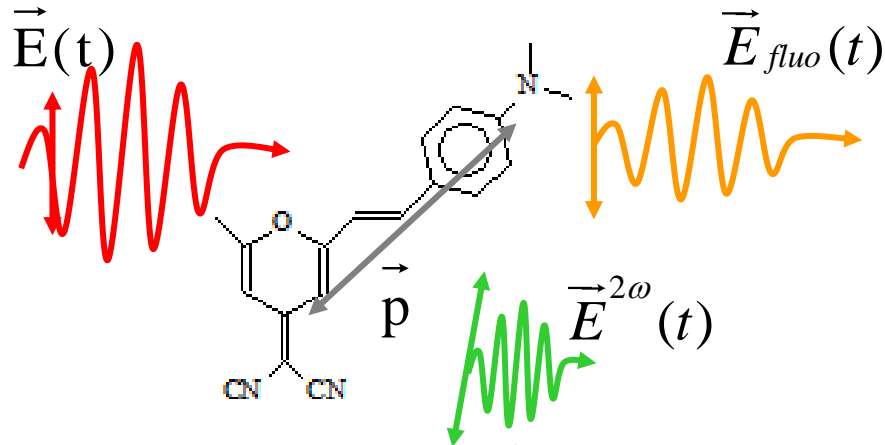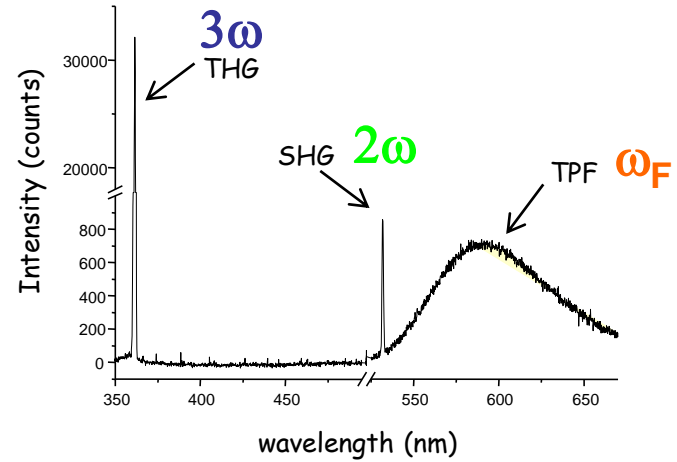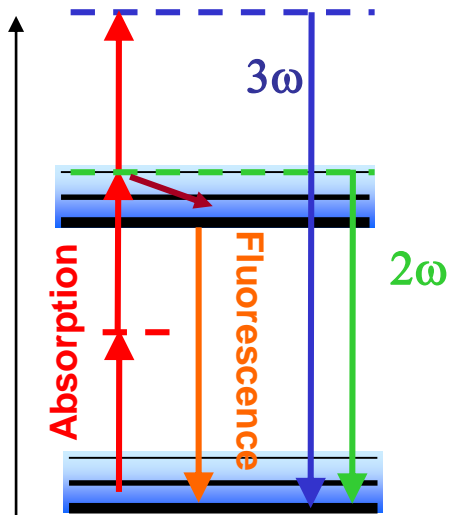
$$\vec{P}^{2\omega} = \chi^{(2)} : \vec{E}^{\omega} \vec{E}^{\omega}$$

$$\vec{P}^{3\omega} = \chi^{(3)} : \vec{E}^{\omega} \vec{E}^{\omega} \vec{E}^{\omega}$$

Is SHG efficient enough for microscopy imaging?

$$\boldsymbol{P}^{SHG} = \chi^{(2)}(2\omega; \omega, \omega) : \boldsymbol{E}^{\omega}\,\boldsymbol{E}^{\omega}$$

SHG requires non-centrosymmetry

SHG from a molecule to an ensemble

$$\mathbf{p}^{SHG} = \beta(2\omega; \omega, \omega) : \mathbf{E}^{\omega}\mathbf{E}^{\omega}$$

Single molecule response

$$p_i^{SHG} = \sum_{jk} \beta_{ijk} E_j^{\omega} E_k^{\omega}$$

Typically

$$\beta = 10^{-48} \text{ to } 10^{-38} \text{ m}^4/\text{V}$$

$$\beta_{zzz}(2\omega; \omega, \omega)$$

$$= \frac{3\,\mu_{01}^z\,(\mu_{11}^z - \mu_{00}^z)\,\mu_{01}^z}{2\,(\hbar\omega_0)^2} \cdot \frac{\omega_0^4}{(\omega_0^2 - 4\omega^2)(\omega_0^2 - \omega^2)}$$

involves $\boldsymbol{\mu_{01}} \sim\, <\boldsymbol{\psi_0(r).\,r.\,\psi_1(r)}>$

40
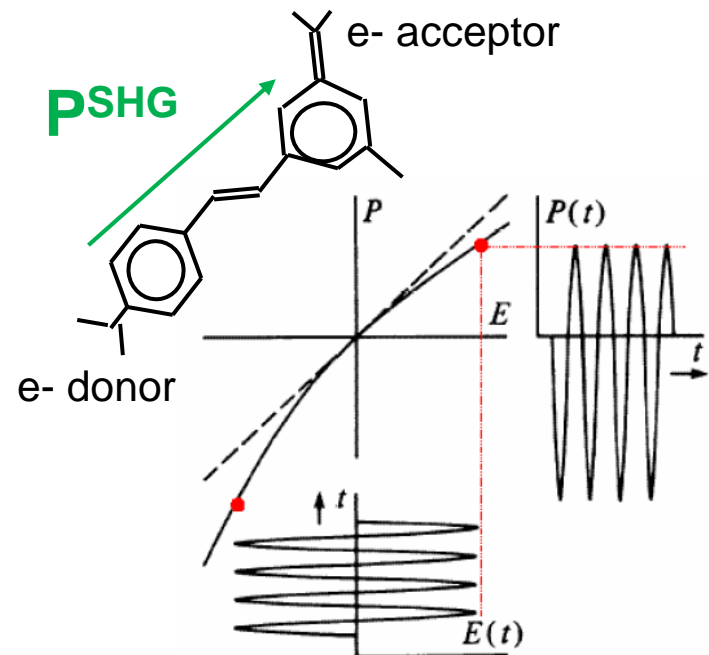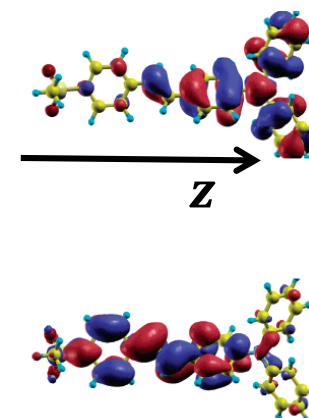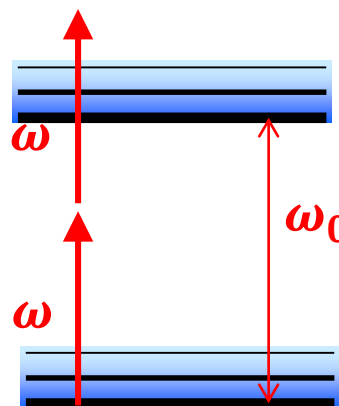
SHG from a molecule to an ensemble
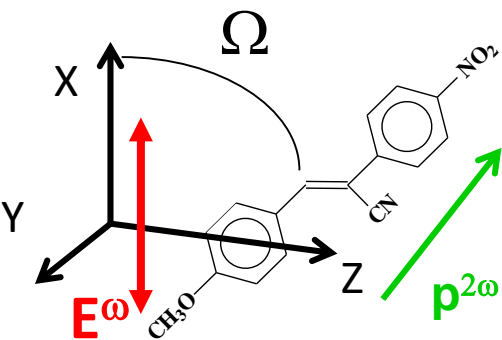
$$\mathbf{p}^{SHG} = \beta(2\omega; \omega, \omega) : \mathbf{E}^{\omega}\mathbf{E}^{\omega}$$

$$p_i^{SHG} = \sum_{jk} \beta_{ijk} E_j^{\omega} E_k^{\omega}$$

Single molecule response

Typically

$\beta = 10^{-48}$ to 10^{-38} m^4/V

$\beta_{zzz}(2\omega; \omega, \omega)$,
$\beta_{zxx}(2\omega; \omega, \omega), \beta_{zyy}(2\omega; \omega, \omega)$

involves $\boldsymbol{\mu_{0n}} \sim <\boldsymbol{\psi_0(r). r. \psi_n(r)}>$

41

SHG from a molecule to an ensemble

$$\mathbf{p}^{SHG} = \beta(2\omega;\omega,\omega) : \mathbf{E}^\omega \mathbf{E}^\omega$$

Single molecule response

$$p_I^{SHG}(\Omega) = \sum_{JK} \beta_{IJK}(\Omega) \, E_J^\omega E_K^\omega$$

Ensemble response : coherent in-phase oscillation

$$P_I^{SHG} = N \int_\Omega \; p_I^{SHG} f(\Omega) \, d\Omega$$

$$I_I^{SHG} = \left| P_I^{SHG} \right|^2 = \left| \sum_{JK} \chi_{IJK}^{(2)} E_J^\omega E_K^\omega \right|^2$$

$$I_I^{SHG} = N^2 \cdot C \cdot \sigma^{SHG} \cdot (I^\omega)^2$$
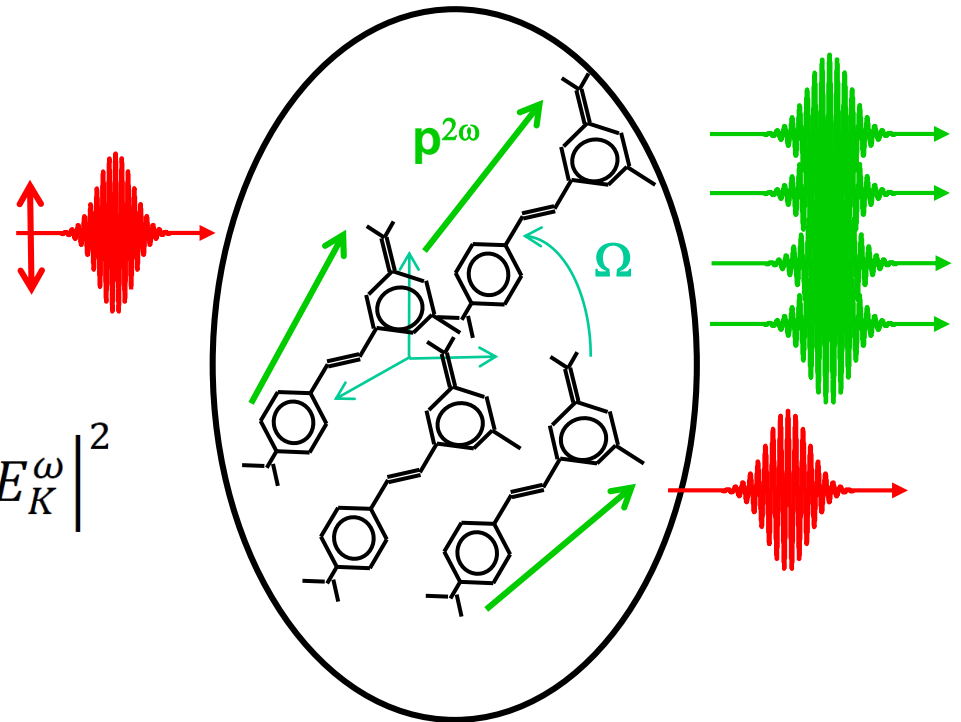
N molecules : sum of dipoles/radiated fields (coherent process) 42

Nonlinear coherent effects : efficiency?
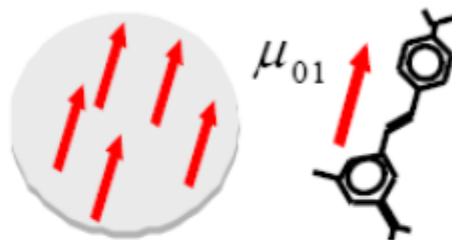
Emission rate

$$I_I^{2-ph} = N \cdot \Phi_f \cdot C \cdot \sigma^{(2)} \cdot (I^\omega)^2$$

$$I_I^{SHG} = N^2 \cdot C \cdot \sigma^{SHG} \cdot (I^\omega)^2$$

$$\sigma^{2PA} \approx 10^{-49} \ cm^4 s \ photon^{-1}$$

$$\sigma^{SHG} \approx 10^{-53} \ cm^4 s \ photon^{-1}$$

1 molecule : 1000 – 10000 ph/s

1 molecule : 0.0001 – 0.01 ph/s
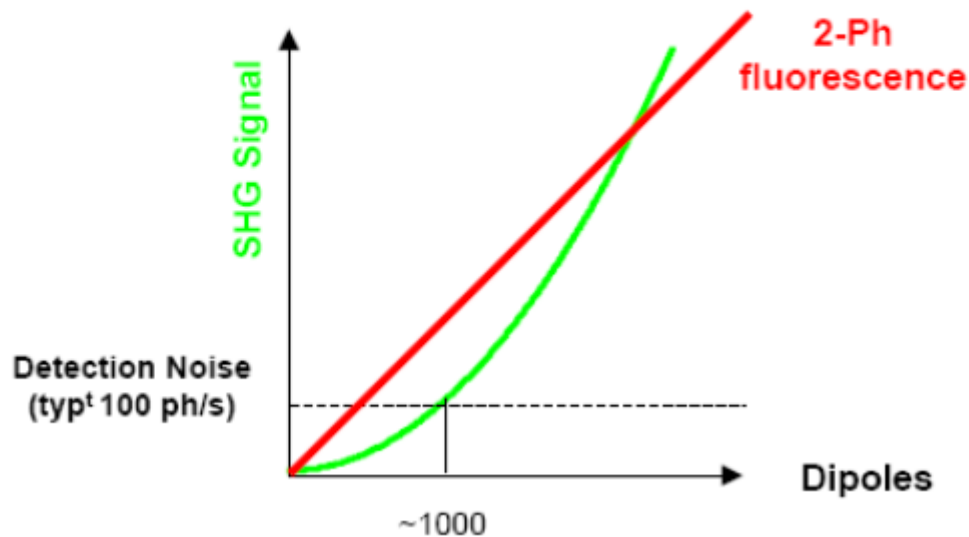
$\beta \sim 10^{-38} \ m^4/V$

$I^\omega \sim 10^{24} \ ph/s/cm^2$

10 nm **molecular nanocrystal** ~1000 dipoles

43

S. Brasselet et al. PRL (2004)

SHG and THG Microscopy imaging

SHG excitation / radiation in a microscope

$$\mathbf{p}^{2\omega}(\Omega, \mathbf{r}) = \beta(2\omega; \omega, \omega) : \mathbf{E}^\omega \mathbf{E}^\omega$$
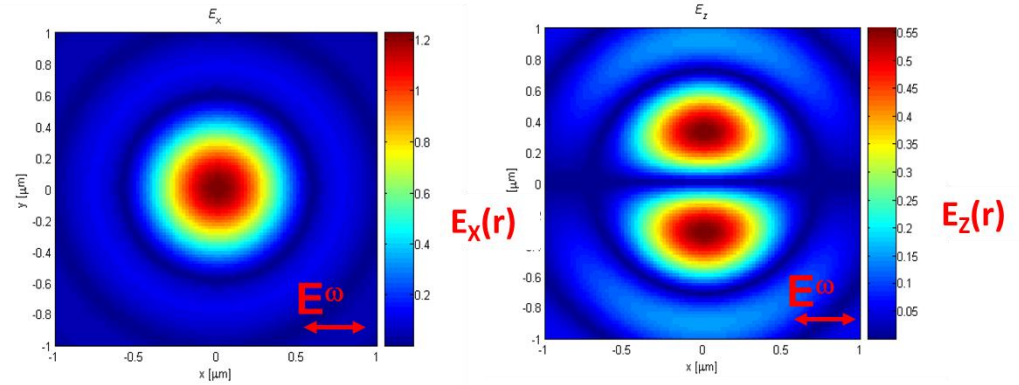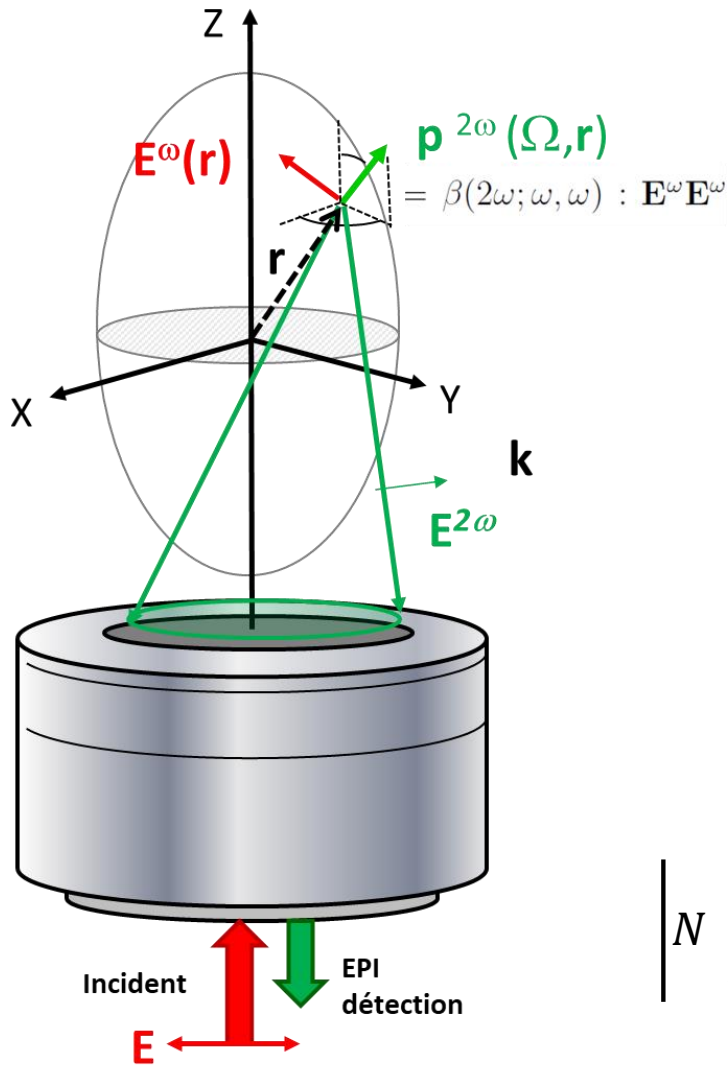
Coherent addition:

$$I_u^{SHG} =$$

$$\left| N \int_{NA} \int_V \int_\Omega E_u^{SHG}(\Omega, \mathbf{r}, \mathbf{k}) \, f(\Omega) \, d\Omega \, \mathrm{d}\mathbf{r} \, \mathrm{d}\mathbf{k} \right|^2$$

45

Phase matching effects in SHG imaging

L : Dimension of the
 focal volume
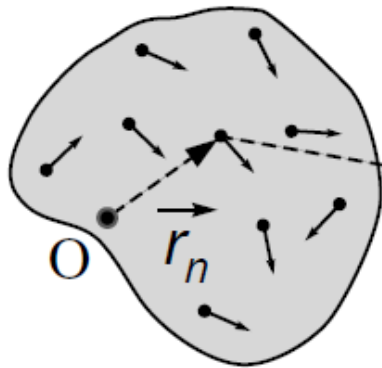
Propagation towards detector
 or microscope objective

$$\vec{R}_n$$

$$\vec{E}_n^{2\omega} \left(t - \frac{R_n}{c} \right)$$

O $\vec{r}_n$
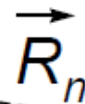
M

$$I^{SHG} \propto |\beta : \mathbf{E}_0 \vec{E}_0|^2 \sum_{n,n'} \exp\left(i(2\mathbf{k}_\omega - \mathbf{k}_{2\omega}) \cdot (\mathbf{r}_n - \mathbf{r}_{n'})\right)$$

$$\Delta \mathbf{k} = \mathbf{k}_{2\omega} - 2\mathbf{k}_\omega$$ Phase matching wave vector

SHG phase matching under tight focusing :

$$\Delta k = \Delta k^{SHG} + \Delta k^{Gouy}$$

Forward

Medium

Excitation volume

Small object

Epi

$\vec{k}^{\omega}$

KTP nanocrystal simulation:

k_ω

10nm

100nm

-40 -20 0 20 40
z nm

-200 0 200
z nm

Aprox. : radiation in vacuum

Forward $\left|\overrightarrow{\Delta k}^{SHG}\right| = 0 + \dfrac{2.\pi}{2\lambda}$

$\vec{k}^{2\omega}$

$\overrightarrow{\Delta k}^{SHG}$

Fwd efficient for
r < 2λ ~2μm

Object of dimension « r »

$\vec{k}^{2\omega}$

Epi

$\left|\overrightarrow{\Delta k}^{SHG}\right| = \dfrac{8\pi}{\lambda} + \dfrac{2.\pi}{2\lambda} = \dfrac{9\pi}{\lambda}$

$\overrightarrow{\Delta k}^{SHG}$

Epi vanishes if

$$r > \dfrac{\lambda}{4} \approx 250\,\text{nm}$$

47
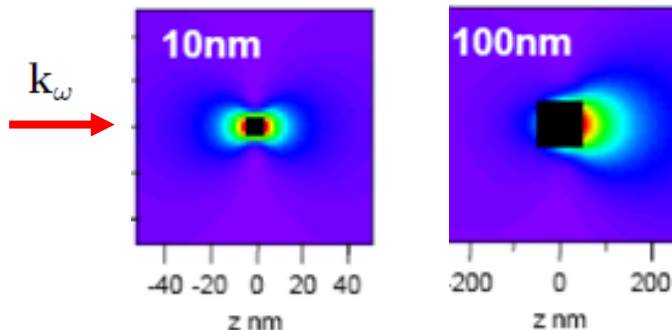
SHG imaging in biological molecules (collagen)
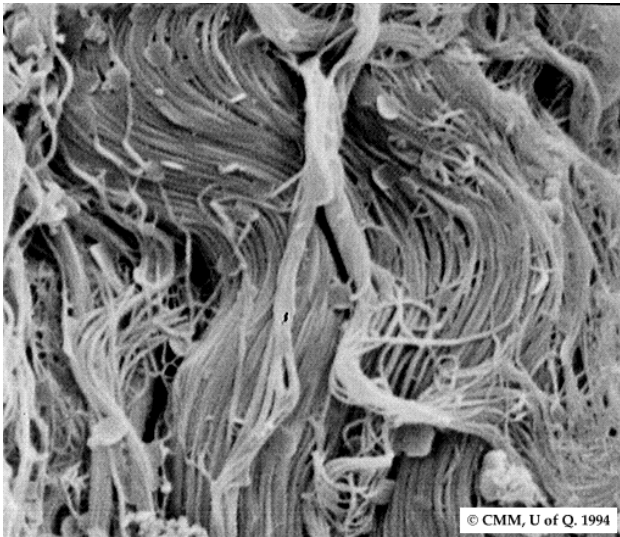
Collagen (EM)

Collagen I is non-centrosymmetric

banding pattern of collagen

collagen fiber 4-10 μ

small fiber bundle

fibrils

60 μm
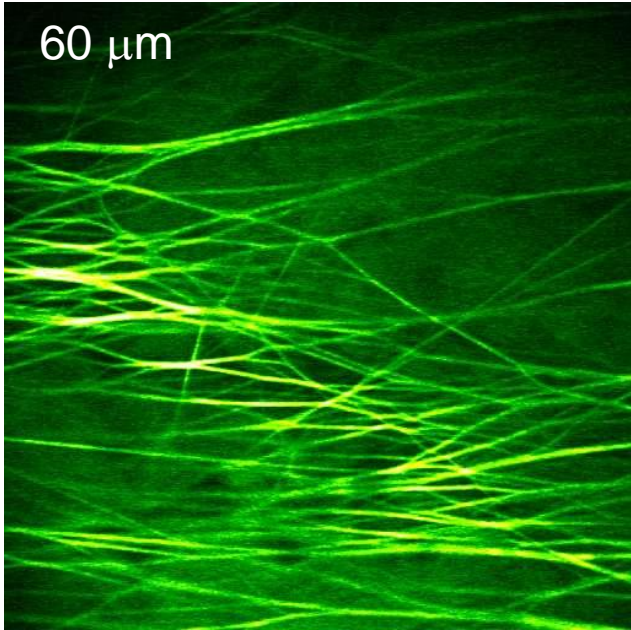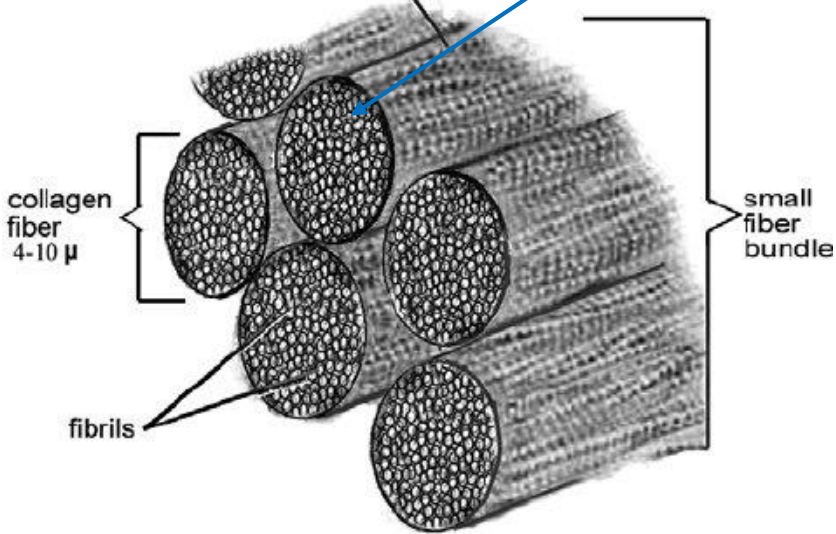
Univ. Exeter, rat tail tendon

SHG fwd image of collagen in a muscle tissue

48

SHG imaging in biological molecules (collagen)
Consequence of phase matching

EPI SHG image   FWD SHG image
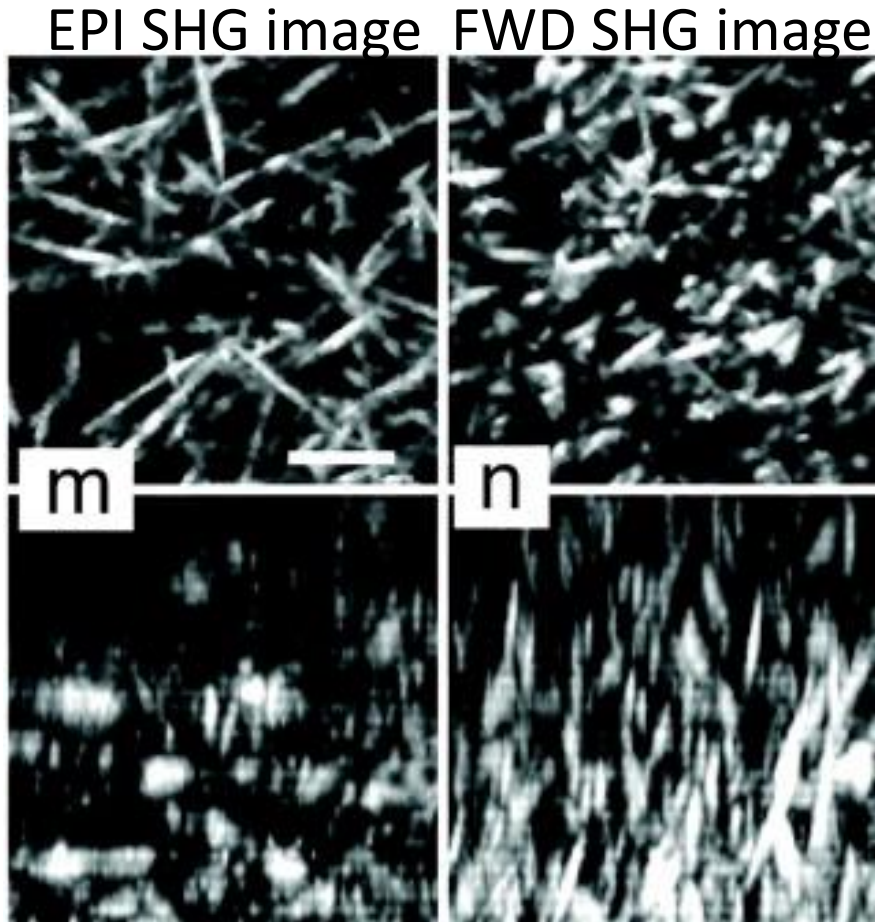
Lateral
projection
(X,Y)

Axial
projection
(Z,X)

Forward
detection

Dichroic
Beamsplitter

EPI detection

scale bar, 5 µm

Collagen gel (10-µm-thick) SHG imaging
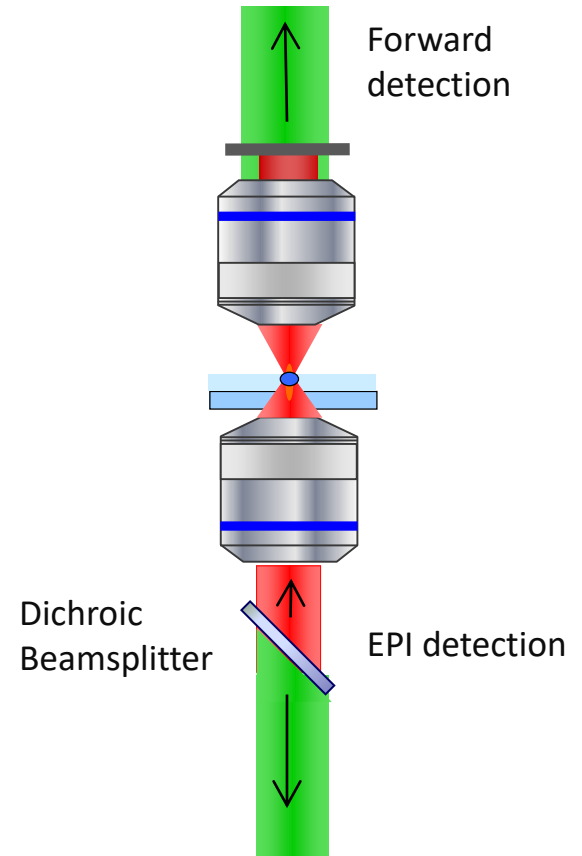
Second Harmonic Generation (SHG) imaging in tissues

Epi

Sample
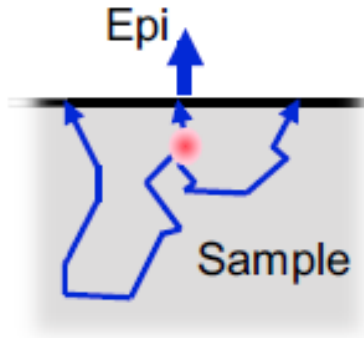
Imaging the collagen structure
in the tissues thanks to backscattering

SHG | TPEF | Combined

Normal Stroma

Neoplastic Stroma

30μm
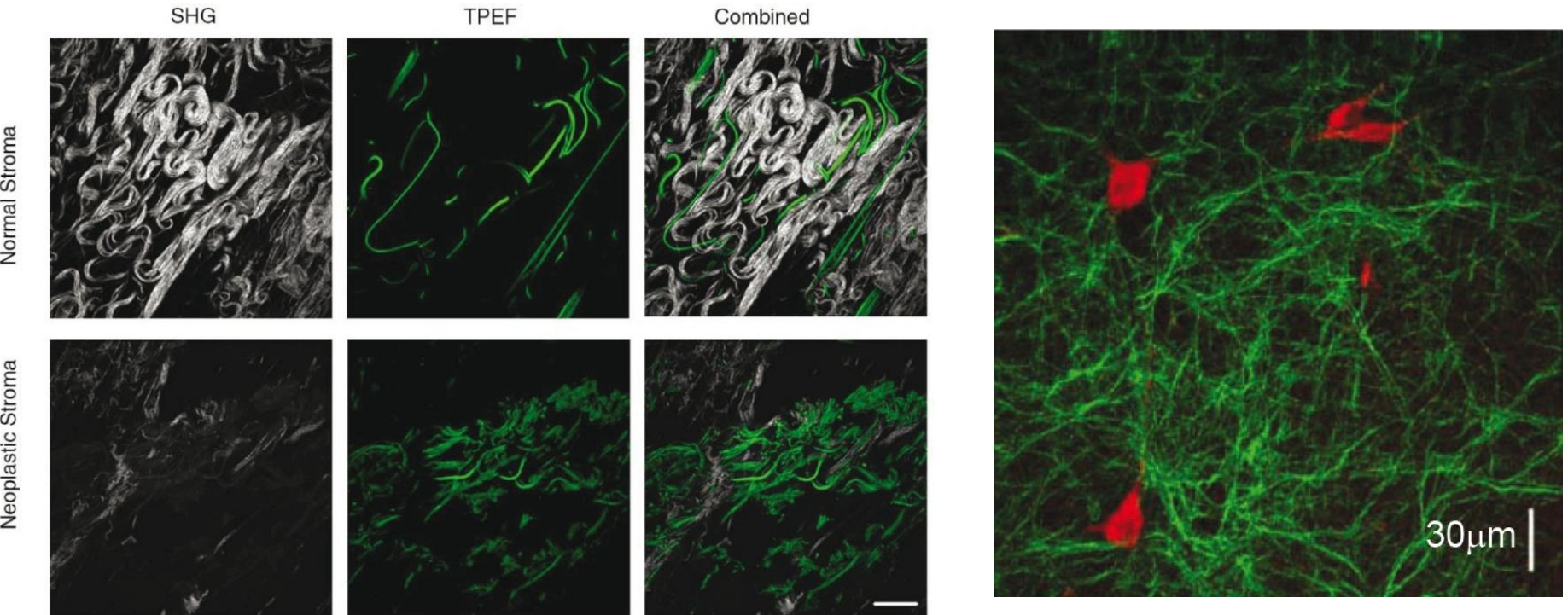
Collagen in the stroma
C. Zhuo et al. J. Biomed. Opt. (2010)

Artificial collagen gel
C. Olive et al. J. Biomed. Opt. (2010)

50

Third Harmonic Generation (THG) imaging

$$P^{THG}(3\omega) = \chi^{(3)}(3\omega; \omega, \omega, \omega): E^{\omega} E^{\omega} E^{\omega}$$

Low efficiency
No symmetry condition
Stringent phase matching conditions
THG sensitive to interfaces
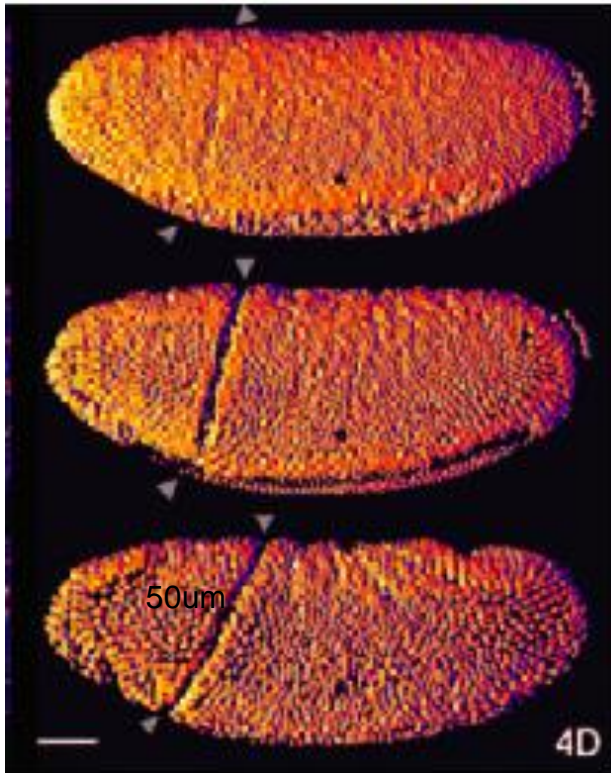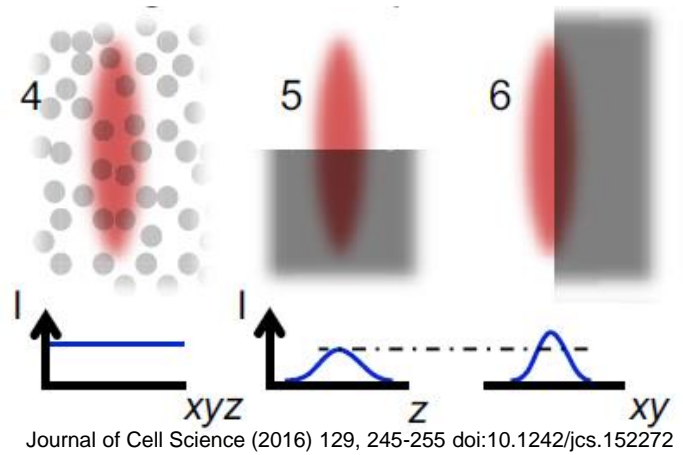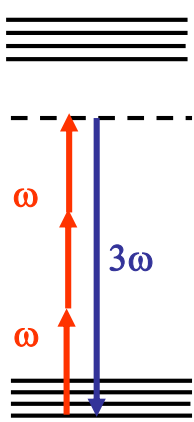
Detection of lipid bodies in the drosophila embryo
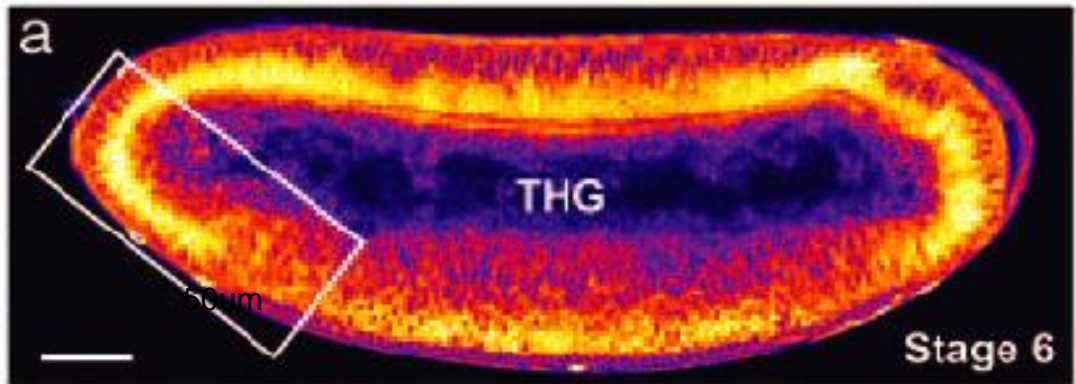
Intrinsic THG from lipid bodies Exc. 1.180um

E. Beaurepaire, LOB, Palaiseau, France

W. Supatto et al., PNAS (2005)

3D imaging of motion of gastrulation in embryos. Intrinsic TPF : in nuclei

Coherent Anti-Stokes Raman Scattering (CARS)

$$P^{CARS}(\omega_{AS}) = \chi^{(3)}\left(\omega_{AS}; \omega_p, \omega_p, -\omega_S\right) : E^{\omega_p}\, E^{\omega_p}\, E^{\omega_S*}$$

ω_p ω_S ω_p ω_{AS} $\updownarrow\ \Omega$

Generated frequency by frequency mixing :

$$\omega_{as} = \omega_p + \omega_p - \omega_s = 2\omega_p - \omega_s$$

Third order process

$$\chi^{(3)} = \frac{A_R}{\Omega_R - (\omega_p - \omega_s) + i\Gamma_R} + \chi^{(3)}{}_{NR}$$

ω_P

AntiStokes

ω_{AS}

ω_S

Stokes

Ω

Strong signal from a Raman – active band

3.1µm   2.9µm   6.6µm
99 GHz   102 GHz   45 GHz

if ω_p-ω_s = Ω : ω_{as} enhanced

52

Coherent Anti-Stokes Raman Scattering (CARS)

$$P^{CARS}(\omega_{AS}) = \chi^{(3)}\left(\omega_{AS}; \omega_p, \omega_p, -\omega_s\right):E^{\omega_p}\,E^{\omega_p}\,E^{\omega_s\,*}$$

Generated frequency by frequency mixing :

$$\omega_{as} = \omega_p + \omega_p - \omega_s = 2\omega_p - \omega_s$$

Third order process

$$\chi^{(3)} = \frac{A_R}{\Omega_R - (\omega_p - \omega_s) + i\Gamma_R} + \chi^{(3)}{}_{NR}$$

ω_p ω_S ω_p ω_{AS} Ω
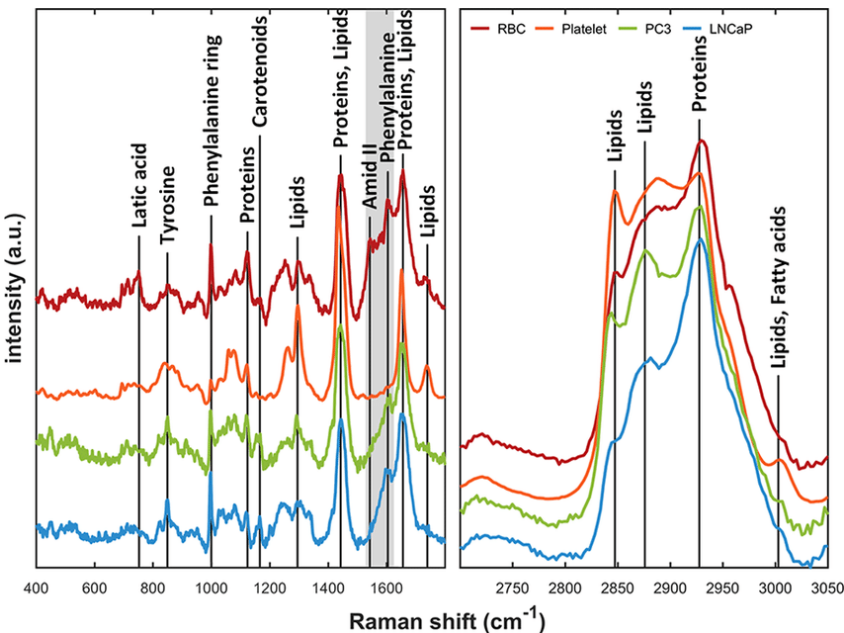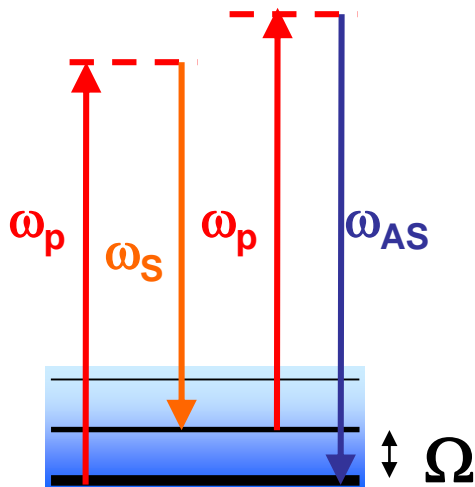
Strong signal from a Raman – active band
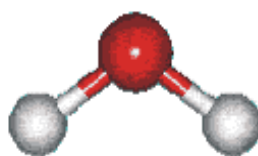
3.1μm
99 GHz

2.9μm
102 GHz

6.6μm
45 GHz

intensity (a.u.)

Latic acid
Tyrosine
Phenylalanine ring
Proteins
Carotenoids
Lipids
Proteins, Lipids
Amid II
Phenylalanine
Proteins, Lipids
Lipids

RBC   Platelet   PC3   LNCaP

Lipids
Lipids
Proteins
Lipids, Fatty acids

400 600 800 1000 1200 1400 1600 2750 2800 2850 2900 2950 3000 3050

Raman shift (cm^{-1})

W. Lee et al. Anal Chem 2018

53
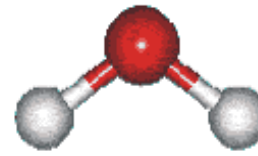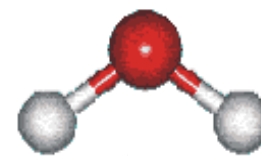
Coherent Anti-Stokes Raman Scattering (CARS)

$$\chi^{(3)} = \frac{A_R}{\Omega_R - (\omega_p - \omega_s) + i\Gamma_R} + \chi^{(3)}_{NR}$$

Coherent superposition of
two contributions
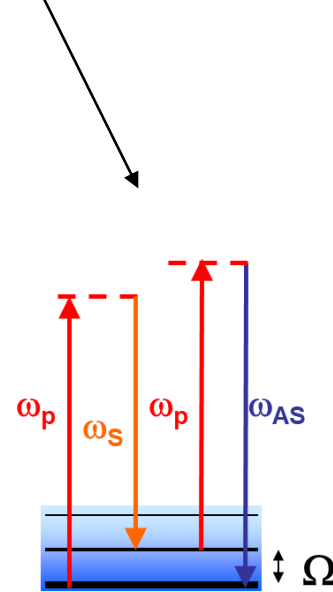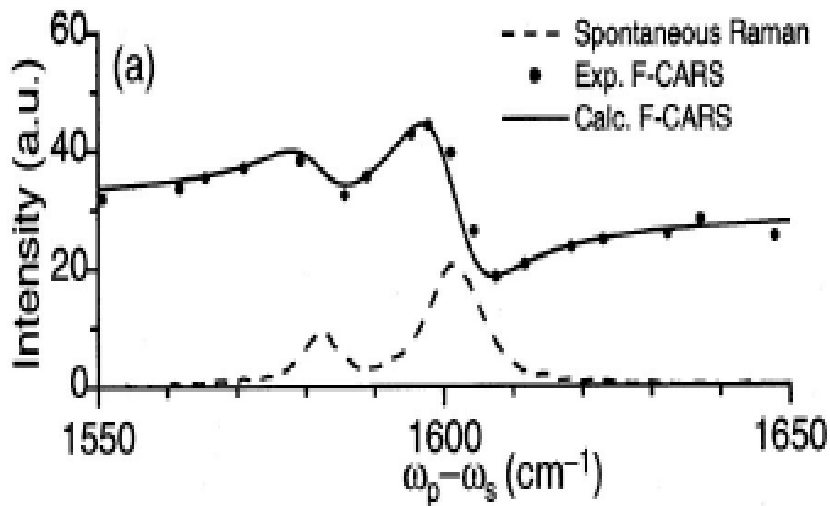
Resonant
vibrational
response
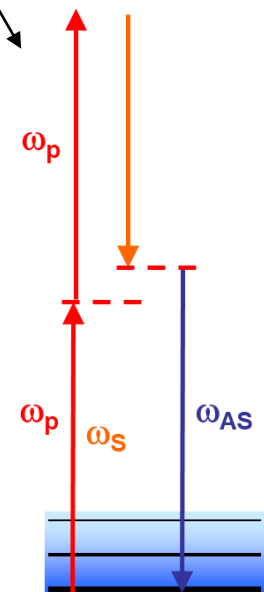
Nonresonant
electronic
response (FWM)

Cheng J. Opt. Soc. Am. B, 19, 1363 (2002)

CARS is a resonant process

$$I_{CARS} = |\chi_R^{(3)}(\omega_{as}):\mathbf{E}_p\mathbf{E}_p\mathbf{E}_S^* + \chi_{NR}^{(3)}(\omega_{as}):\mathbf{E}_p\mathbf{E}_p\mathbf{E}_S^*|^2$$

1003cm^{-1} →

Source: http://www.aist.go.jp

POLYSTYRENE
SDBSNO = 1957   (C$_8$H$_8$)   RM-01-00002 : 4579A.200M.GRAIN(NBS 706)

Polystyrene spontaneous **Raman** spectrum

Polystyrene **CARS** spectrum

← CARS resonance

Off-resonance →
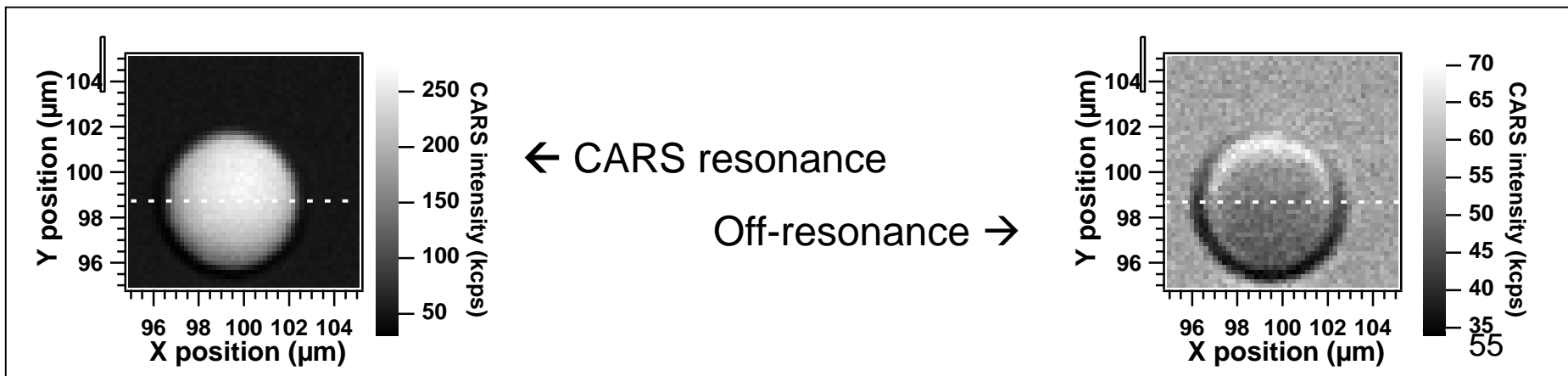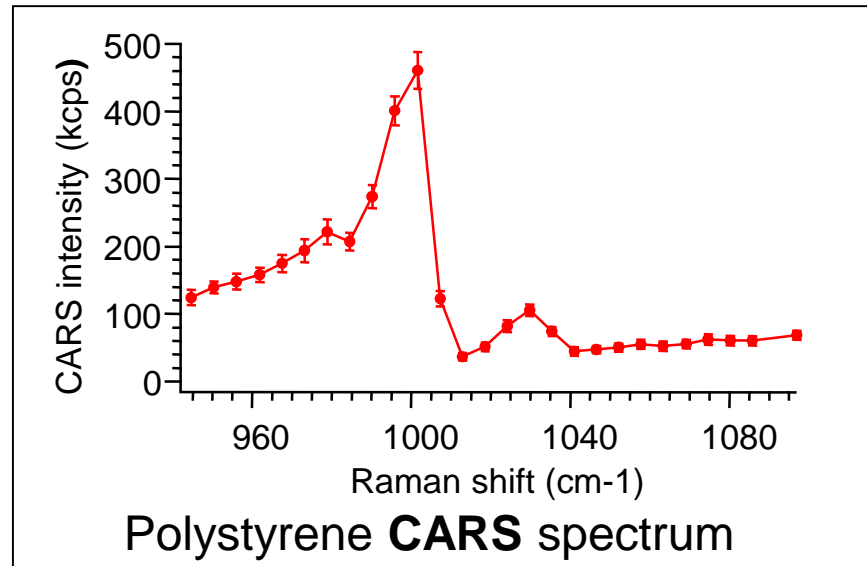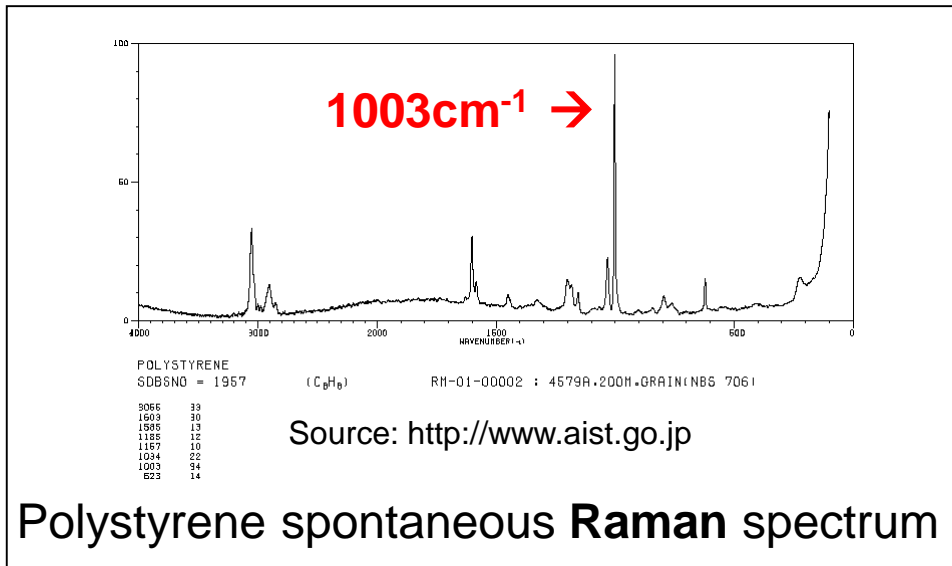
Coherent Anti-Stokes Raman Scattering (CARS) microscopy

Brustlein et al. , JBO 2011
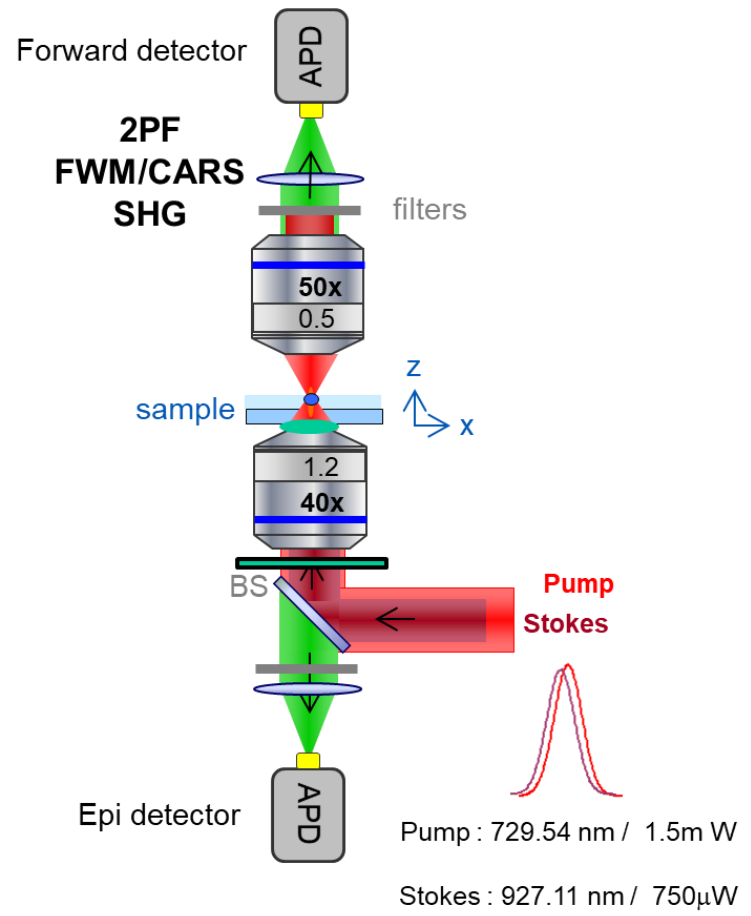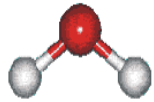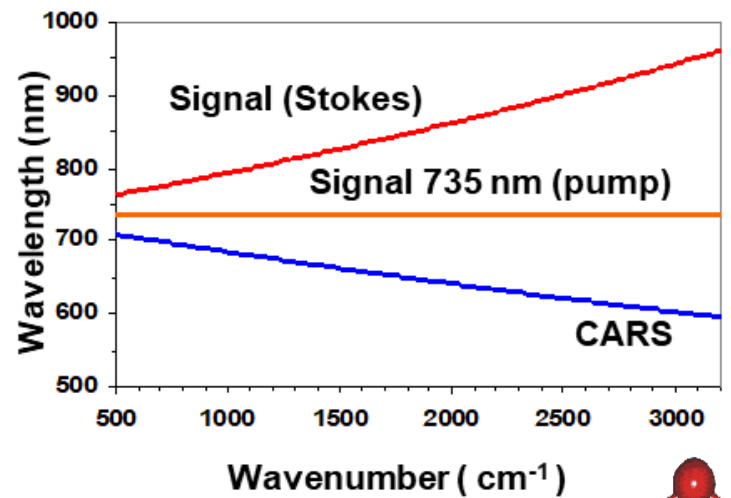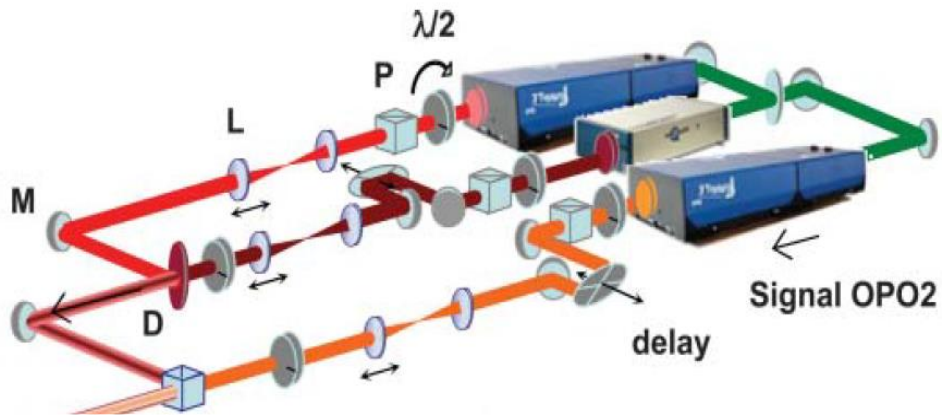
Multimodal imaging for cancer detection

Rat mammary tumor / S. Boppart lab

CARS (3050 cm^{-1})
AutoFluo2P
AutoFluo 3P
SHG
THG

Tu et al. Sc. Adv. 2017

57
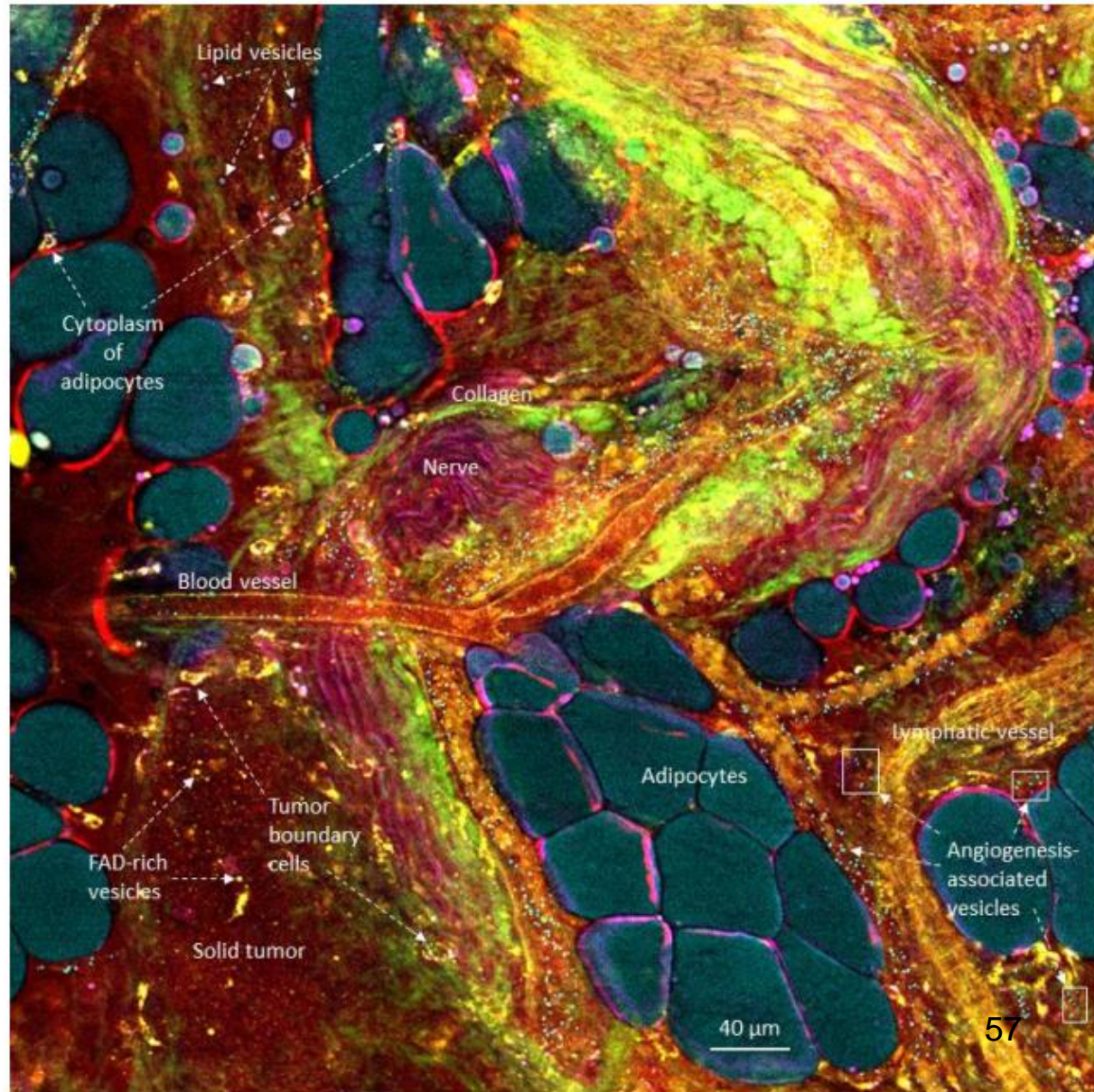
Multimodal imaging for neurosciences

CARS

Mouse spinal cord; Collab. F. Debarbieux INT Marseille
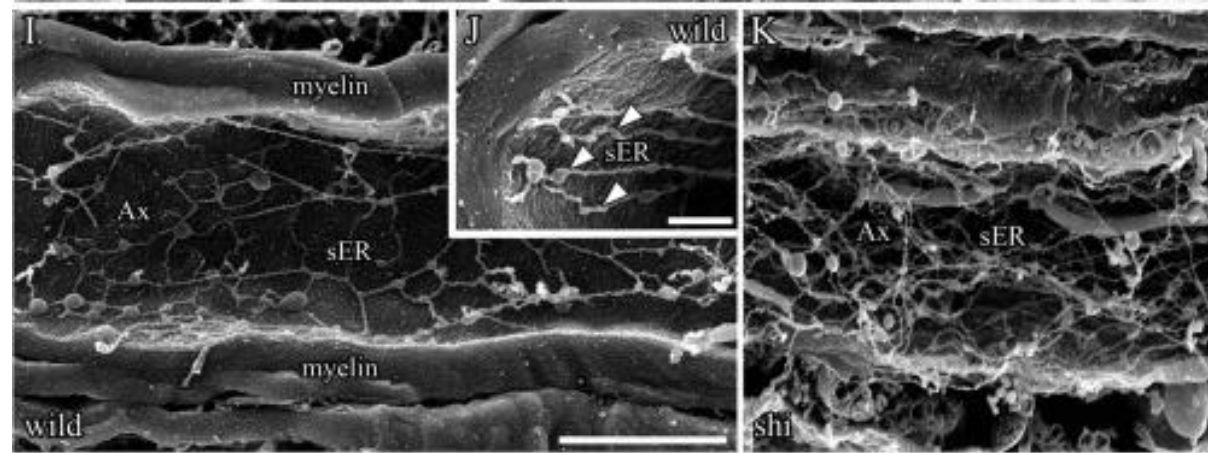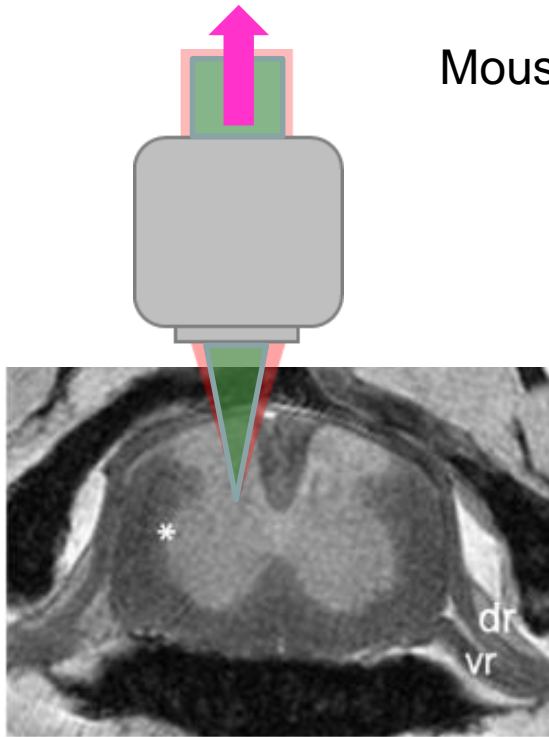
Myelin (SEM)

T. Nomura et al. Neurosci Res. 2013

Neuron

Lipid bilayer

Myelin sheath
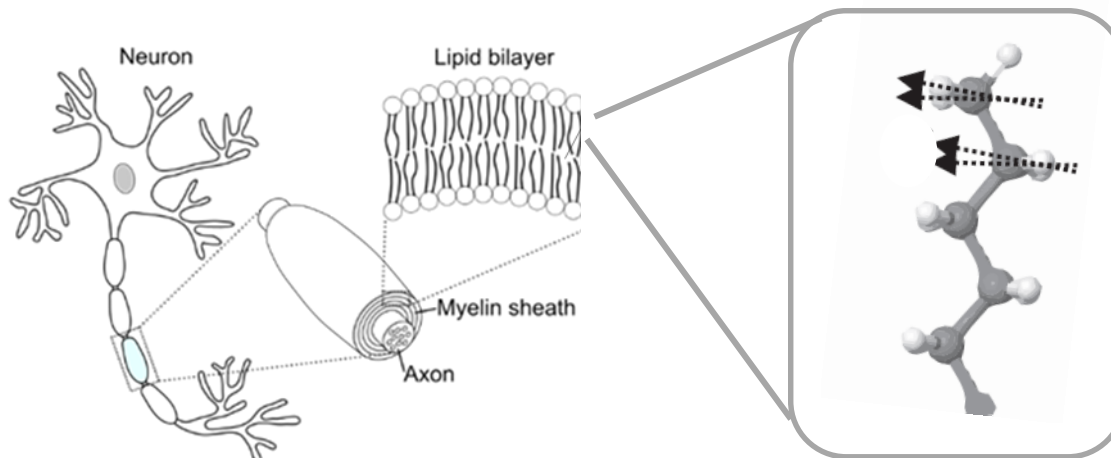
Axon

Myelin imaging in the mouse spinal cord

Collaboration F. Debarbieux (INT, Marseille, France)

Spinal cord

Myelin sheath

Lipids (70%)
Proteins (30%)
water

higheredbcs.wiley.com

D. Sherman, P. Brophy, 2005
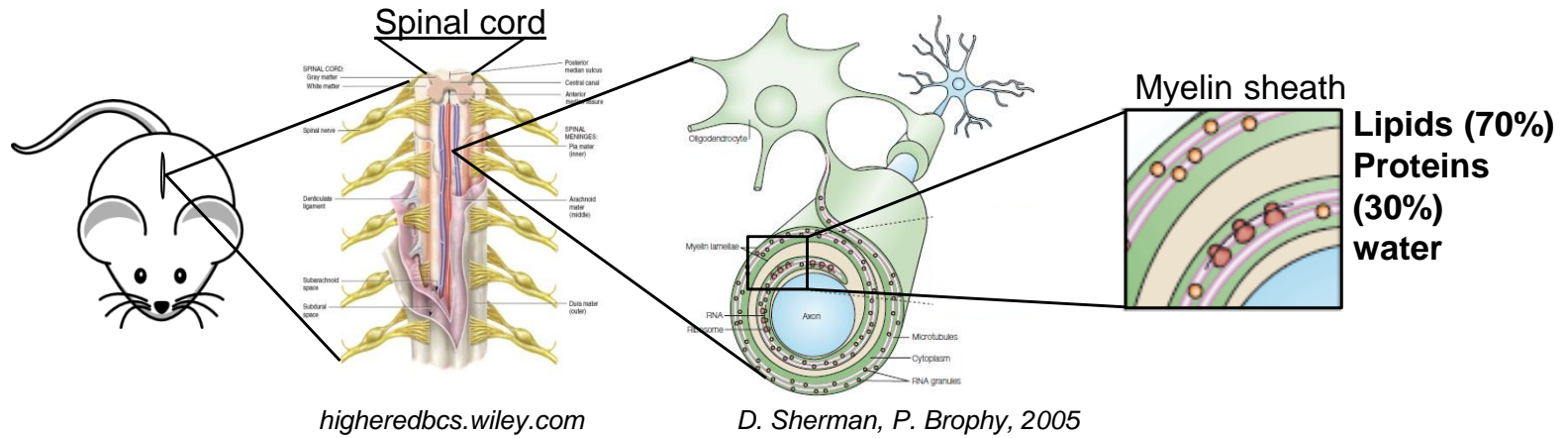
Myelin (CARS – CH2 stretch. vib.) Axons (TPEF - CFP)

10µm

10µm

10µm
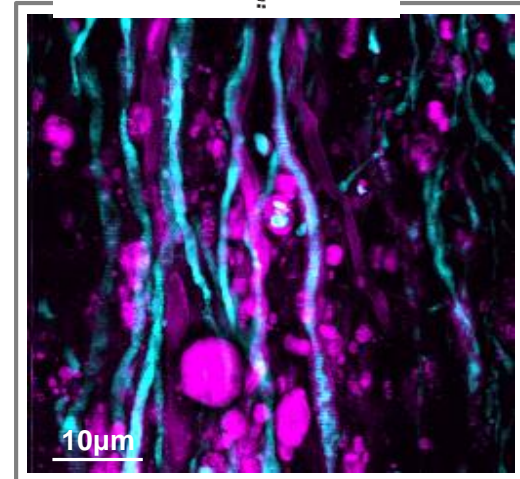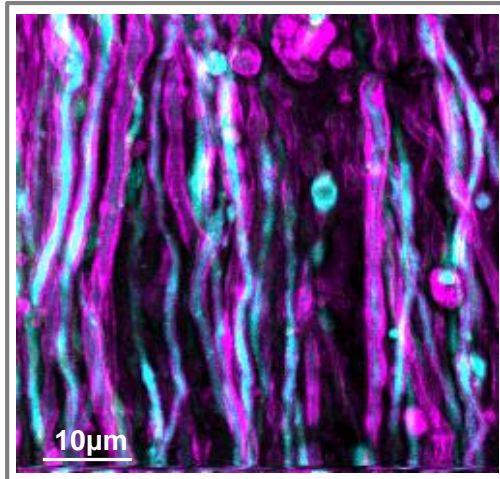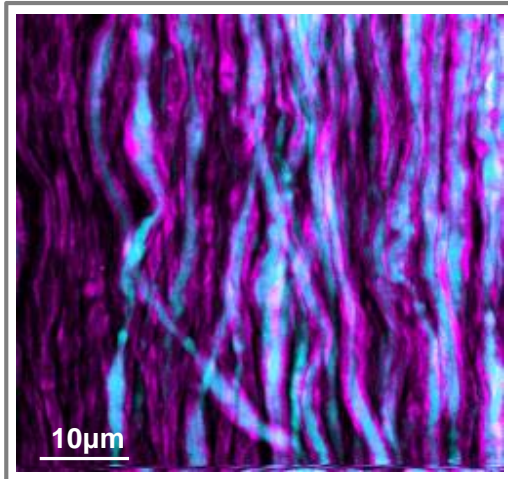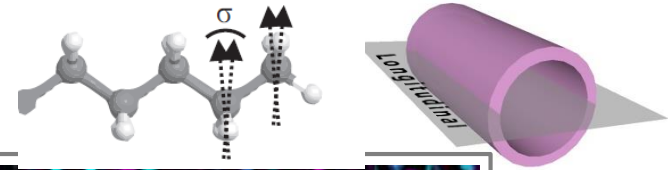
Progression of the EAE disease

P. Gasecka et al., Biophys. J. (2017)

CARS imaging in fixed mouse spinal cords : depth 30-50 µm

Myelin (CARS, 2845 cm^{-1} CH$_2$)   Axons (2PF, CFP)

Immune cells (YFP, GFP)

100µm

5µm

ωs ωf ωas

ωp

2PF   CARS

60

P. Gasecka et al., Biophys. J. (2017)
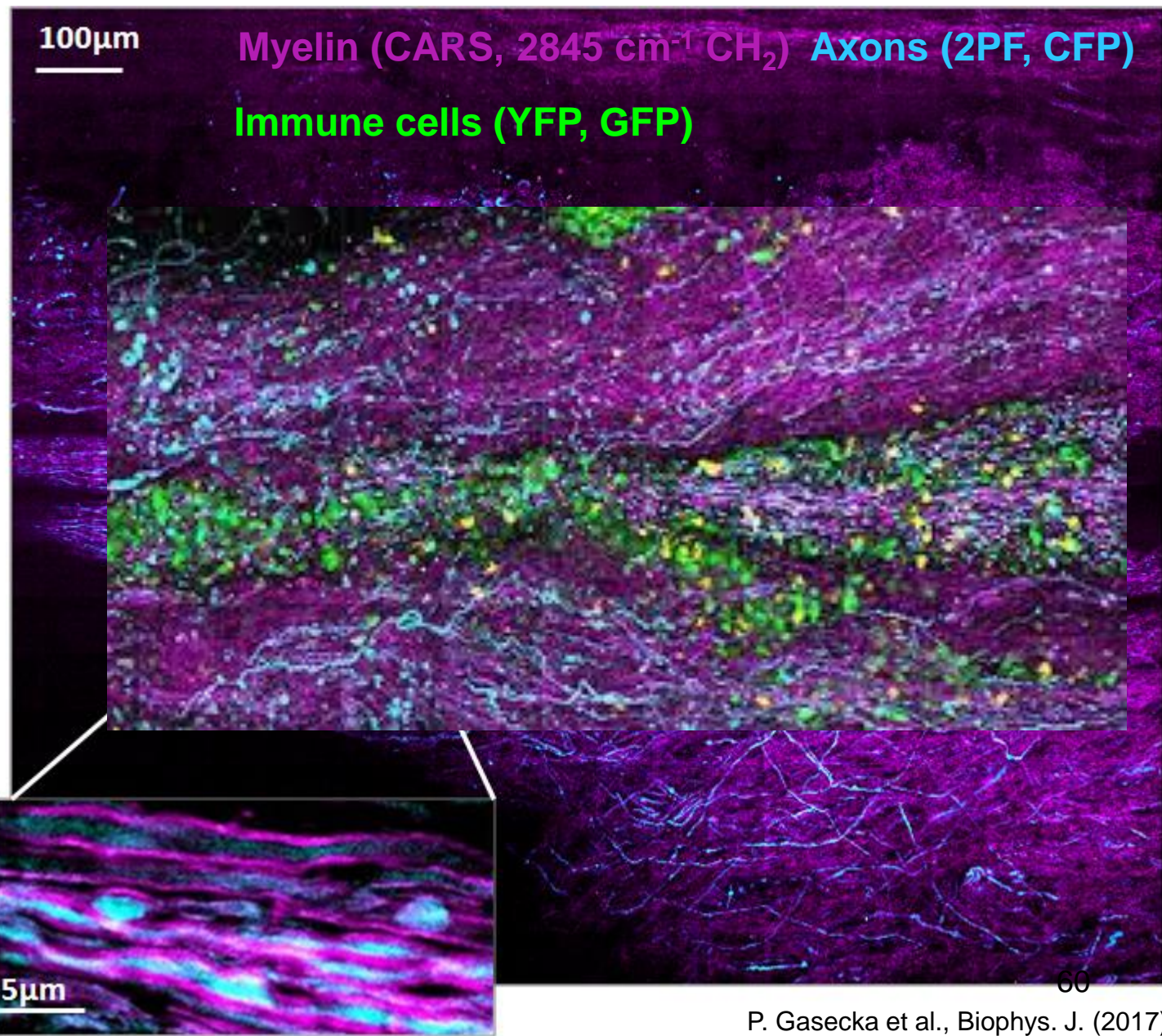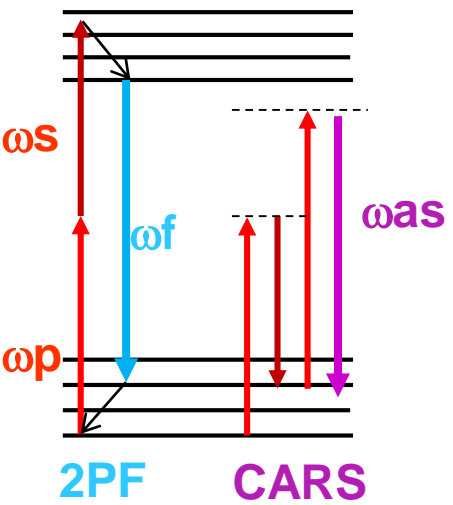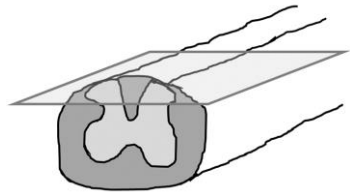
Short pulses and nonlinear microscopy

Short pulses and nonlinear microscopy
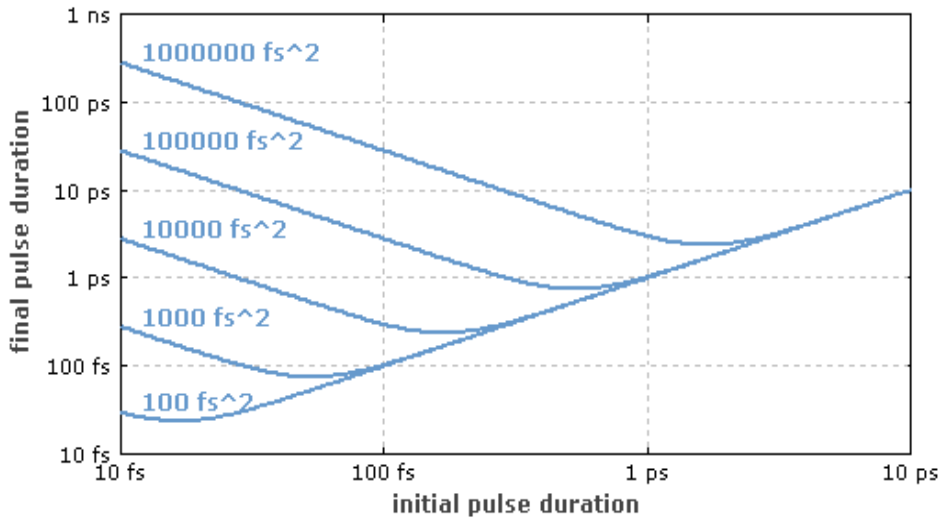
At 800nm :
Fused silica : GVD = 36.11 fs^2/mm
BK7 : GVD = 50.60 fs^2/mm
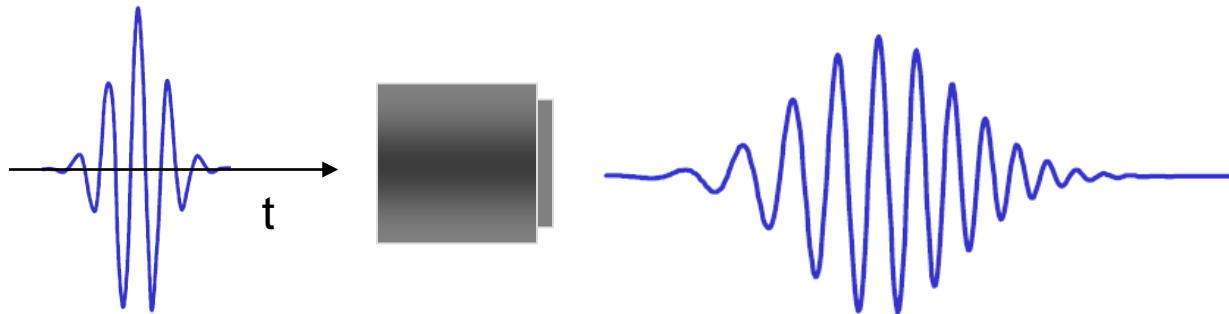
A microscope objective : typically 3000 fs^2

Short pulses and nonlinear microscopy
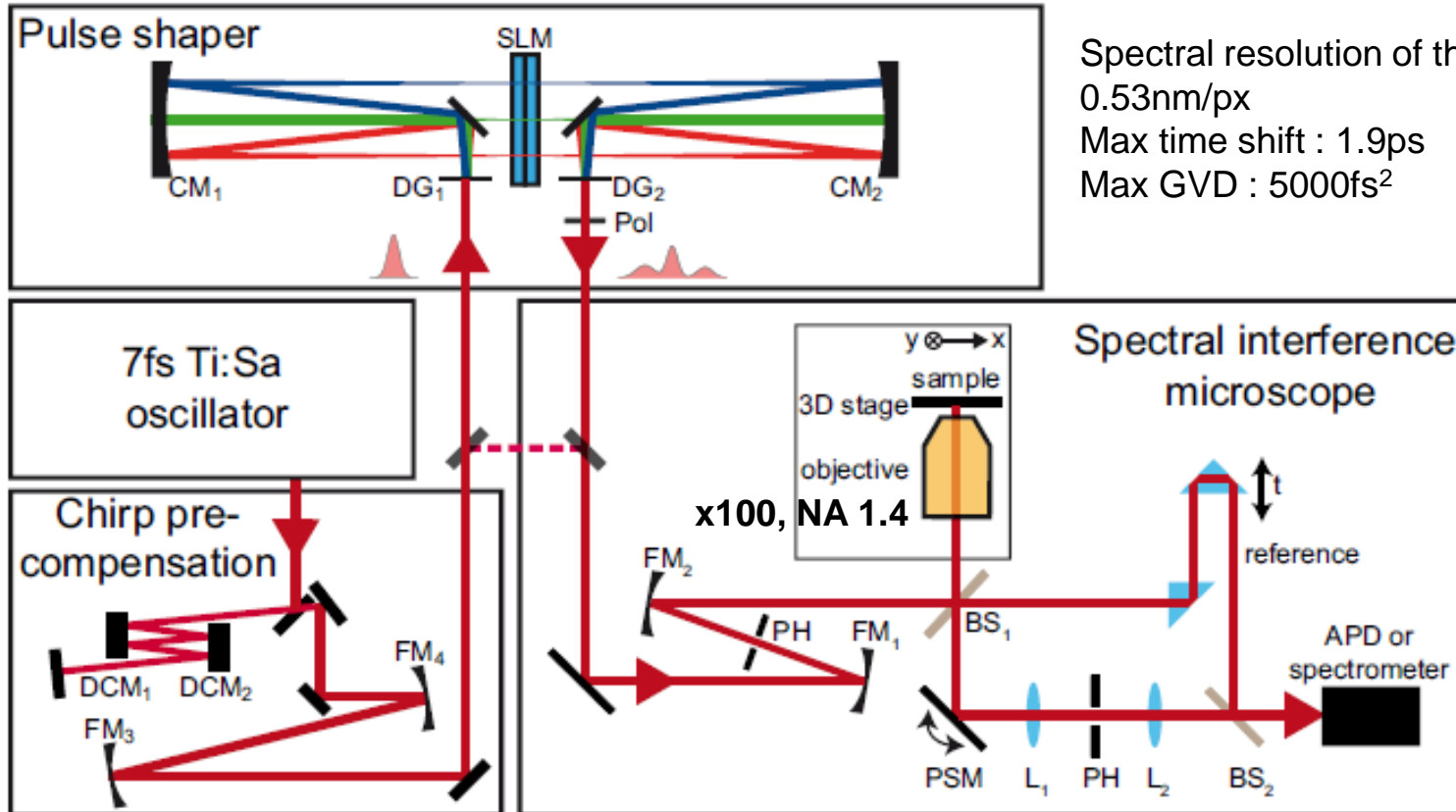
Spectral resolution of the shaper :
0.53nm/px
Max time shift : 1.9ps
Max GVD : $5000fs^2$

(sub-10fs pulses, M Pawlowska et al. OE 2014)

Short pulses and nonlinear microscopy

Distorsion occurs both in space and time (space-time coupling)

Nanoscatterers:
gold nanorods (34 nmx25 nm)
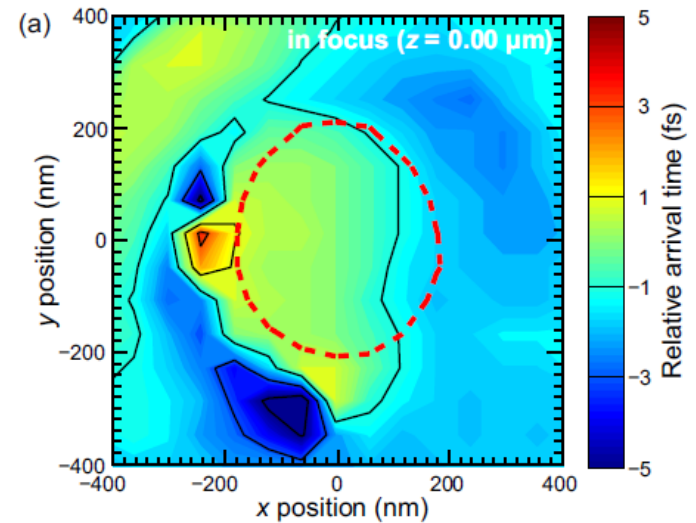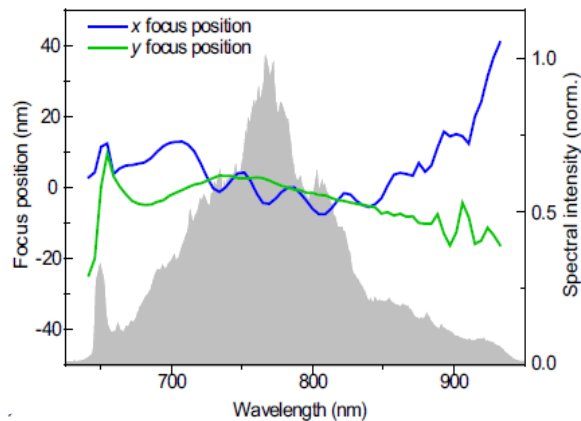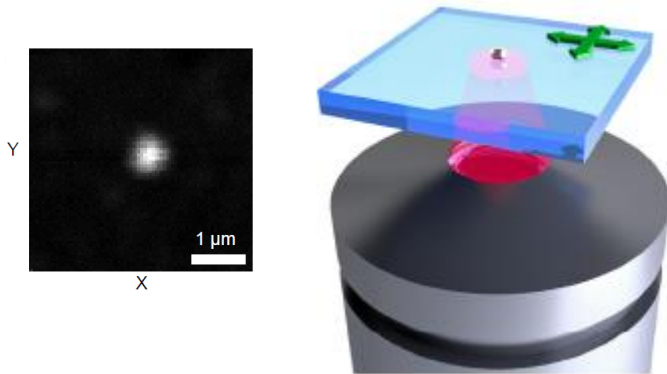
After pulse
shaping
optimization

M Pawlowska et al. OE 22 (2014)

Optimizing spectral conditions in 2P processes

coherent control for selective nonlinear microscopy

Two-photon excitation process

2nd Order Time-Dependent Perturbation Analysis

2P excitation :

$$a_f(\infty) \propto \int E^2(t) \exp(i\omega_{fg}t)dt$$

$$a_f(\infty) \propto \int E(\omega)E(\omega_{fg} - \omega)d\omega$$

$|f\rangle$

$|g\rangle$
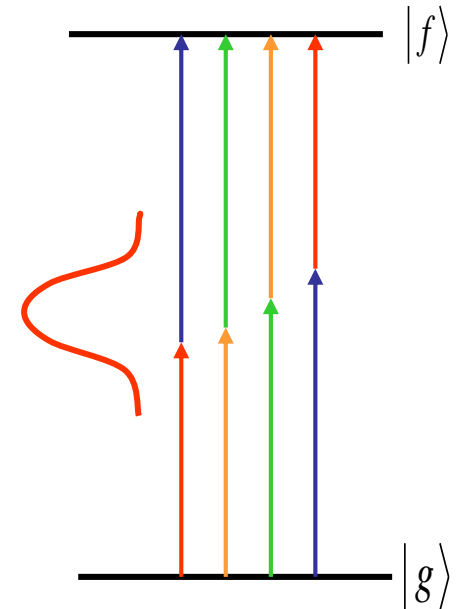
Many combinations of the frequency pairs determine the total excitation

Two-photon excitation process

$$a_f(\infty) \propto \int d\delta\omega\, E(\omega_0 + \delta\omega)E(\omega_0 - \delta\omega) =$$

$$= \int d\delta\omega\, |E(\omega_0 + \delta\omega)||E(\omega_0 - \delta\omega)| \cdot e^{i[\Phi(\omega_0 + \delta\omega) + \Phi(\omega_0 - \delta\omega)]}$$

Transition probability is controlled by the spectral phase of the incident field

At ω_0 : antisymmetric phase is unaffected by transition probability

Transform limited pulses are the most efficient :

$$\omega_0 = \omega_{fg}/2$$

$|f\rangle$

$|g\rangle$
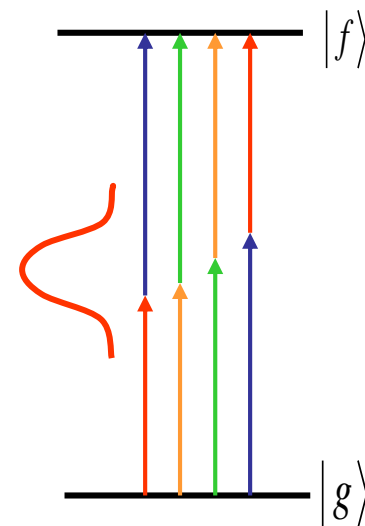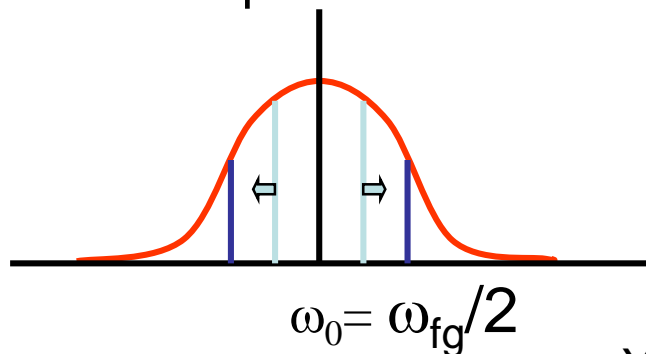
Phase coherent control of 2P processes in molecular systems

$$\text{TPF} \propto \int \sigma^{(2)}(\omega) \left| \int E\left(\frac{\omega}{2} - \Delta\right) E\left(\frac{\omega}{2} + \Delta\right) d\Delta \right|^2 d\omega$$

TPA large spectrum

2-photon excitation spectrum
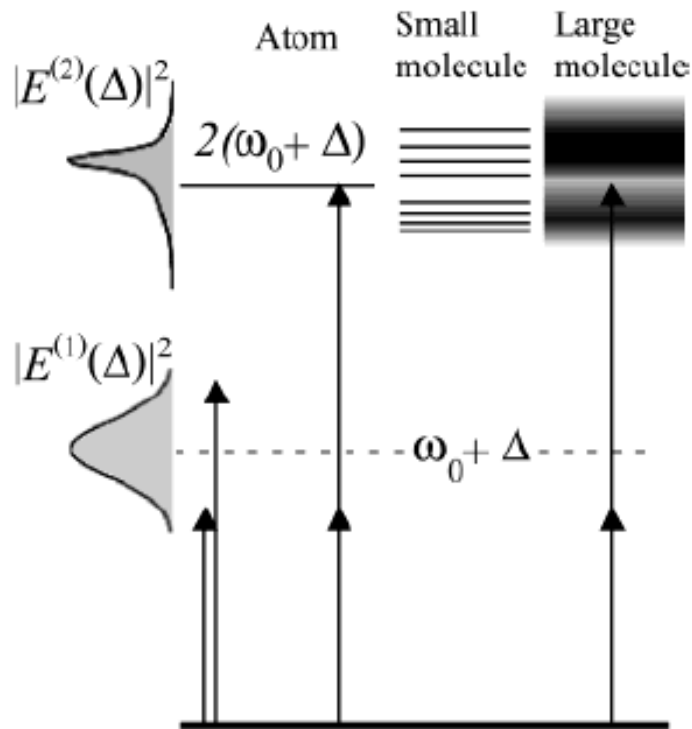
- **Flat phase** : Optimum over the whole spectrum
- **Phase antisymmetric point** : no destructive interference
- **Elsewhere** : phase is not optimal : weak or zero-signal

68

V.V. Lozovoy et al. J. Chem. Phys. 118 (2003)
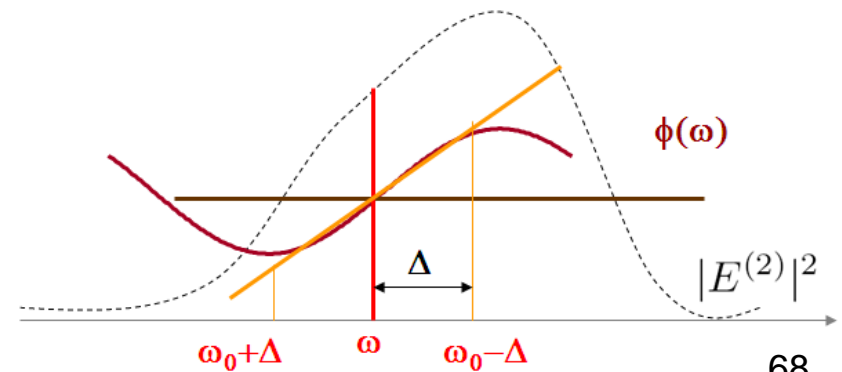
Matching the molecular absorption profile

$$\text{TPF} \propto \int \sigma^{(2)}(\omega) \left| \int E\left(\frac{\omega}{2} - \Delta \right) E\left(\frac{\omega}{2} + \Delta \right) d\Delta \right|^2 d\omega$$

Molecular absorption profile

V.V. Lozovoy et al. J. Chem. Phys. 118 (2003)
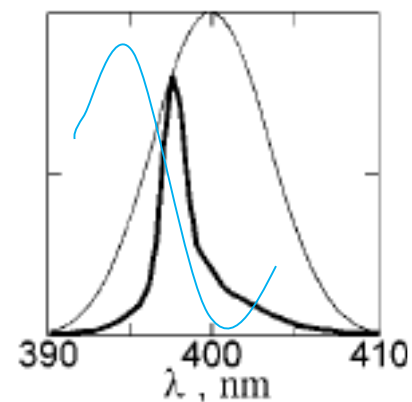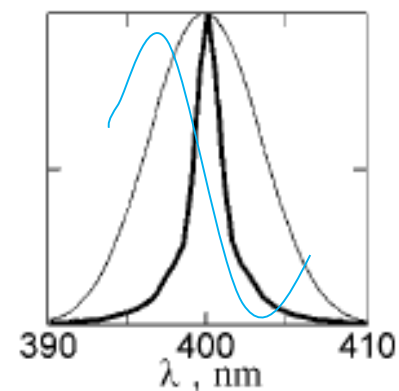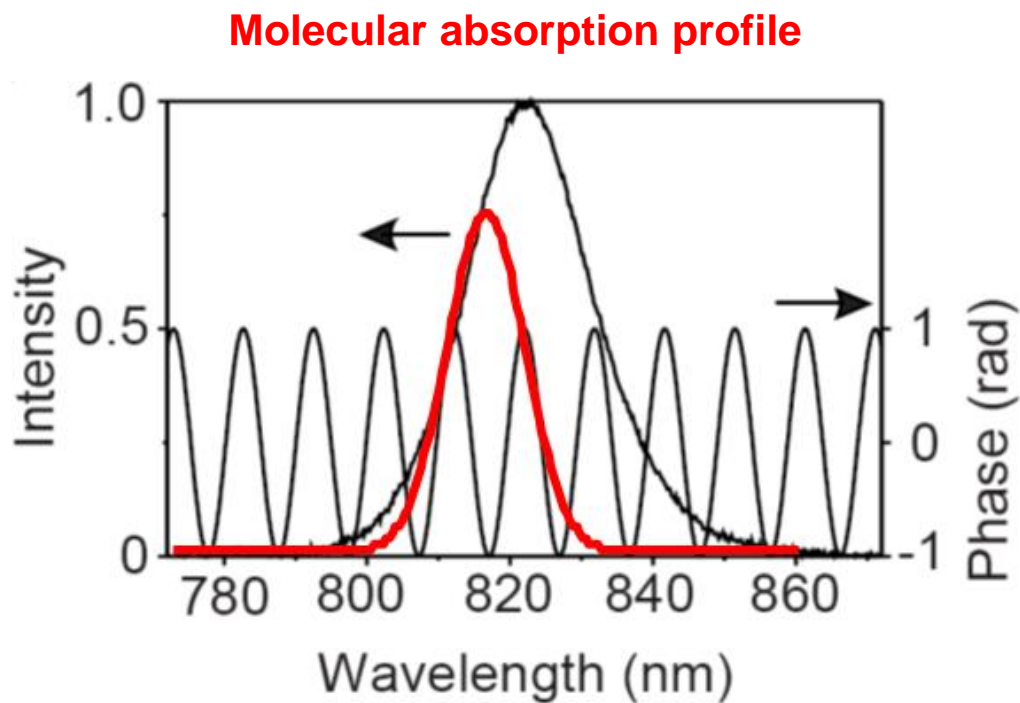
Coherent control for selective two-photon fluorescence microscopy of live organisms

Drosophila embryo
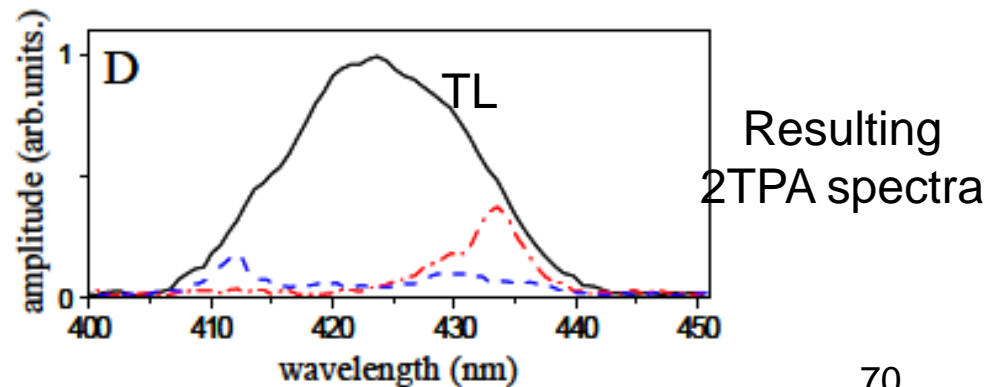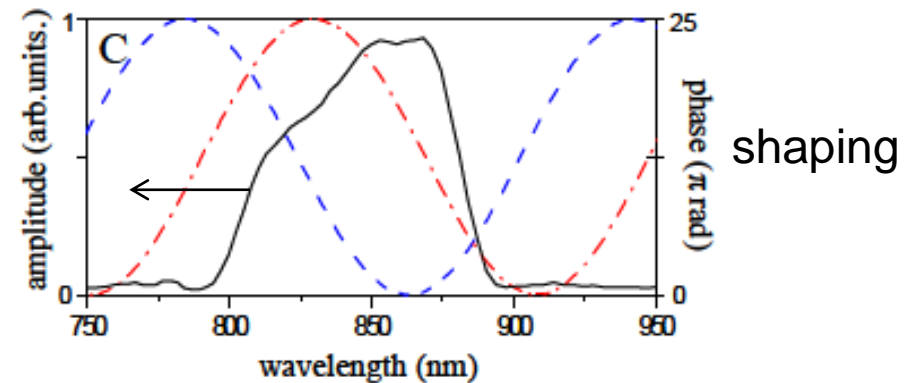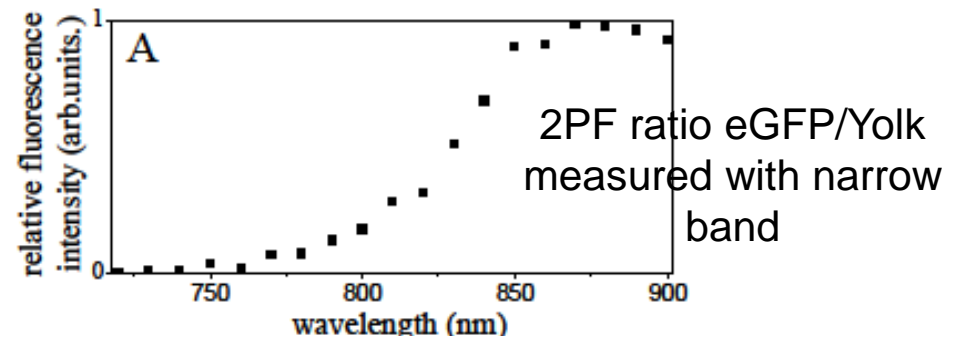
2PF ratio eGFP/Yolk measured with narrow band

shaping

Resulting 2TPA spectra

J.P. Ogilvie, …. E. Beaurepaire, M. Joffre, OE (2006)

70

Coherent control for selective two-photon fluorescence microscopy of live organisms

Shaper

Microscope

B
Ti:Sapph oscillator

BS
BS
PC
Dazzler
X-Y scanner
objective
sample
condenser
filters
PMT
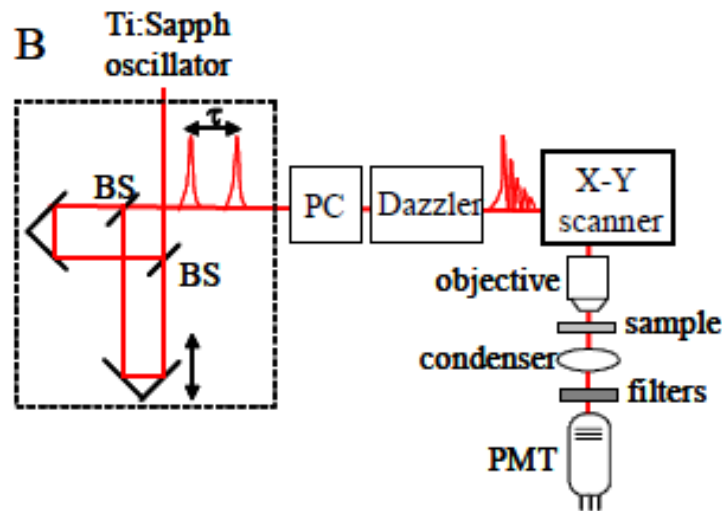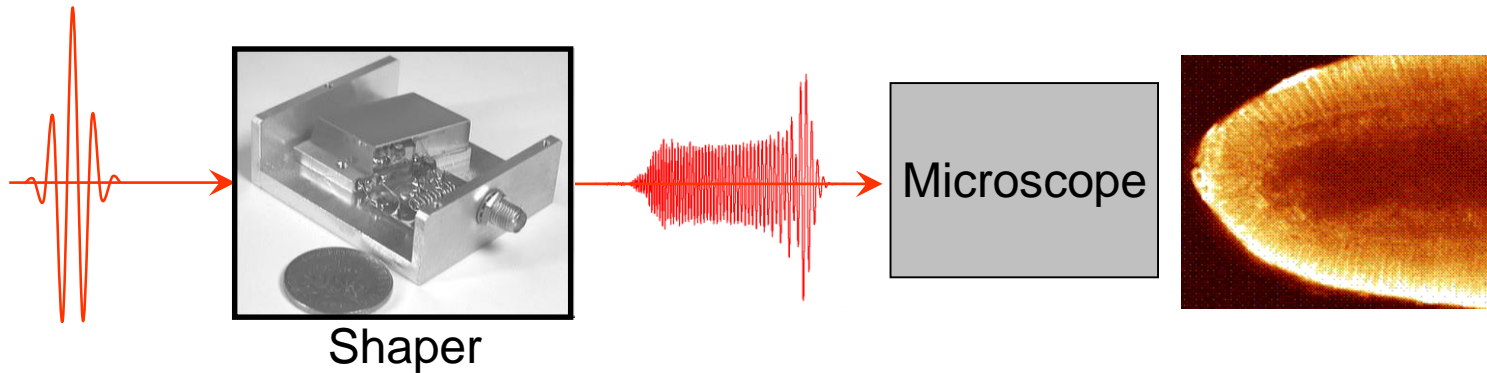
J.P. Ogilvie, …. E. Beaurepaire, M. Joffre, OE (2006)

Also Marcos Dantus group, Michigan State

Linear combinations yield
two selective images of Drosophila embryo

Blue pulse

Yolk emission

Red pulse

GFP emission

25 µm

J.P. Ogilvie, …. E. Beaurepaire, M. Joffre, OE (2006)
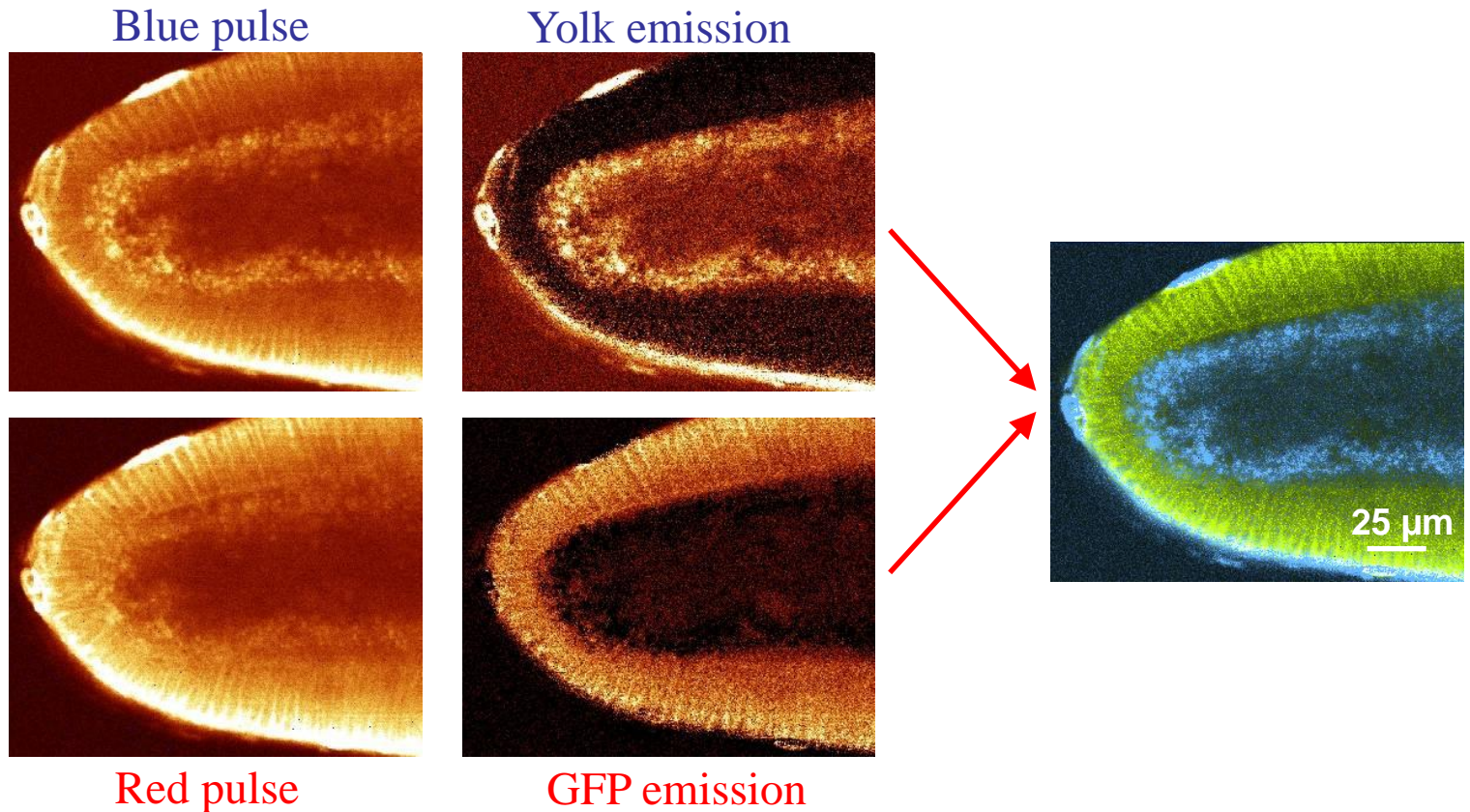
Phase coherent control for specific imaging : pH selectivity

I. Pastirk et al. OE **11** (2003)
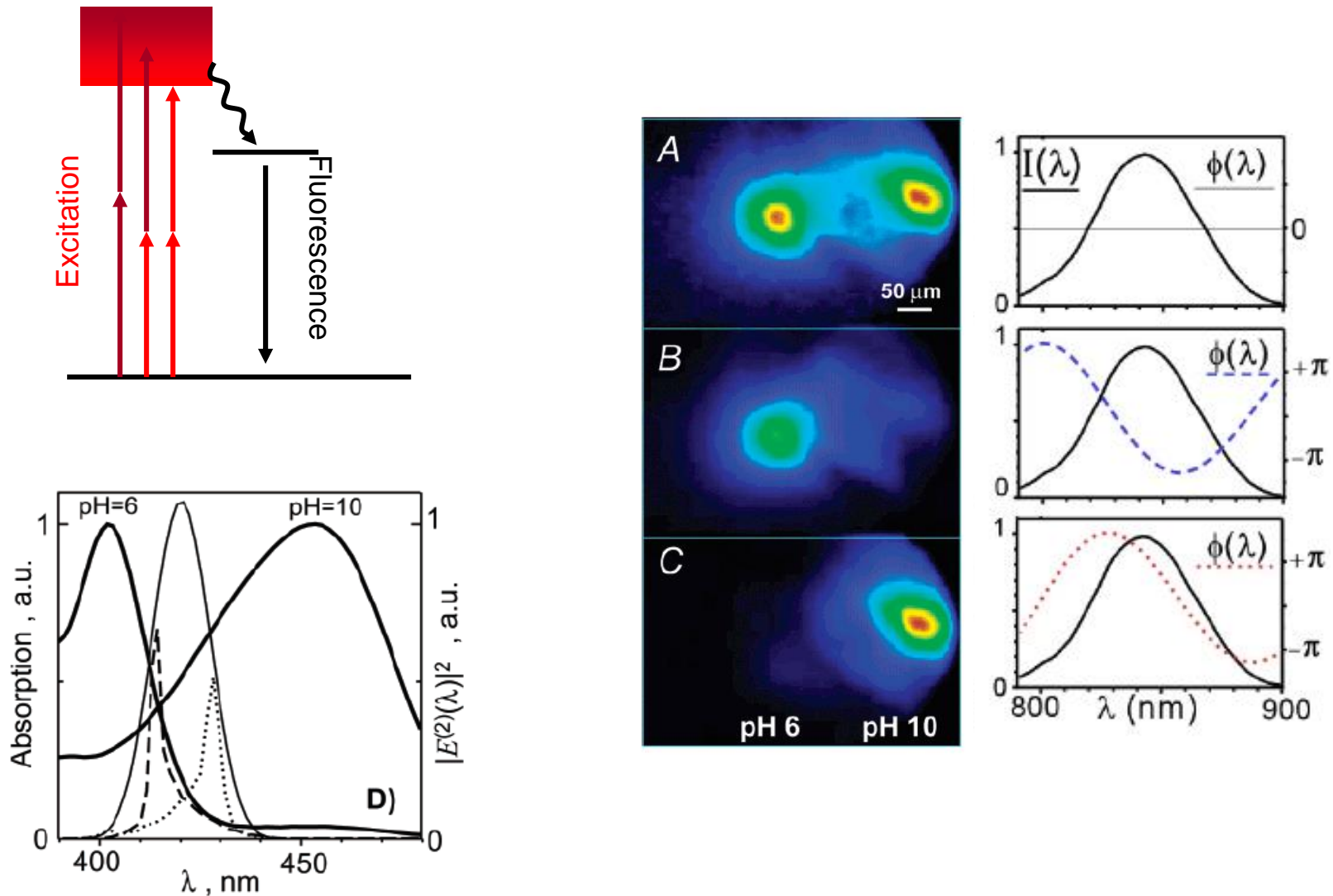
Nonlinear processes involve intra-pulse interferences

$$\mathbf{P}^{(1)}(\mathbf{k}, \omega) = \chi^{(1)}(\omega){:}\mathbf{E}(\mathbf{k}, \omega)$$

$$\mathbf{P}^{(2)}(\mathbf{k} = \mathbf{k}_i + \mathbf{k}_j, \omega = \omega_i + \omega_j) = \chi^{(2)}(\omega_i + \omega_j){:}\mathbf{E}(\mathbf{k}_i, \omega_i)\mathbf{E}(\mathbf{k}_j, \omega_j)$$

$$\mathbf{P}^{(3)}(\mathbf{k} = \mathbf{k}_i + \mathbf{k}_j + \mathbf{k}_l, \omega = \omega_i + \omega_j + \omega_l) = \chi^{(3)}(\omega_i + \omega_j + \omega_l){:}\mathbf{E}(\mathbf{k}_i, \omega_i)\mathbf{E}(\mathbf{k}_j, \omega_j)\mathbf{E}(\mathbf{k}_l, \omega_l)$$

SHG :

$$P_I(2\omega) = \int_{-\infty}^{\infty} \sum_{JK} \chi^{(2)}_{IJK}(\omega, \Omega) E_J(\omega - \Omega) E_K(\omega + \Omega) \mathrm{d}\Omega$$

ω_2

$\omega_1 + \omega_2$

ω_1
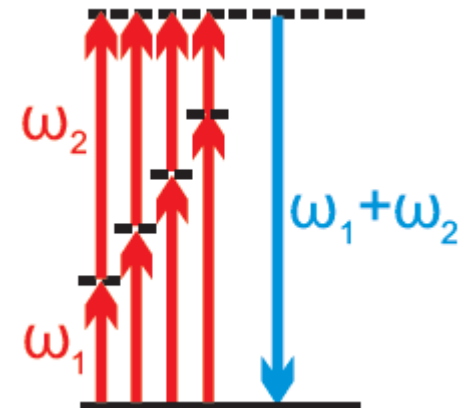
Polarized NLO imaging

Imaging bio-molecular organization

5μm
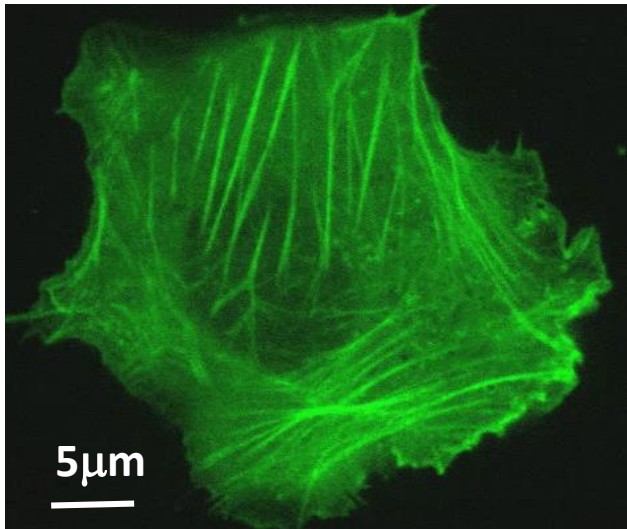
Zeiss- Human Osteosarcoma - Actin

200nm

Detergent extracted actin cytoskeleton SEM- Ian Wells, DB Stolz

20μm
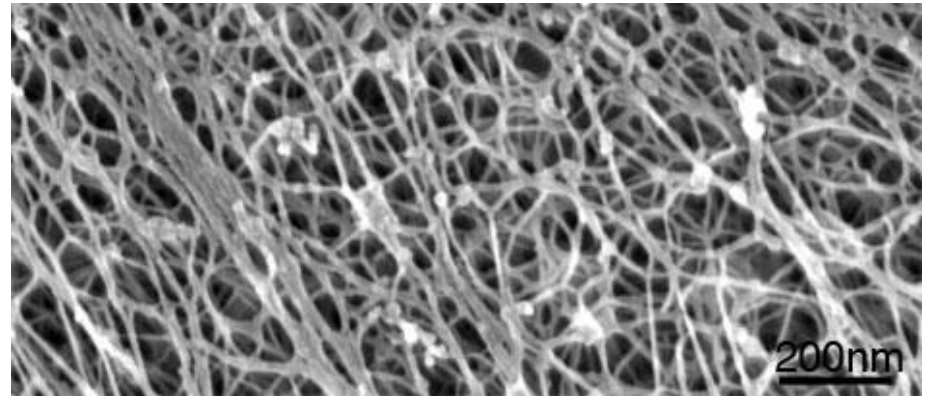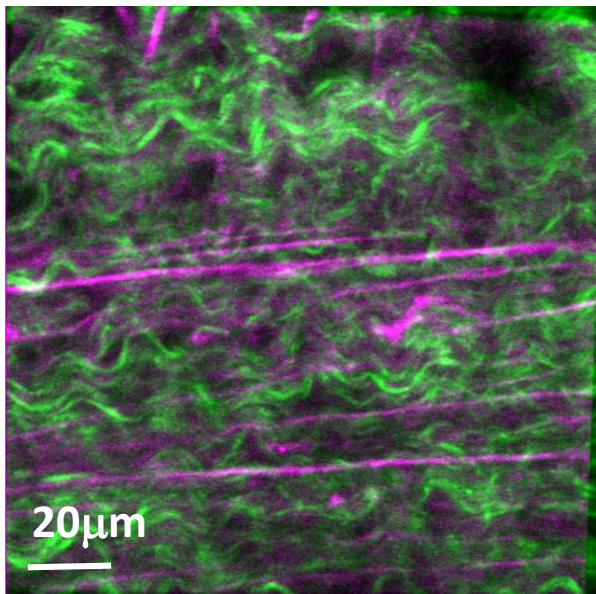
Collagen (SHG) / elastin (TPF) chordae,
U. Exeter/I. Fresnel

10 μm

Collagen (SEM)

10 μm

Elastin (SEM)

76
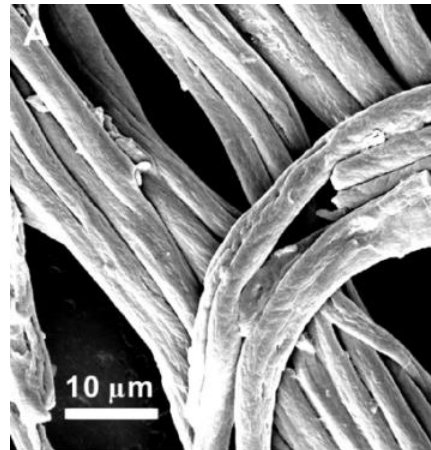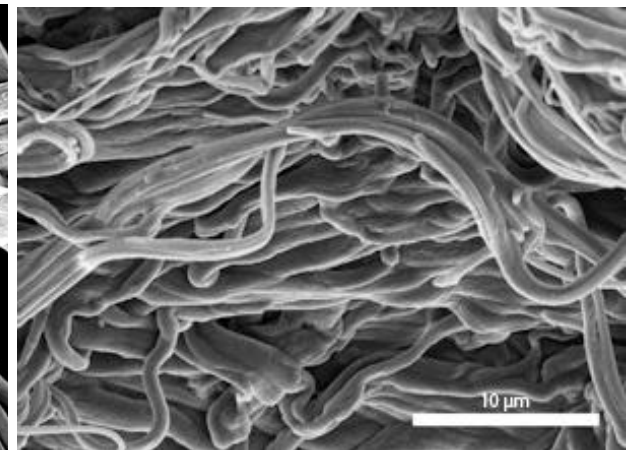
Molecular orientational order reports structural information
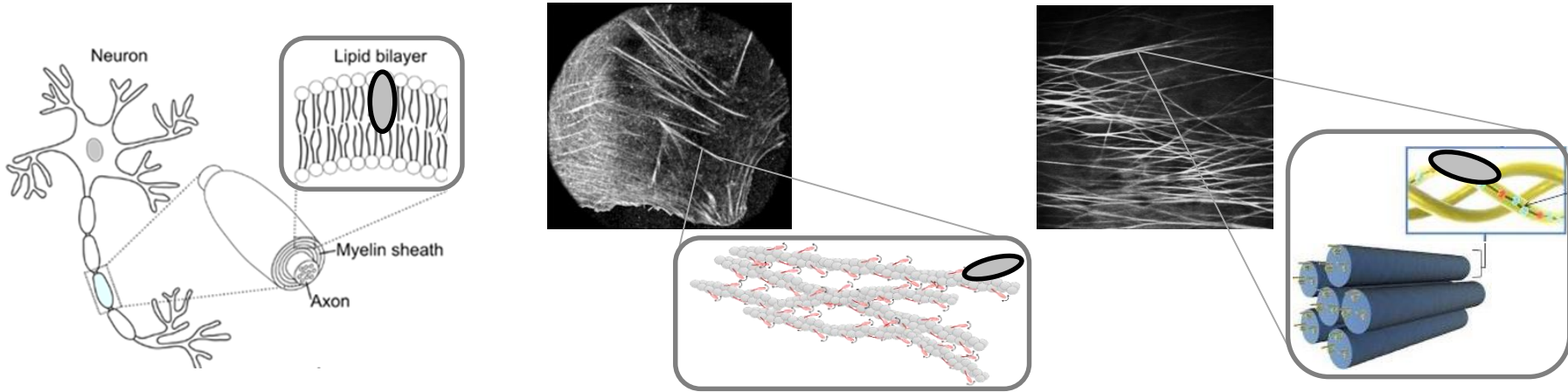
Resolution in nonlinear optical microscopy: ~ 300nm

Ordered

ψ

ψ

$\psi = 180°$

Disorder due to
Spatial rearrangements / Dynamics

disordered
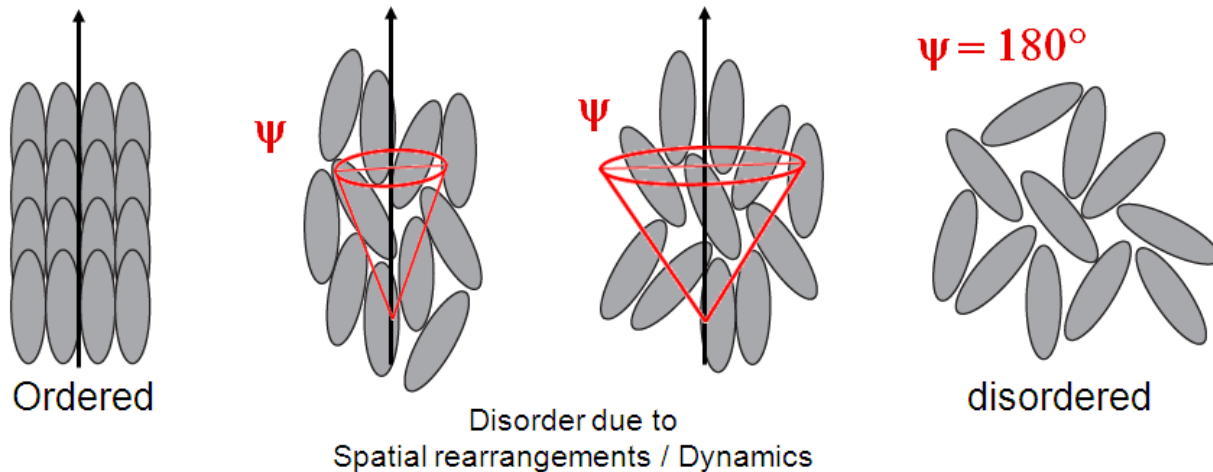
1 photon fluorescence

Fluorescence = Absorption x Emission

Linear excitation

Absorption

$$\mu_{abs} \sim\, < \psi_0(r).r.\psi_1(r) >$$

$$\mu_{abs}$$

$$\psi_1(r)$$
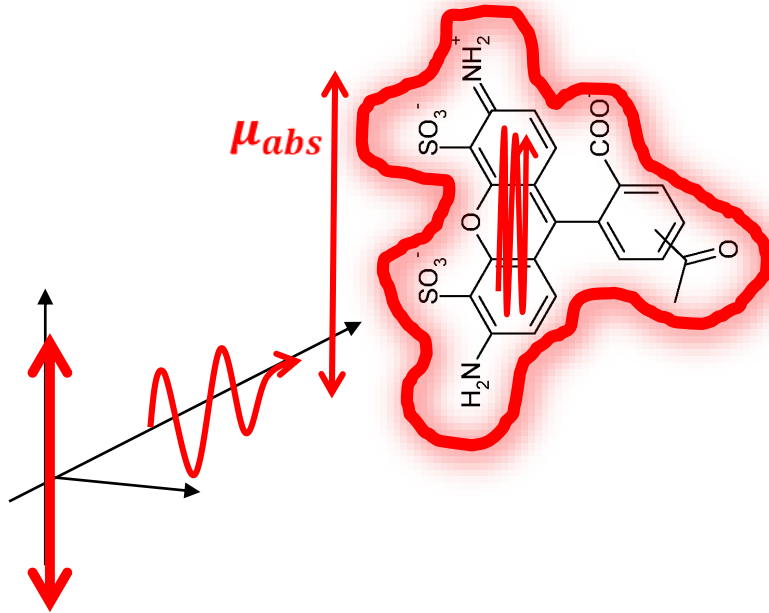
$$\psi_0(r)$$
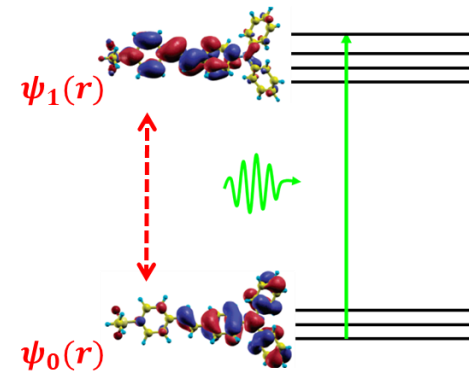
$$P_{abs} \propto |\mu_{abs}.E|^2$$

$$P_{abs} = \sigma_{abs}.I$$

1PF: tuning the excitation - single molecule

$$I(\alpha) \propto \left| \vec{\mu}_{\text{abs}} \cdot \vec{E} \right|^2$$

Absorption dipole

exciting field
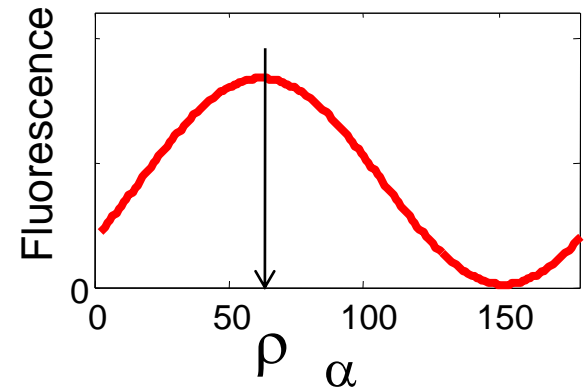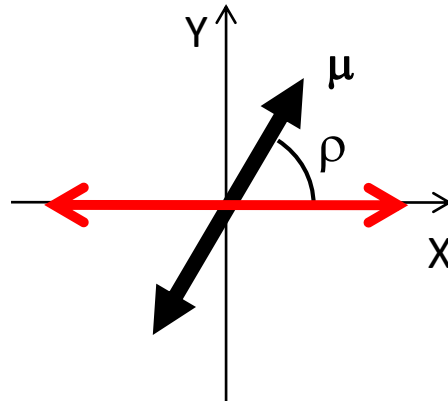
Many molecules

$$I^{1PF}(\alpha) = N \int_{\Omega} |\mu_{abs}(\Omega) \cdot \mathbf{E}|^2 f(\Omega) d\Omega$$
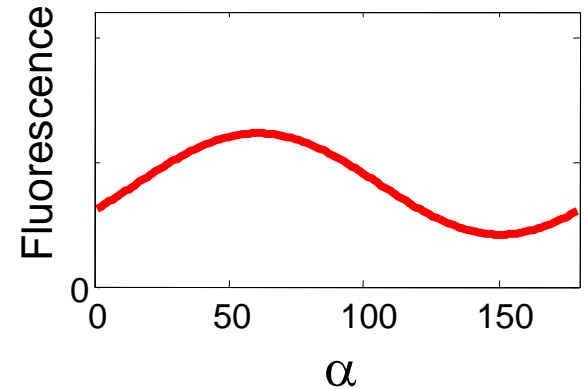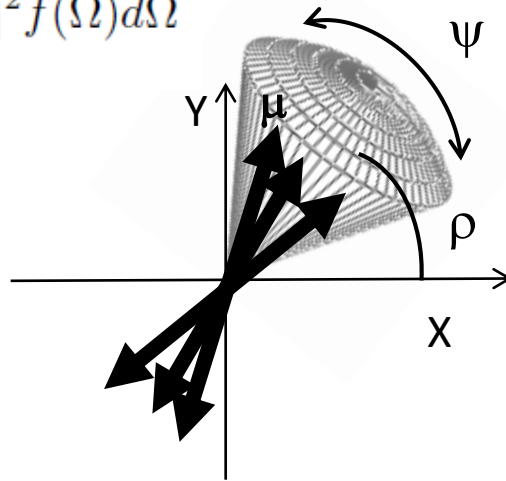
Time and space averaging

80

S. Brasselet et al. in Springer Series Fluoresc, Springer-Verlag (2013)

Polarimetric Fluorescence (1PF) imaging
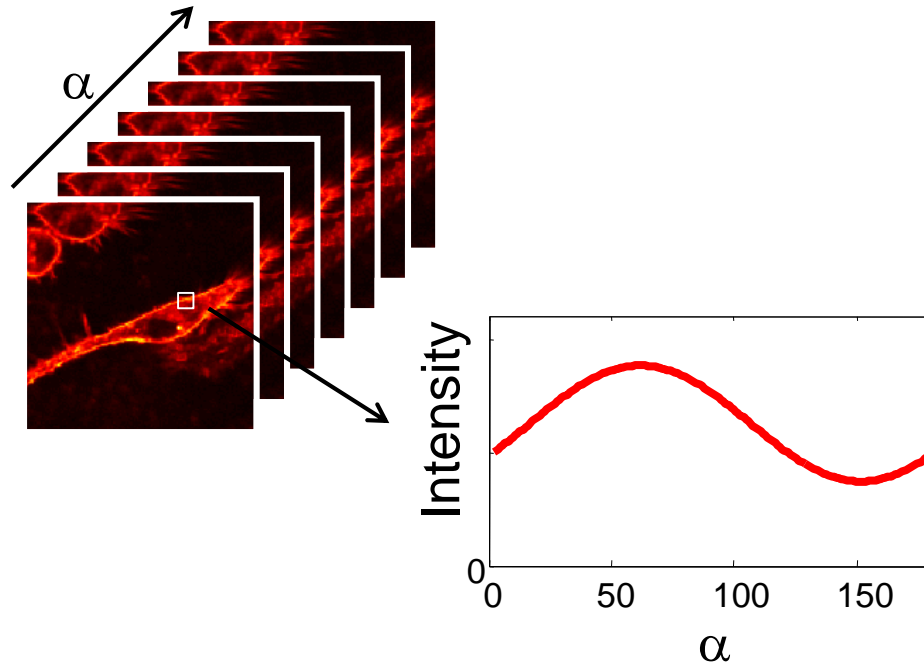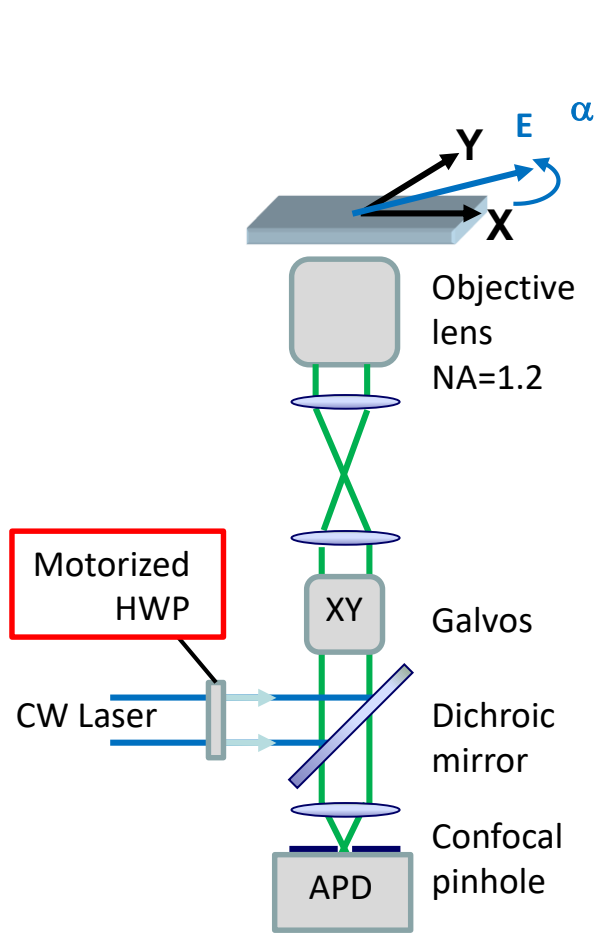
$$I(\alpha) = \boxed{A_0}\left[1 + \boxed{\frac{A_2}{A_0}}\cos(2\alpha) + \boxed{\frac{B_2}{A_0}}\sin(2\alpha)\right]$$

$(A,B) \Leftrightarrow (\rho,\psi)$
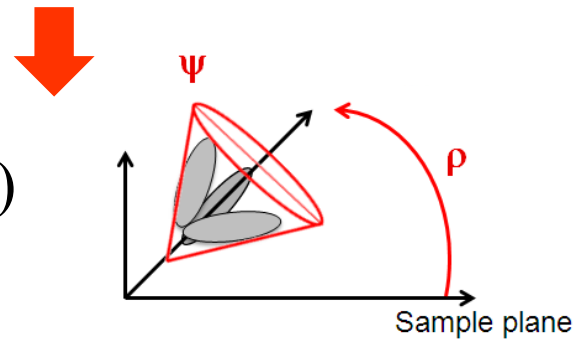
Gasecka et al. Biophys J 2009
Duboisset et al. JPC B 2013
Kress et al., Biophys J 2013

Structural imaging of actin sress fibers

Alexa 488 – phalloidin in fixed COS 7 cells

$\Psi = 119 +/- 3$ deg
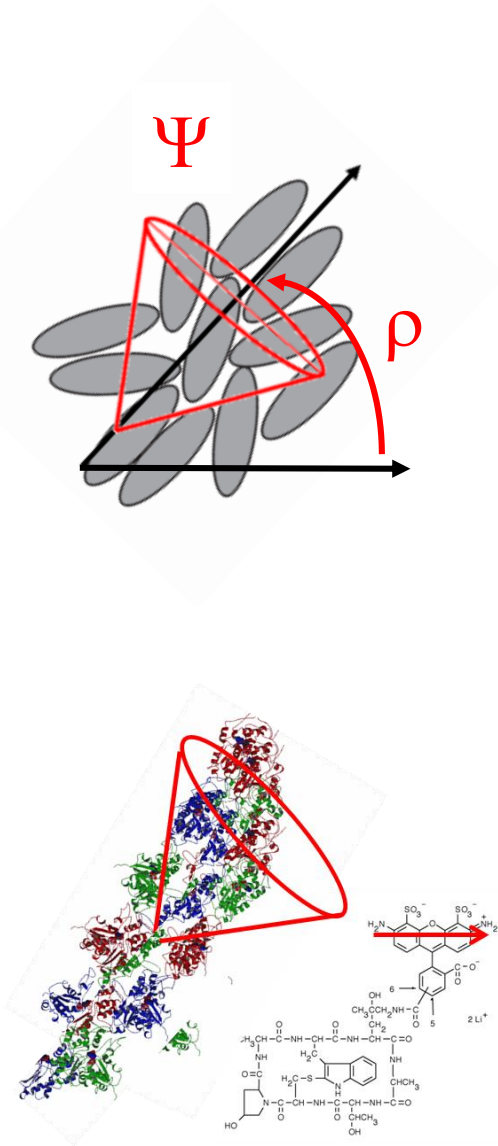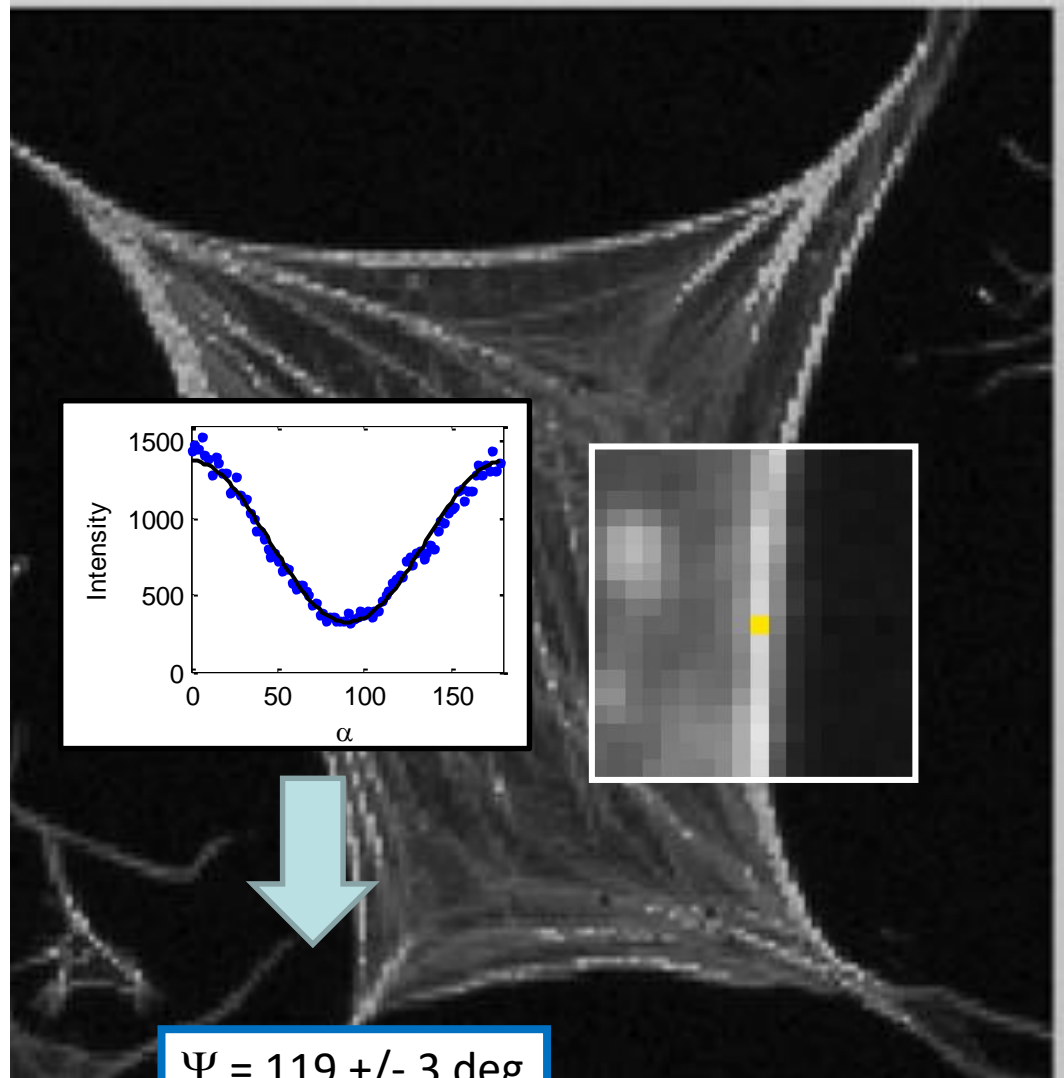
Structural imaging of actin sress fibers

Alexa 488 – phalloidin in fixed COS 7 cells
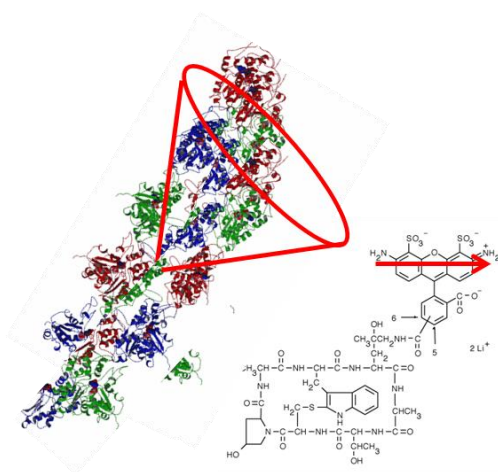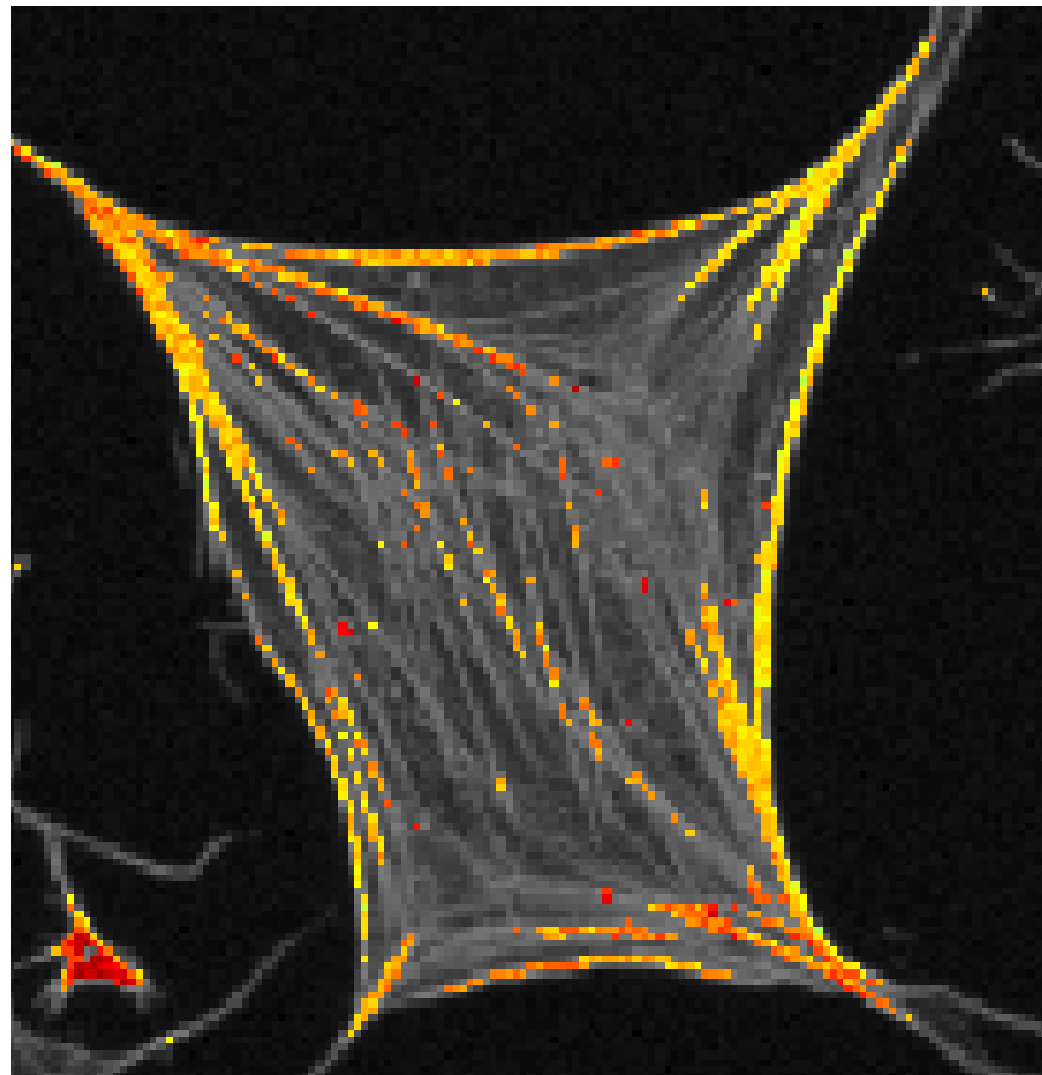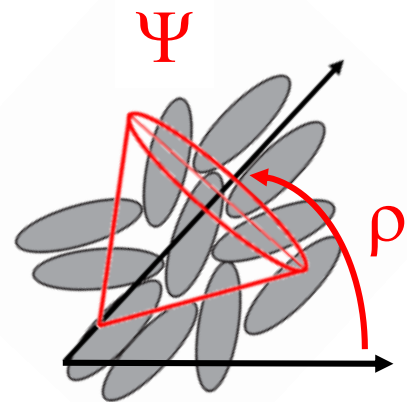
Structural imaging of actin sress fibers

Alexa 488 – phalloidin in fixed COS 7 cells
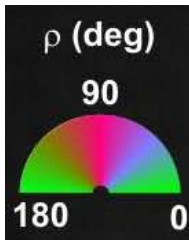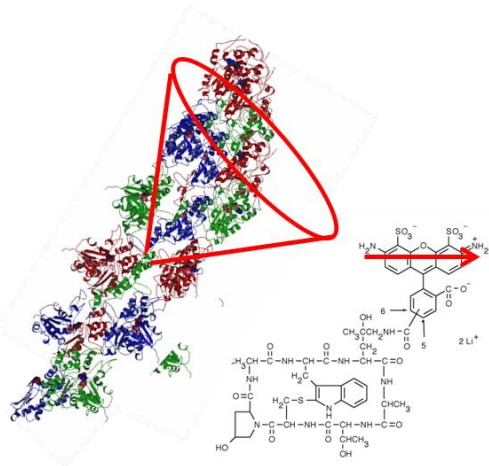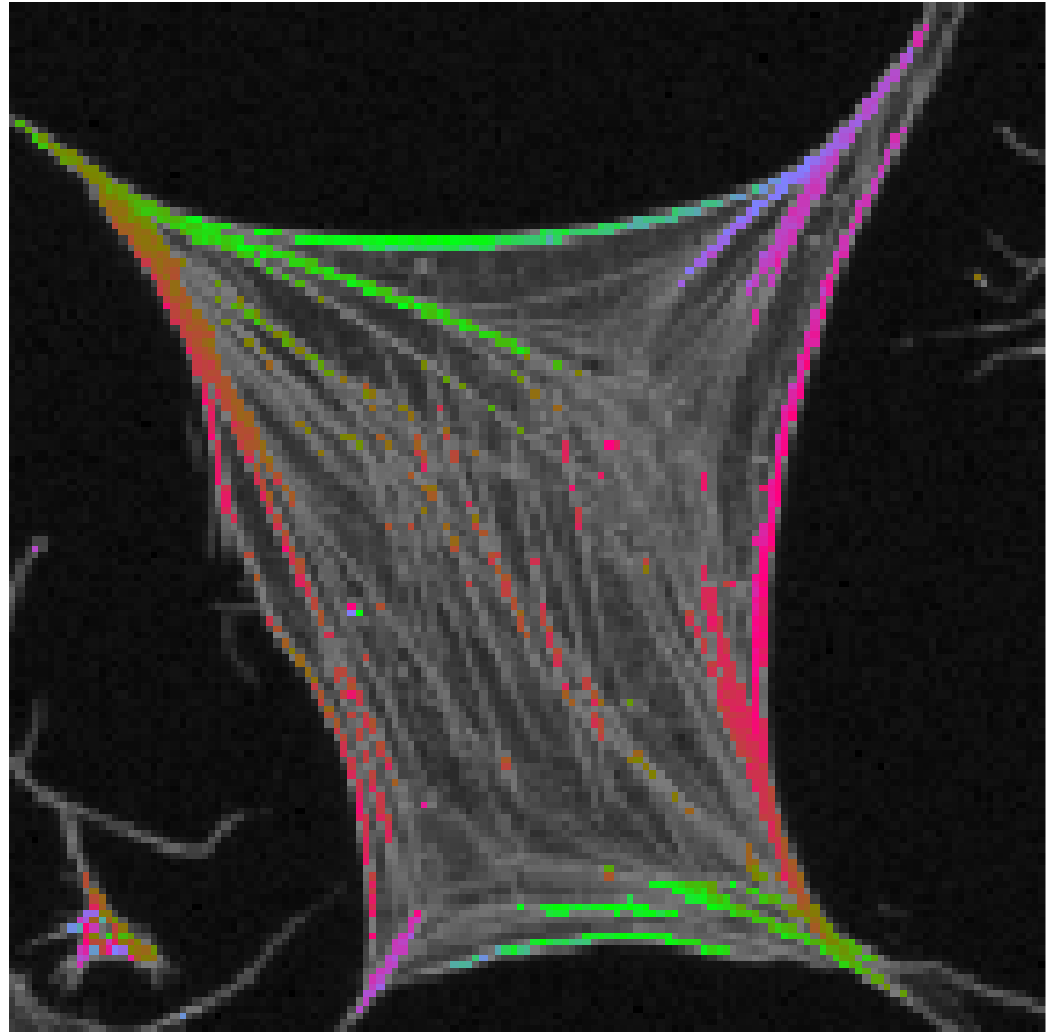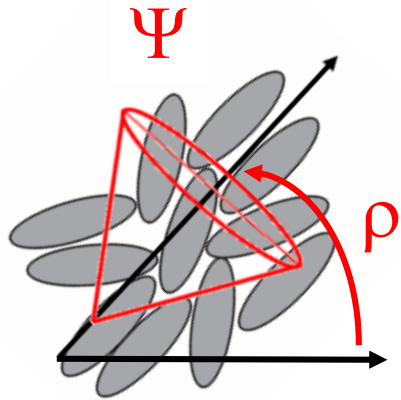
Structural imaging of actin sress fibers

Alexa 488 – phalloidin in fixed COS 7 cells
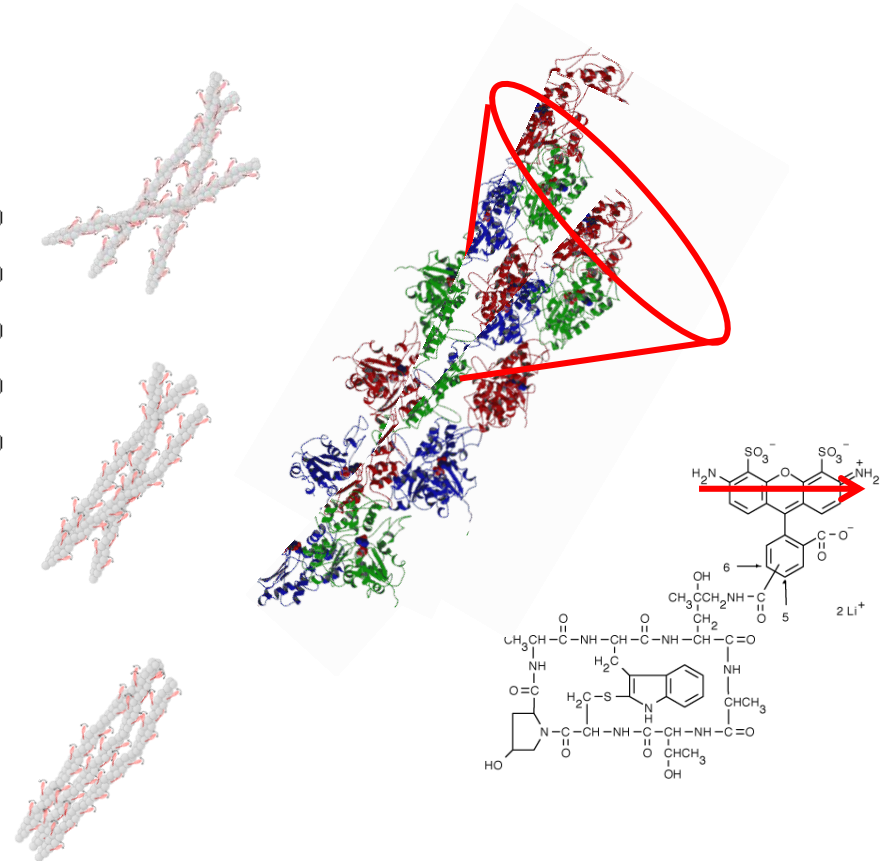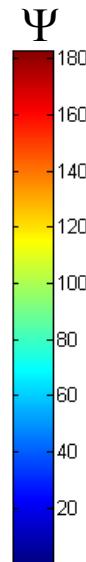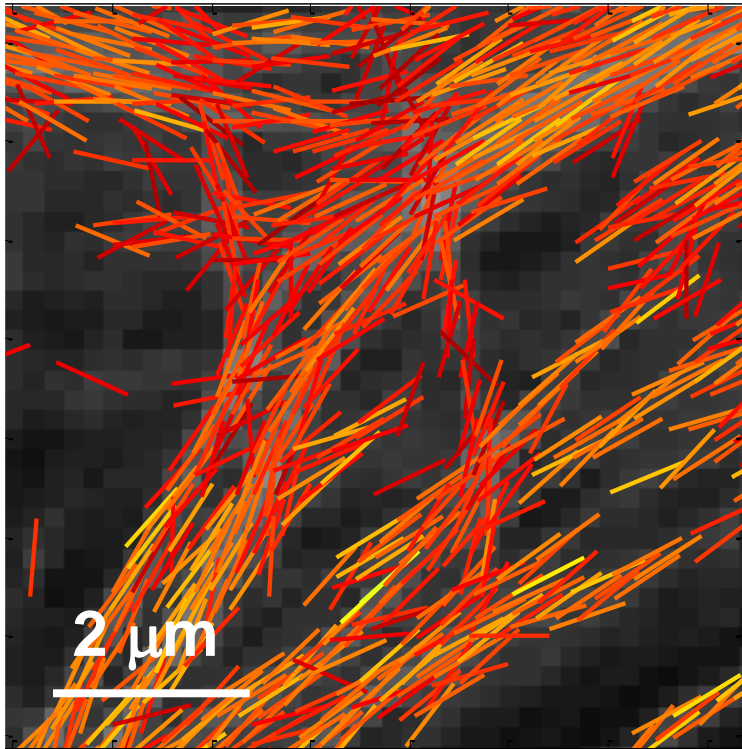
Label-free

Polarization resolved Nonlinear microscopy

$$(E_X^\omega, E_Y^\omega, E_Z^\omega) = E_0 (\cos\alpha, \sin\alpha, 0)$$

Enlarged view of the excitation volume

$$\vec{P} = \varepsilon_0 \vec{\chi}^{(1)} \vec{E} + \varepsilon_0 \vec{\chi}^{(2)} \vec{E}\vec{E} + \varepsilon_0 \vec{\chi}^{(3)} \vec{E}\vec{E}\vec{E} + ...$$

SHG

THG

FWM / CARS

$$\sum_{JKL} \chi_{IJKL}^{(3)} E_J^\omega E_K^\omega E_L^\omega$$

$$\sum_{JK} \chi_{IJK}^{(2)} E_J^\omega E_K^\omega$$

$$\sum_{JKL} \chi_{IJKL}^{(3)} E_J^{\omega_p} E_K^{\omega_p} E_L^{\omega_s*}$$

$$\chi_{IJK}^{(2)} = N \int_\Omega \beta_{IJK}(\Omega) f(\Omega) d\Omega$$

Incident light

EPI detection
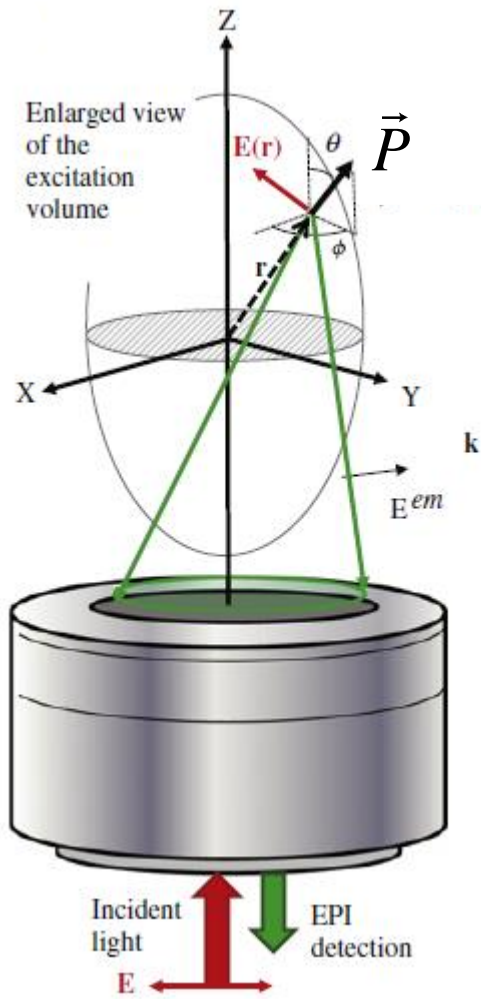
All dipole radiations will add up coherently

87

Polarization resolved nonlinear microscopy

Forward detector

2PF
FWM/CARS
SHG

filters

50x
0.5

sample

z

x

1.2
40x

BS

Rotating polarization

Pump
Stokes

Epi detector

α

CARS
CARS
CARS
CARS

Counts

Experimental
Fit

0° α 180°
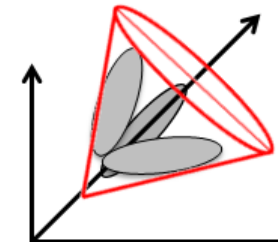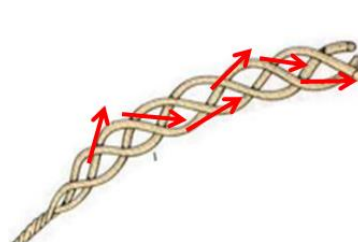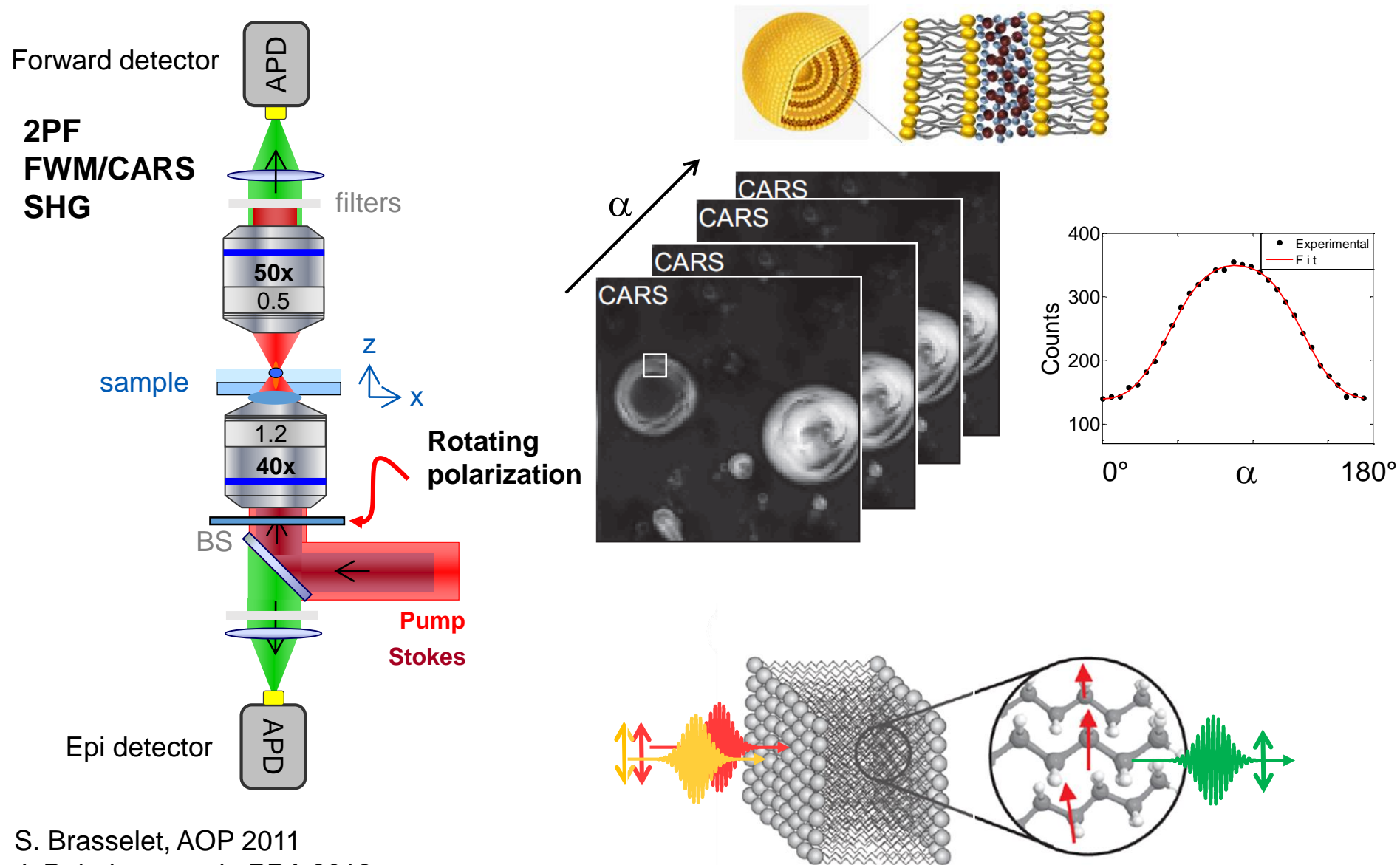
S. Brasselet, AOP 2011
J. Duboisset et al., PRA 2012
F.Z. Bioud et al., PRA 2014

Polarization resolved SHG/TPF

$$(E_X^\omega, E_Y^\omega, E_Z^\omega) = E_0 (\cos\alpha, \sin\alpha, 0)$$

$$P_{\text{SHG}} \propto N \int [\beta(\Omega) : E(\alpha)E(\alpha)] \, f(\Omega) d\Omega$$

$$P_{\text{SHG}} \propto \chi^{(2)} : E(\alpha)E(\alpha)$$

$$I_{\text{2PF}}(\alpha) \propto \int |\mu_{\text{abs}}(\Omega) \cdot E(\propto)|^4 \cdot f(\Omega) d(\Omega)$$

$$I = a_0 + \boxed{a_2 \cos(2\alpha)} + a_4 \cos(4\alpha)$$

$$b_2 \sin(2\alpha) + b_4 \sin(4\alpha)$$

$$f(\Omega) = \bigcirc + \infty + \ldots$$
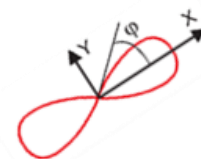
SHG polarized microscopy in collagen

High order

High disorder

Fast SHG polarized microscopy in collagen

SHG Intensity

100 μm

S2,φ2

High order

High disorder
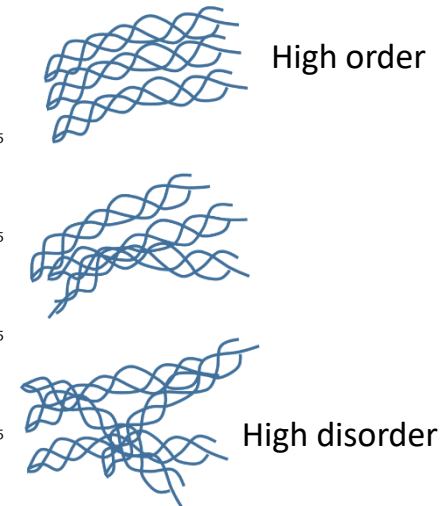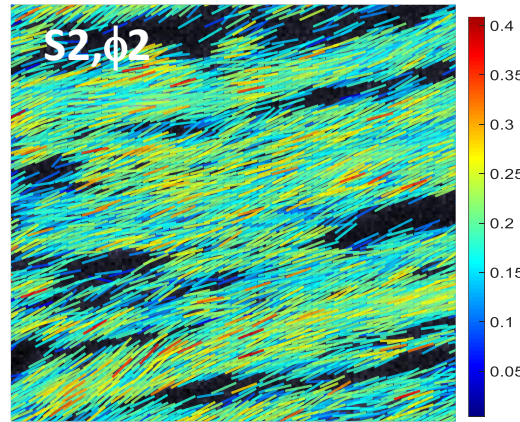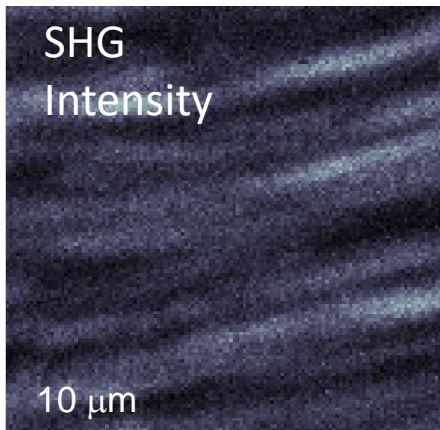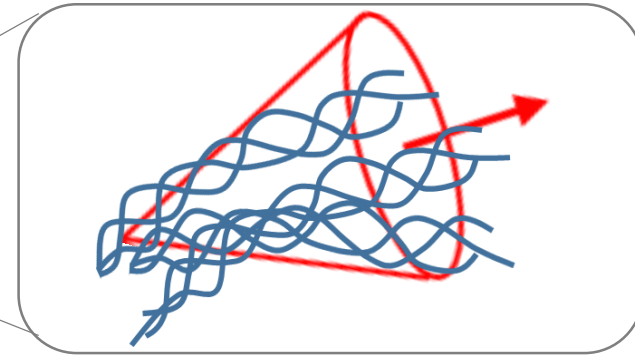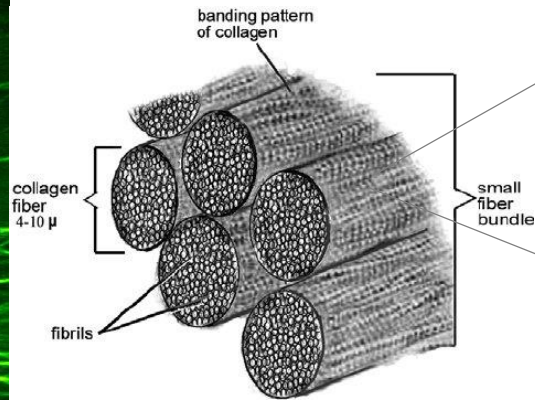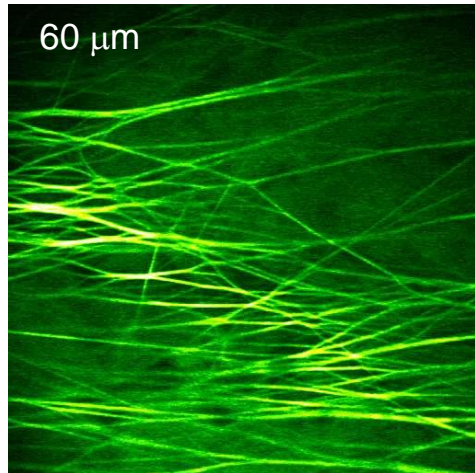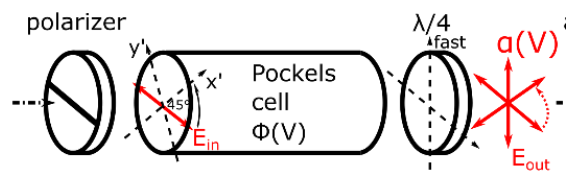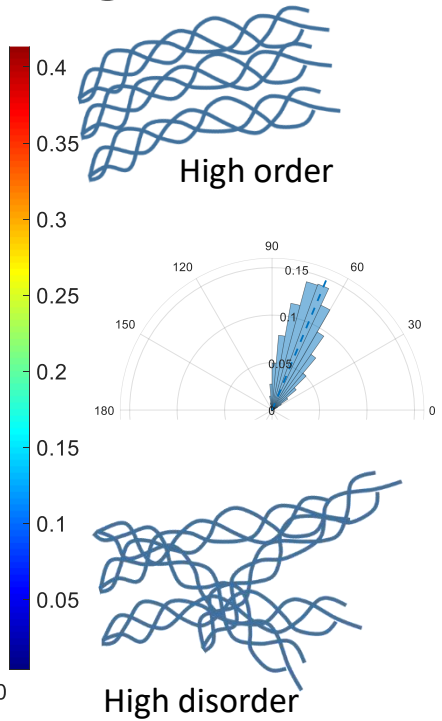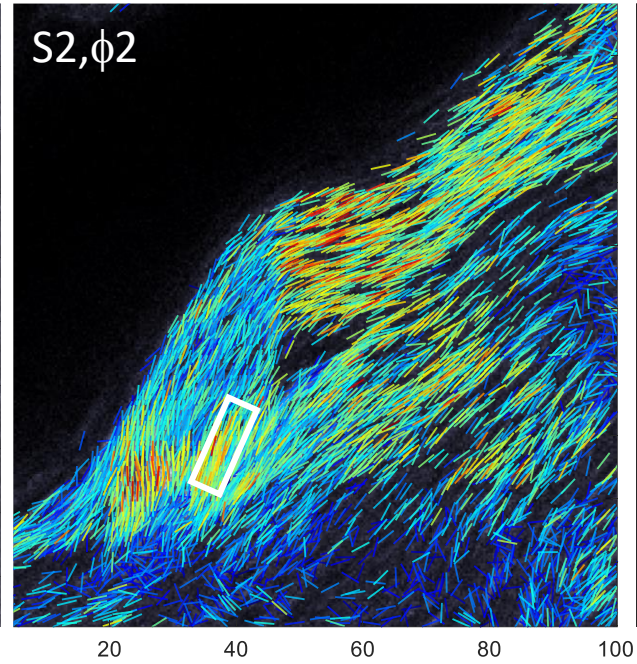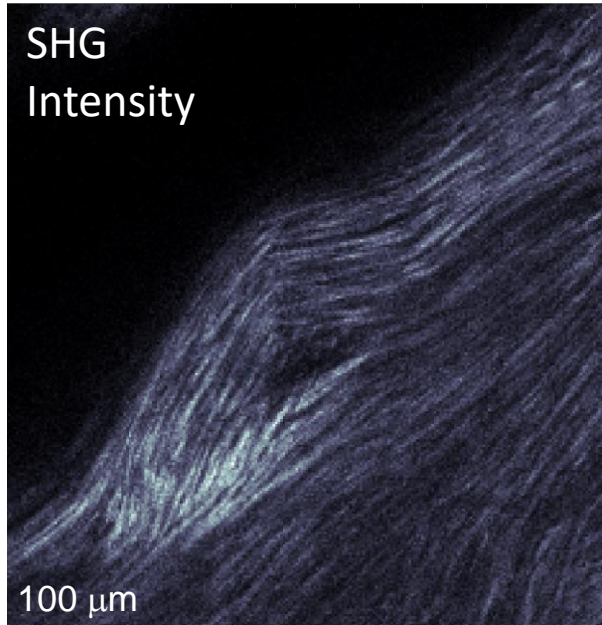
EOM or AOM based
1MHz polarized modulation
+ lock-in detection

1 image/sec

Sison et al. In prep (2021)
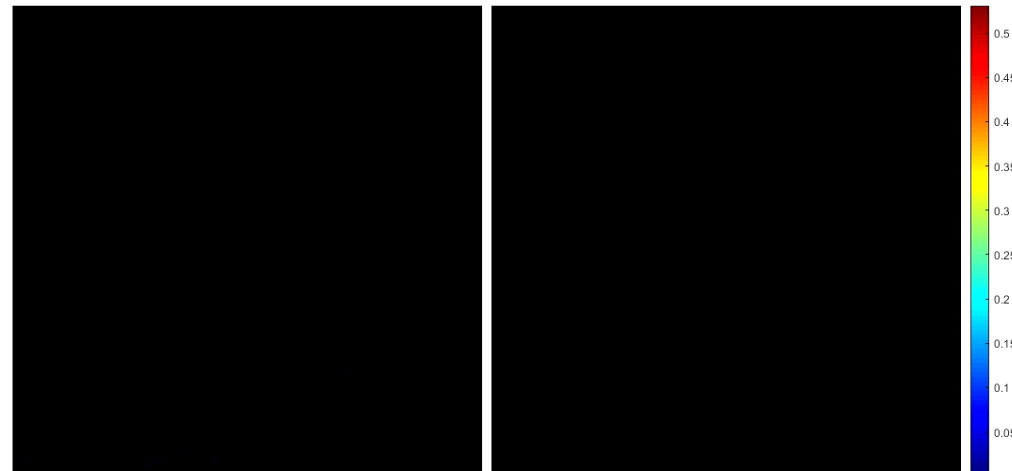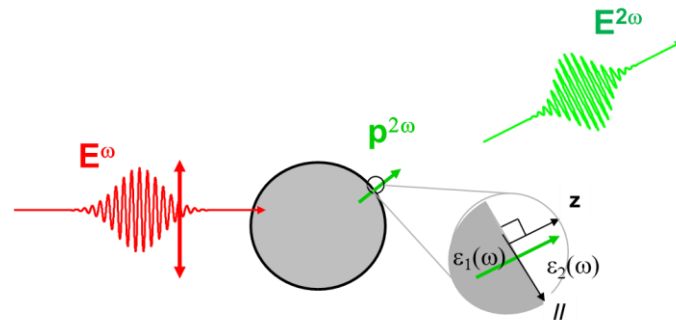
pSHG provides sub-diffraction information
Gold nanorods
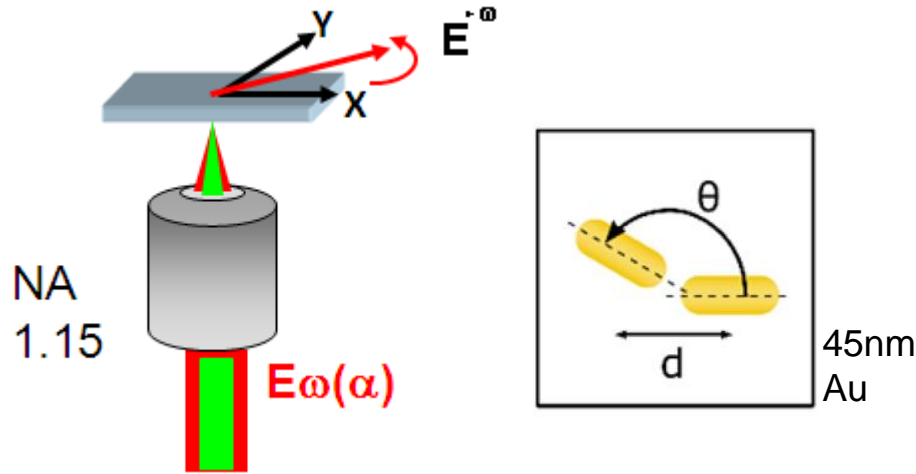
$$I = a_0 + a_2 \cos(2\alpha) + a_4 \cos(4\alpha)$$

$$b_2 \sin(2\alpha) + b_4 \sin(4\alpha)$$

$$I_n = \frac{1}{a_0} \sqrt{a_n^2 + b_n^2} \qquad \varphi_n = \frac{1}{n} \arctan\left(\frac{b_n}{a_n}\right)$$

45nm Au

d = 40 nm

$I_2; \phi_2$

$I_4; \phi_4$

$\theta = -60°$

40nm pixel size

$I_2; \phi_2$

$I_4; \phi_4$

d)

Balla et al. ACS Photonics (2017)
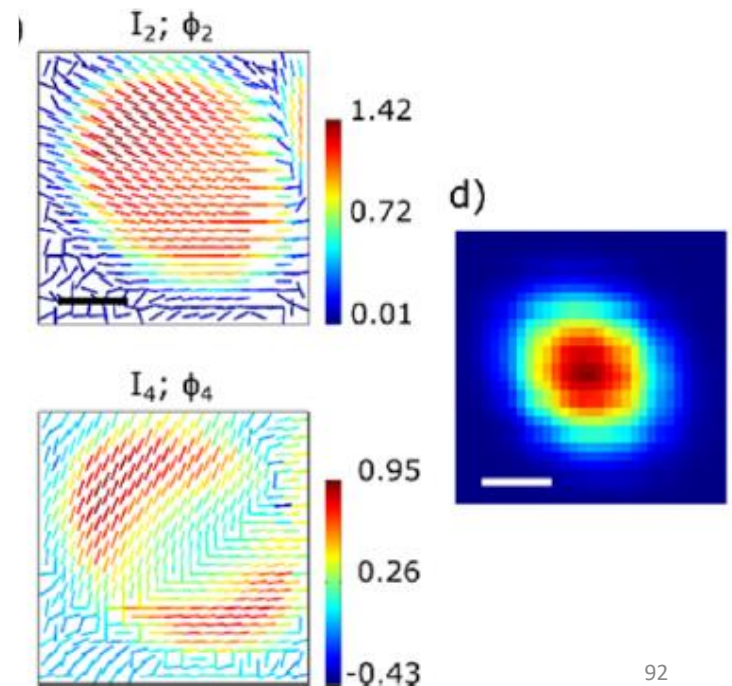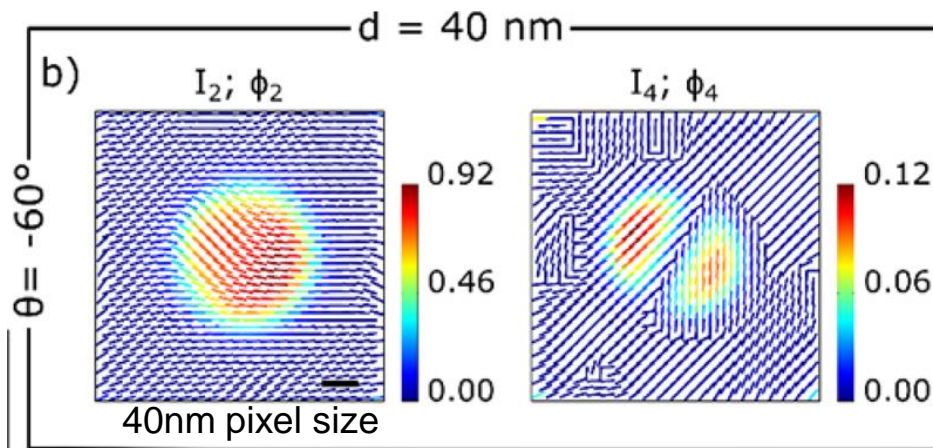
pSHG provides sub-diffraction information
Gold nano-stars
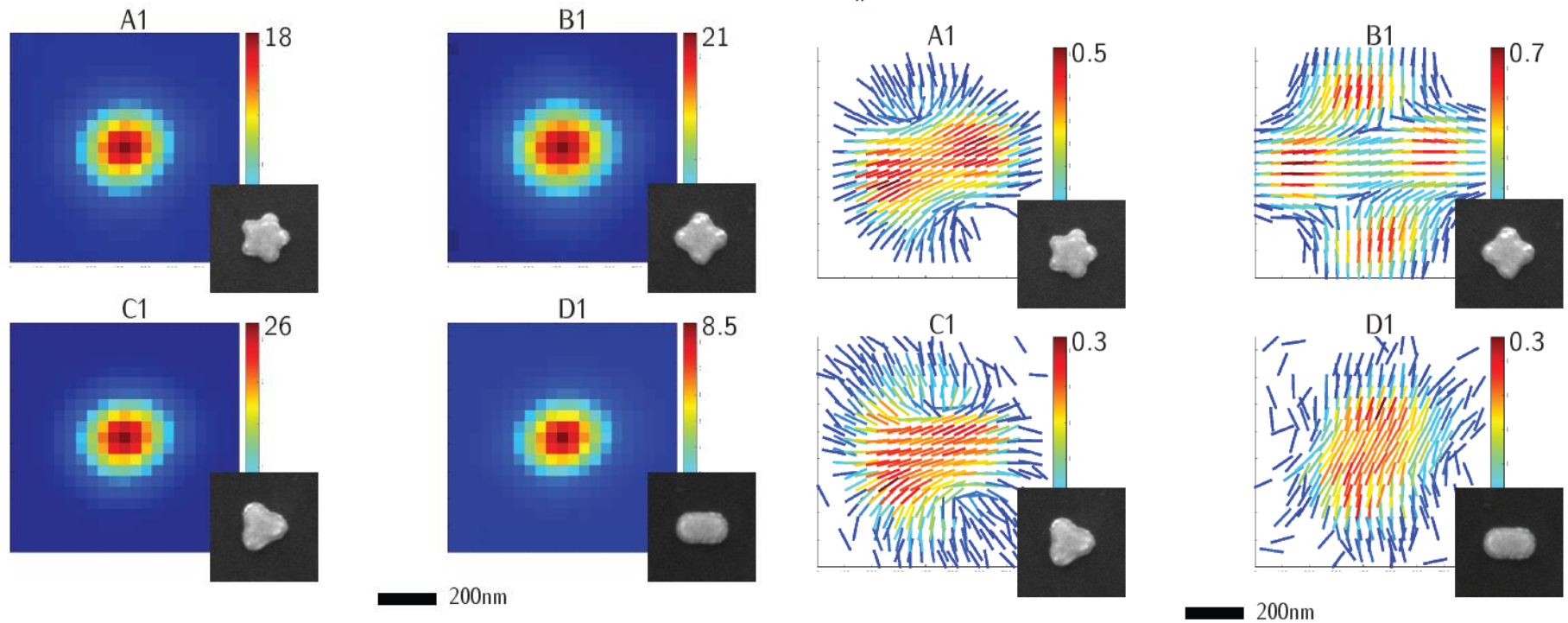
Collaboration R. Quidant, ICFO

Balla et al. ACS Photonics (2017)

Polarization resolved CARS

$$(E_X^\omega, E_Y^\omega, E_Z^\omega) = E_0 \left(\cos\alpha, \sin\alpha, 0 \right)$$

$$I_X^{CARS} \propto \sum_{\substack{JKL \\ MNO}} \chi_{XJKL} \chi_{XMNO}^* E_J^* E_K E_L E_M E_N^* E_O^*$$

$$I = a_0 + a_2 \cos(2\alpha) + a_4 \cos(4\alpha) + a_6 \cos(6\alpha) +$$
$$b_2 \sin(2\alpha) + b_4 \sin(4\alpha) + b_6 \sin(6\alpha)$$

$$f(\Omega) = \bigcirc + \infty + \dots$$
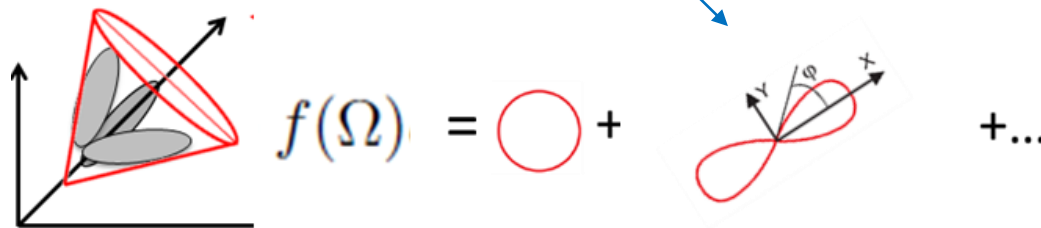
High orders of the molecular angular distribution

$$\chi^{(3)}_{IJKL} = N\gamma \int_{\Omega} (\mathbf{I} \cdot \mathbf{e})(\mathbf{J} \cdot \mathbf{e})(\mathbf{K} \cdot \mathbf{e})(\mathbf{L} \cdot \mathbf{e}) f(\Omega) d\Omega$$
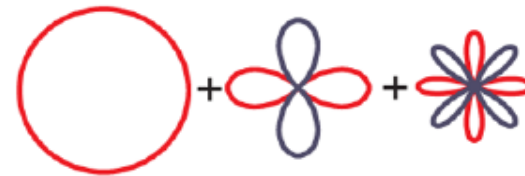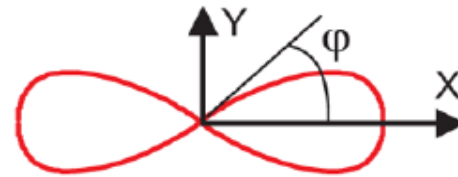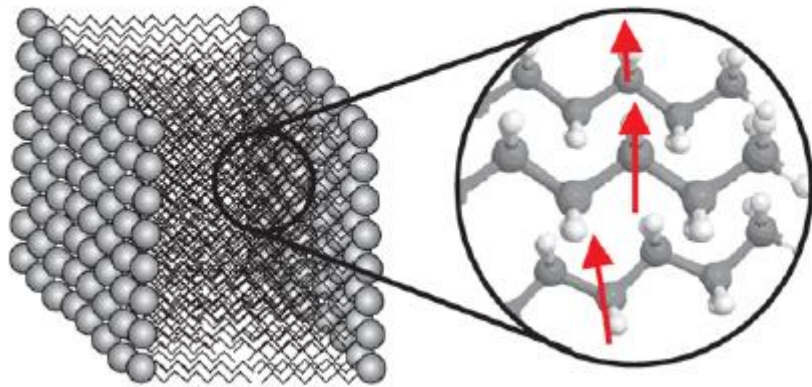
2D incident polarization

$$p(\varphi) = p_0 + \sum_n p_n \cos(n\varphi) + q_n \sin(n\varphi)$$
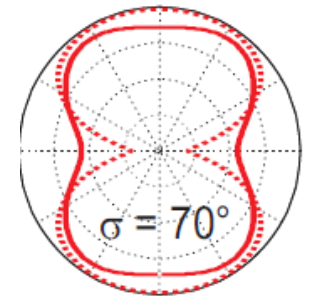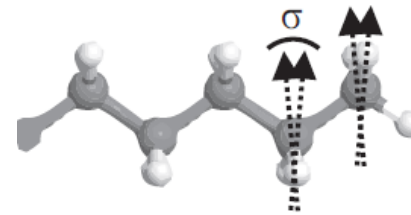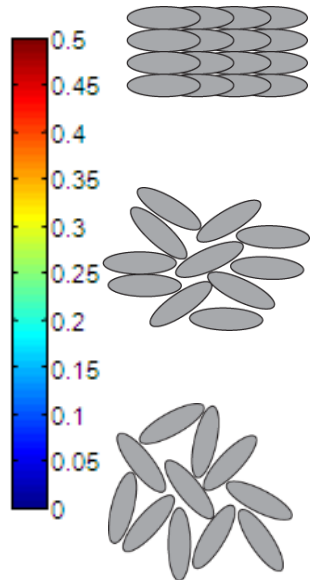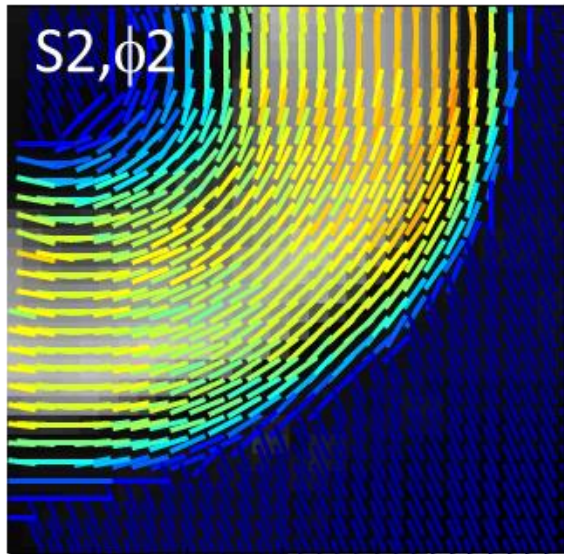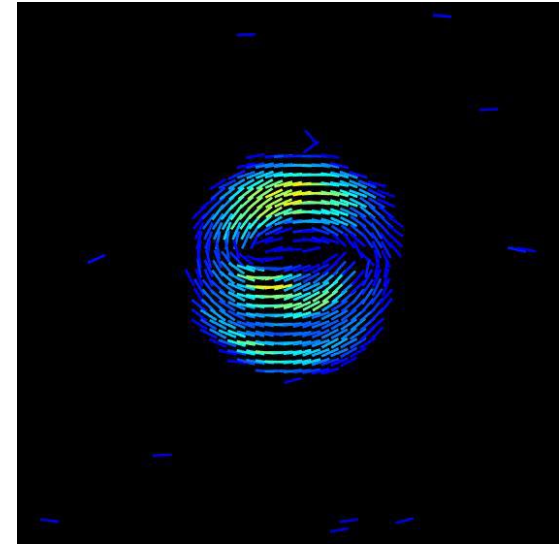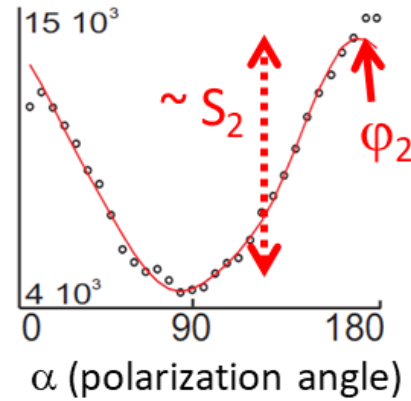
symmetry orders

$$I = a_0 + a_2 \cos(2\alpha) + a_4 \cos(4\alpha) + a_6 \cos(6\alpha) +$$
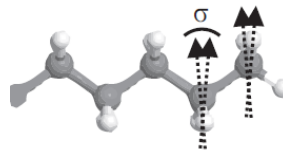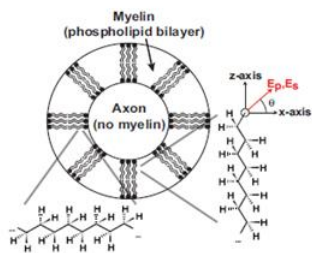$$b_2 \sin(2\alpha) + b_4 \sin(4\alpha) + b_6 \sin(6\alpha)$$

FZ Bioud et al. PRA 2014
J. Duboisset et al. JPCB 2015
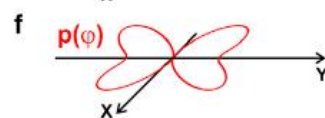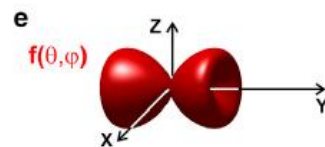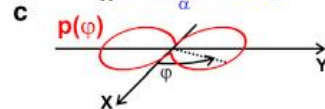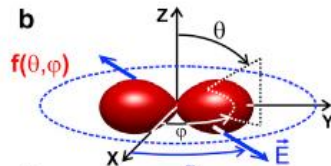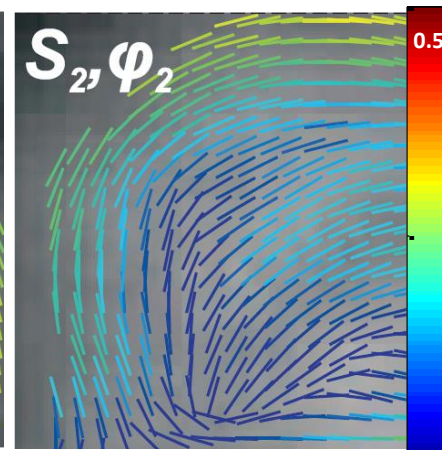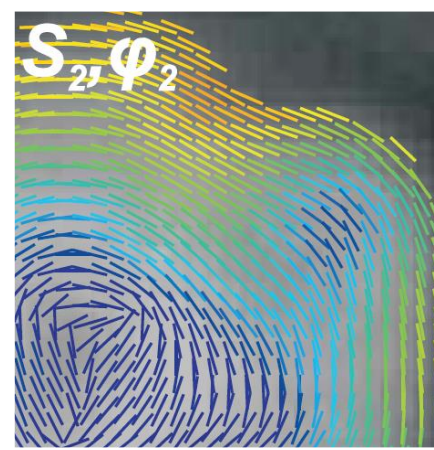
pCARS in MLVs (CH$_2$ stretch. bonds)

CARS

$$a_0 + \boxed{I_2 \cos 2(\alpha - \varphi_2)} + I_4 \cos 4(\alpha - \varphi_4)$$

5 µm

$\sim S_2$

φ_2

15 10^3

4 10^3

0   90   180

α (polarization angle)

1 image/sec

S2,φ2

0.5
0.45
0.4
0.35
0.3
0.25
0.2
0.15
0.1
0.05
0

σ

$\sigma = 70°$

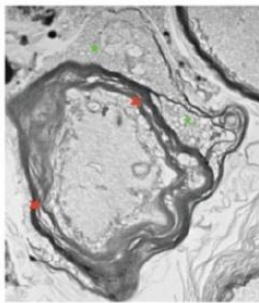F.Z. Bioud et al., PRA 2014
M. Hofer et al. Optica (2017)

96
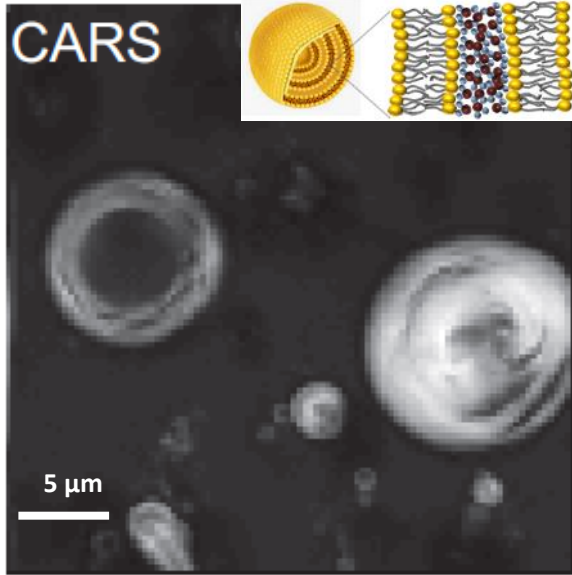
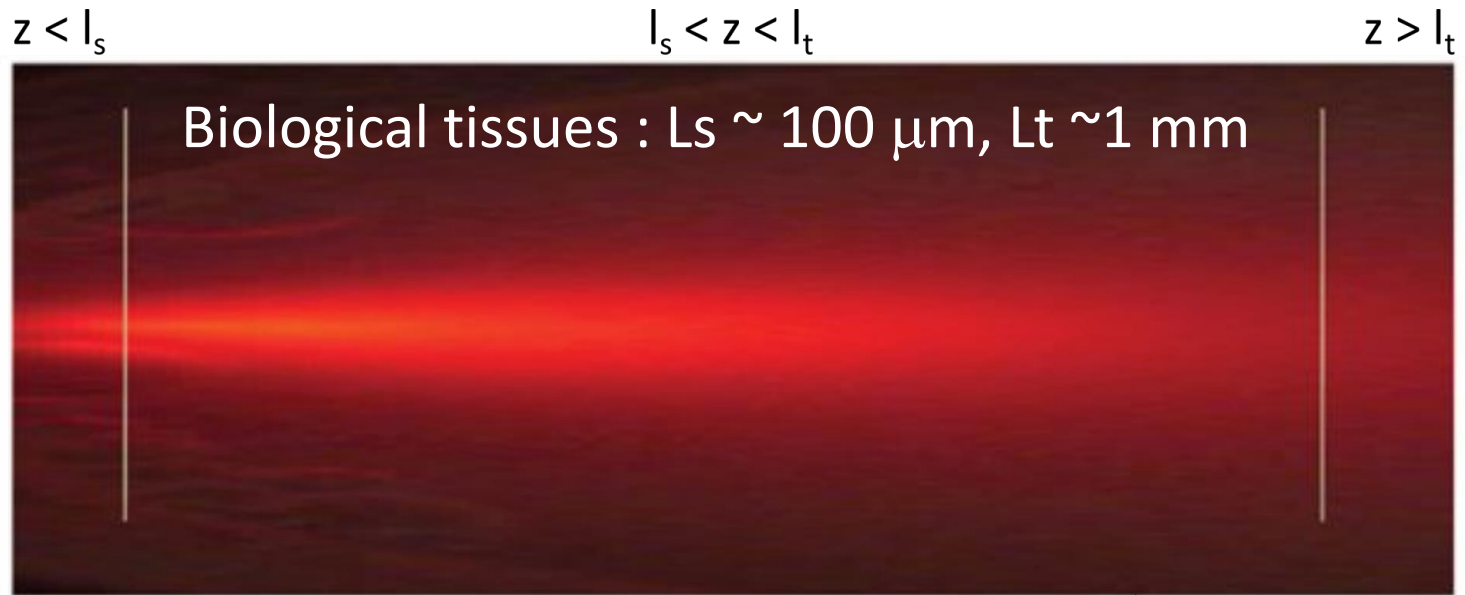# pCARS provides sub-diffraction information

100nm pixel size, PSF ~ 300nm

CARS
EAE Score 2.5

5μm

S_2, φ_2

S_2, φ_2

S_2, φ_2

Myelin
(phospholipid bilayer)

Axon
(no myelin)

EM

demyelination

order — S_2 — disorder

Fu et al. J Neurosci Res. 2007

P. Gasecka et al., Biophys. J. (2017)
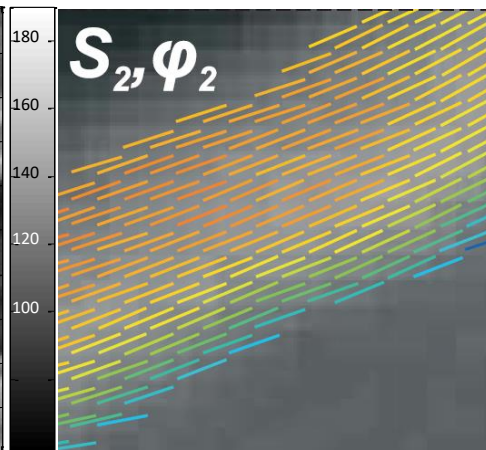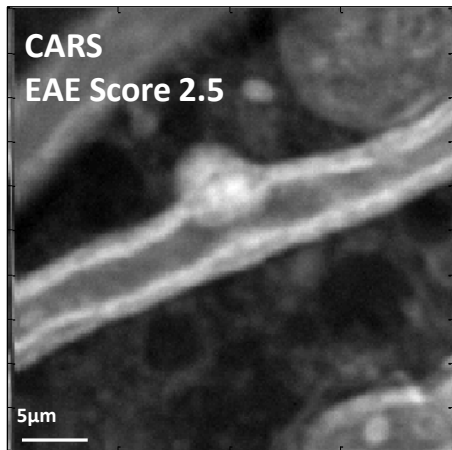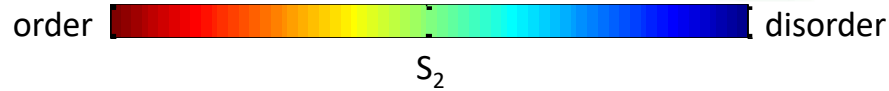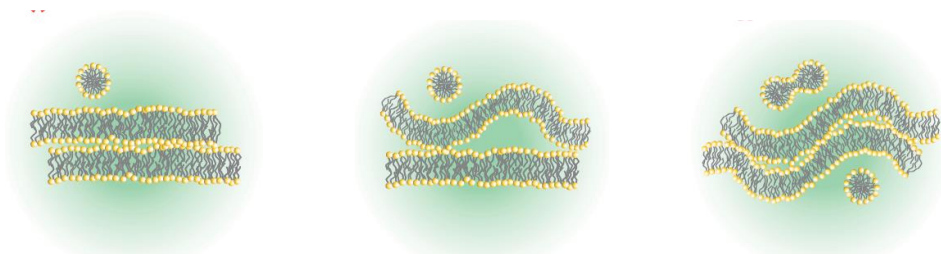
NLO imaging in depth in tissues

Optical imaging at large depths

$z < l_s$ $l_s < z < l_t$ $z > l_t$

Biological tissues : Ls ~ 100 µm, Lt ~1 mm

ballistic
regime

diffusive regime

130–140 µm
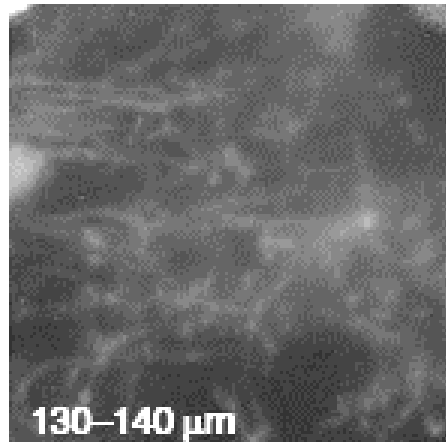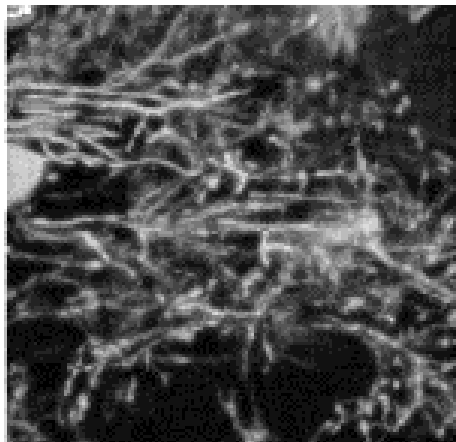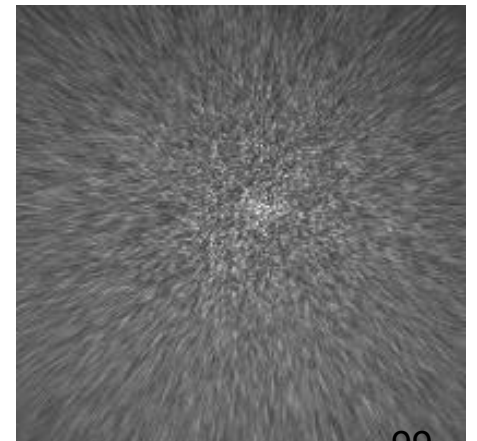
aberrations

scattering

Light propagation in biological media

$l_t \sim$ 1mm

$l_s \sim$ 100μm
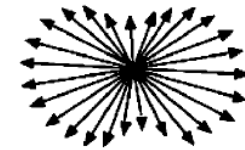
Scattering mean free path
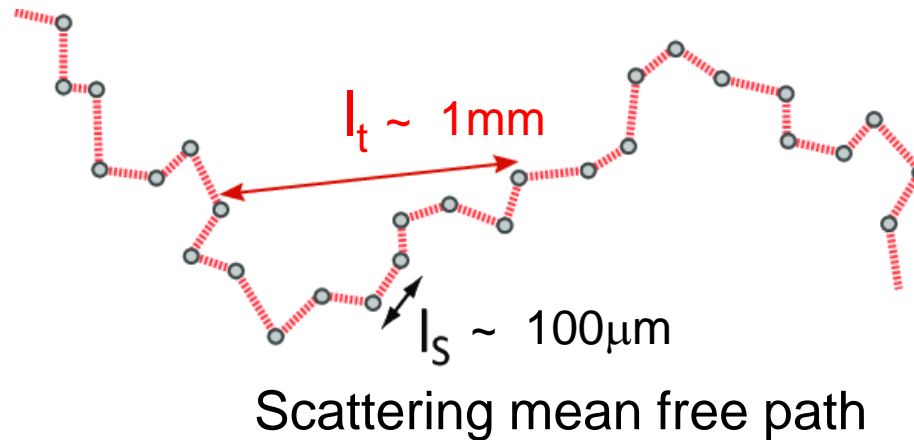
Transport mean free path :

$$L_t = \frac{L_s}{1-g}$$

$g \sim 0$

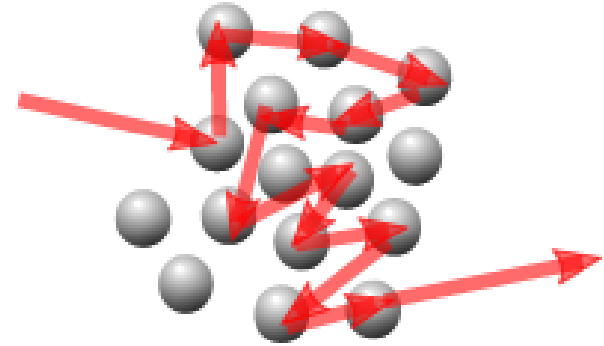Anisotropy:
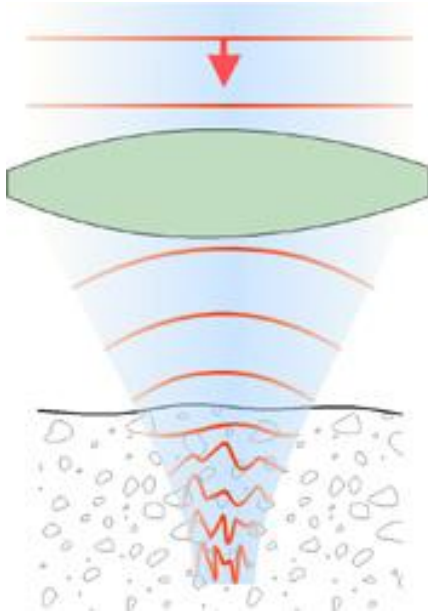
$$g = \langle \cos \theta \rangle$$

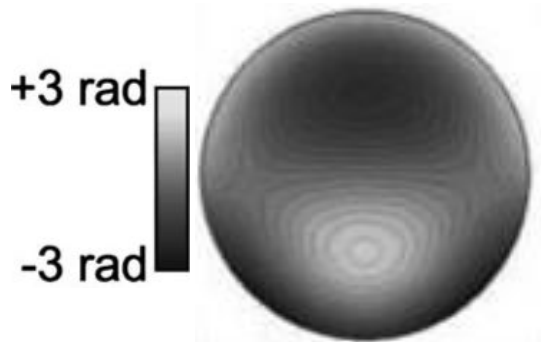$g \sim 1$

Biological media are forward-scattering : g ~0.9

Optics in complex media

Aberrations (ballistic light)

Multiple scattering (diffuse light)

Wavefront distorsions come from :

+3 rad

-3 rad

aberrations of the optics/sample

2π

$\frac{3}{2}\pi$

π

$\frac{1}{2}\pi$

0
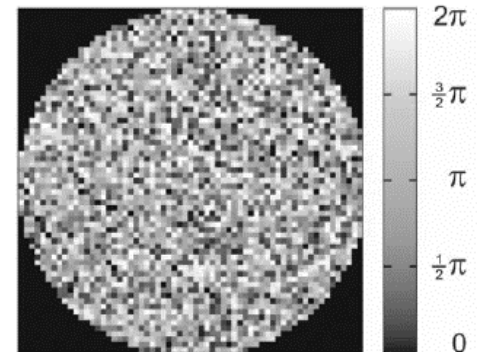
scattering

Adaptive optics
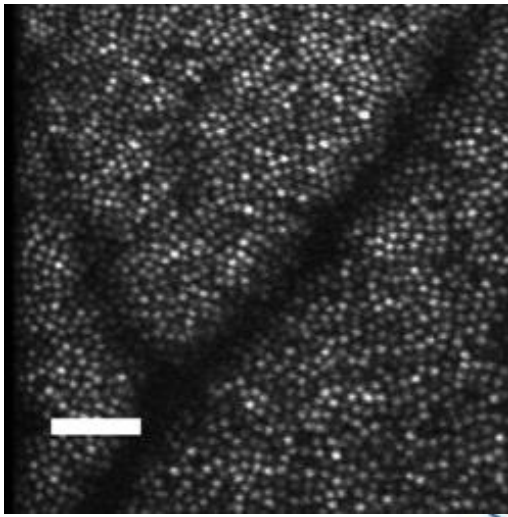
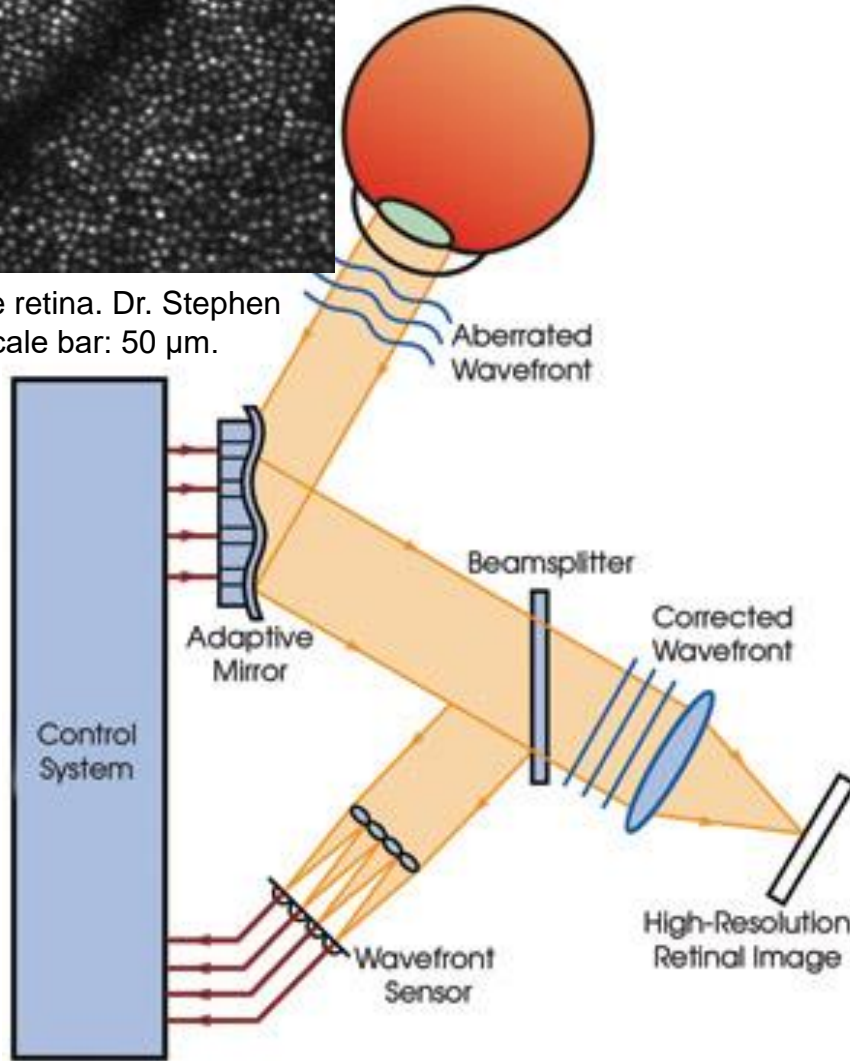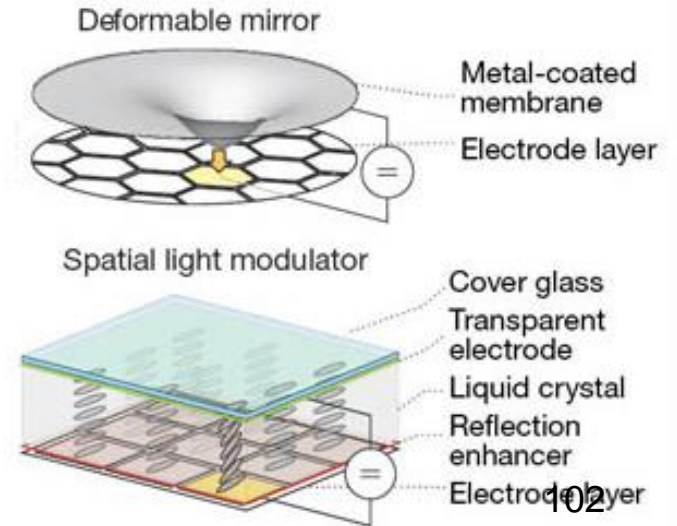Image of the retina. Dr. Stephen A. Burns. Scale bar: 50 μm.

Deformable mirror and feedback loop

Signal

controler

Aberrated Wavefront

Adaptive Mirror

Control System

Beamsplitter

Corrected Wavefront

Wavefront Sensor

High-Resolution Retinal Image

Deformable mirror

Metal-coated membrane

Electrode layer

Spatial light modulator

Cover glass

Transparent electrode

Liquid crystal
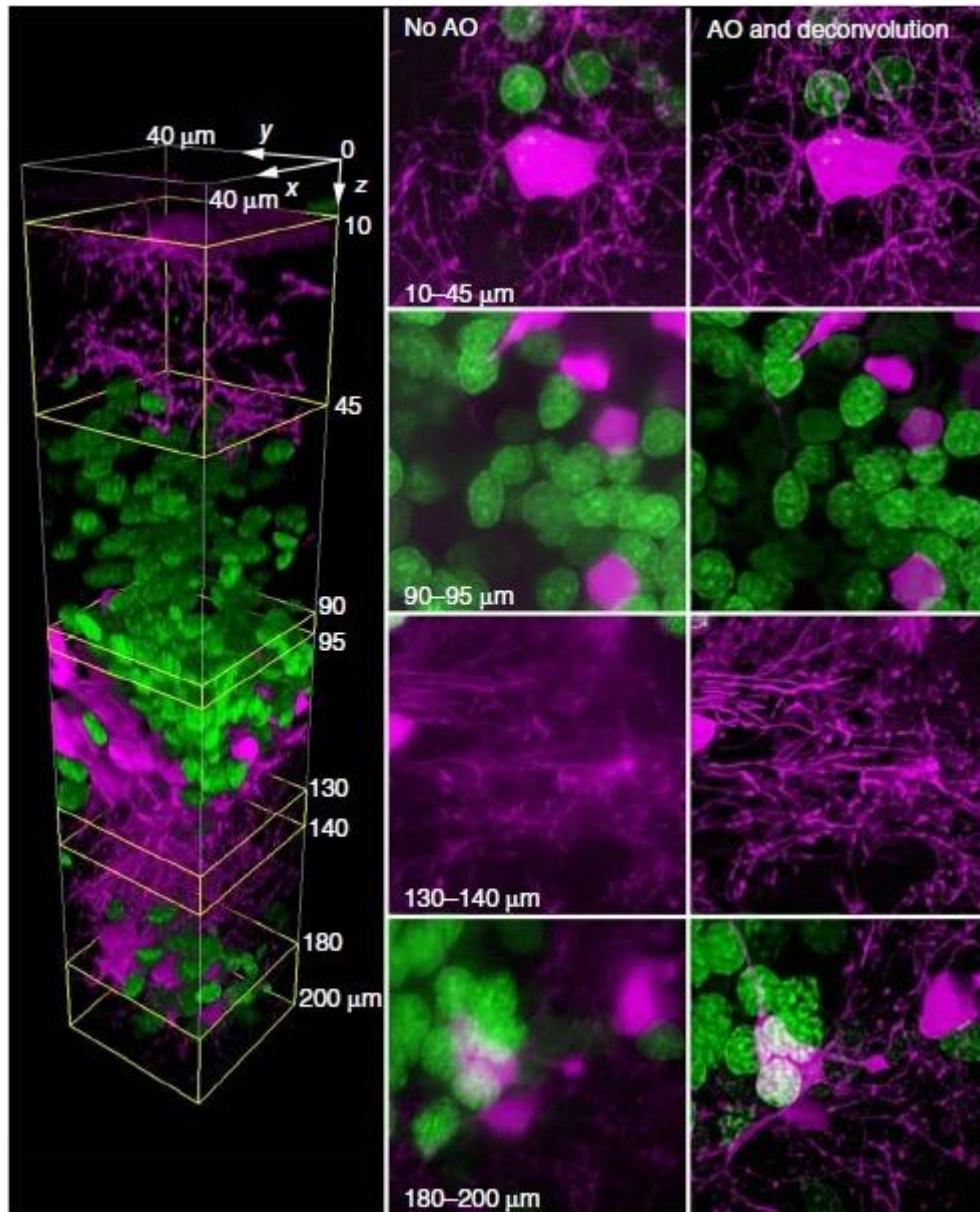
Reflection enhancer

Electrode layer
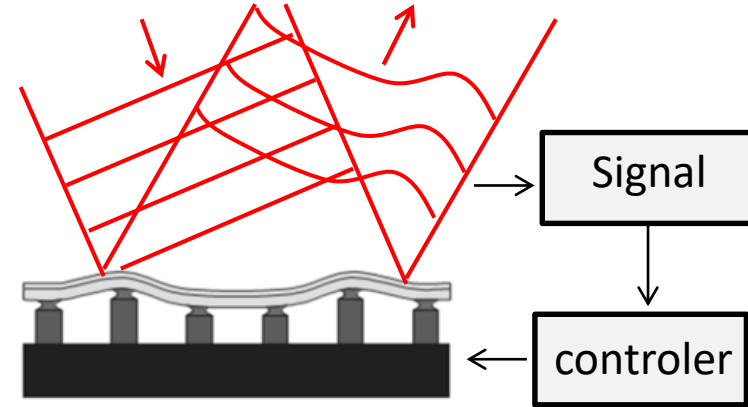
Adaptive optics and 2PF imaging
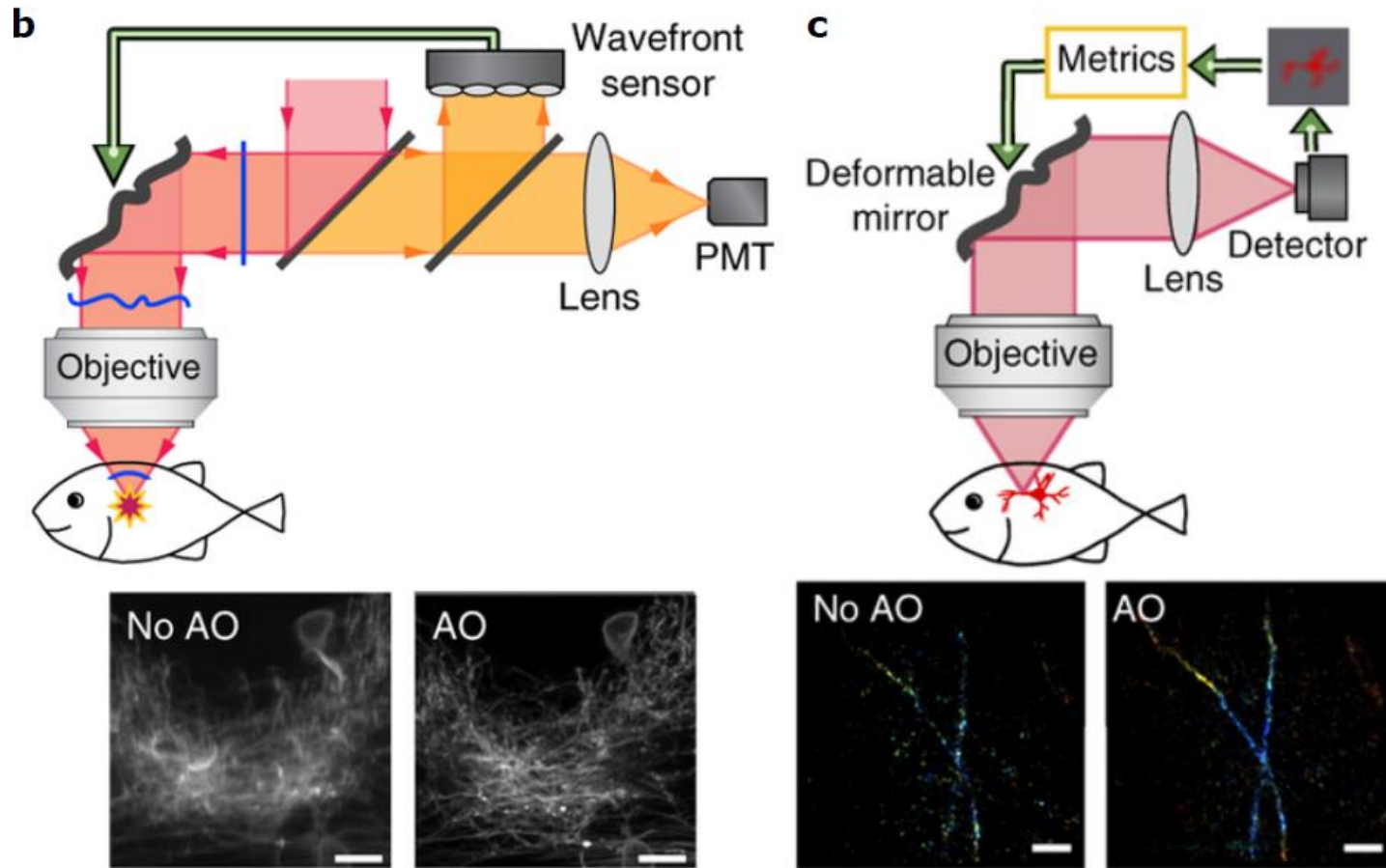
Ji N, Nature Methods, 14(4):374–380 (2017)

Combining fluorescence microscopy with adaptive optics in aberrant/scattering media

No AO

AO and deconvolution

10–45 µm

90–95 µm

130–140 µm

180–200 µm

40 µm

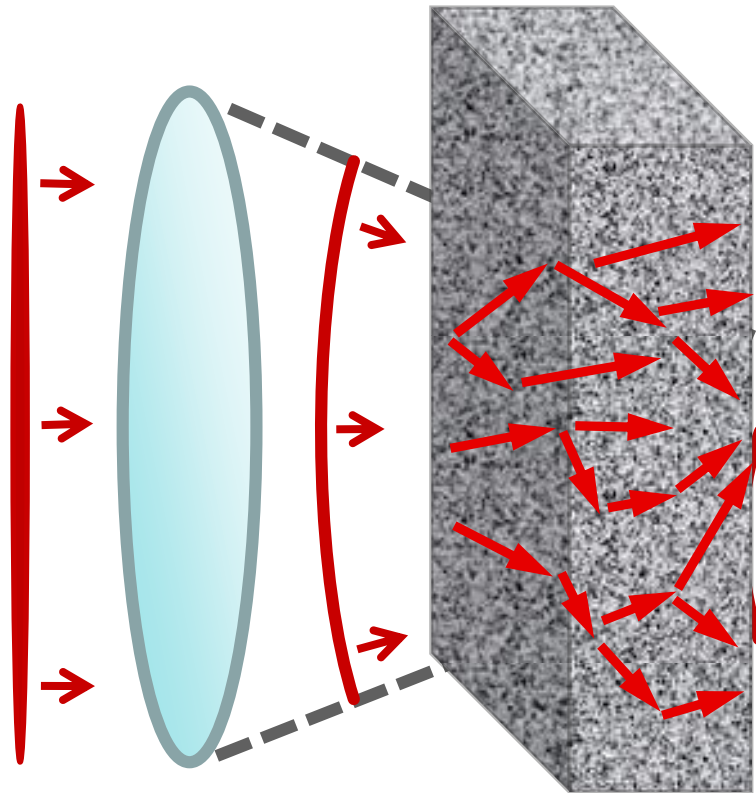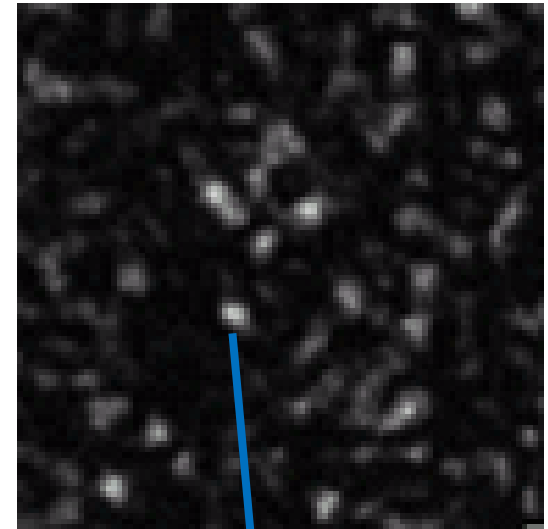E. Betzig lab, Nat Meth 2014

living zebrafish brain

104

Imaging above Lt ? scattering media

Spatial distortions

Speckle

A : illumination area
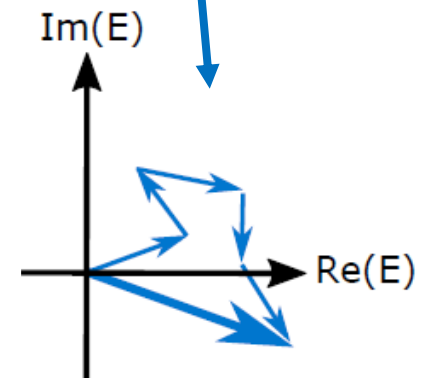
$$N_{modes} = \frac{A}{\lambda^2}$$

Im(E)
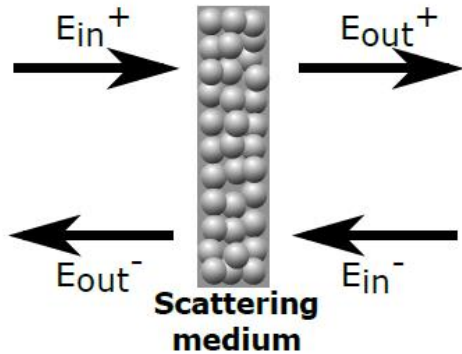
Re(E)

Y. Silberberg

CW Wavefront Shaping
Vellekoop and Mosk, OL 2007
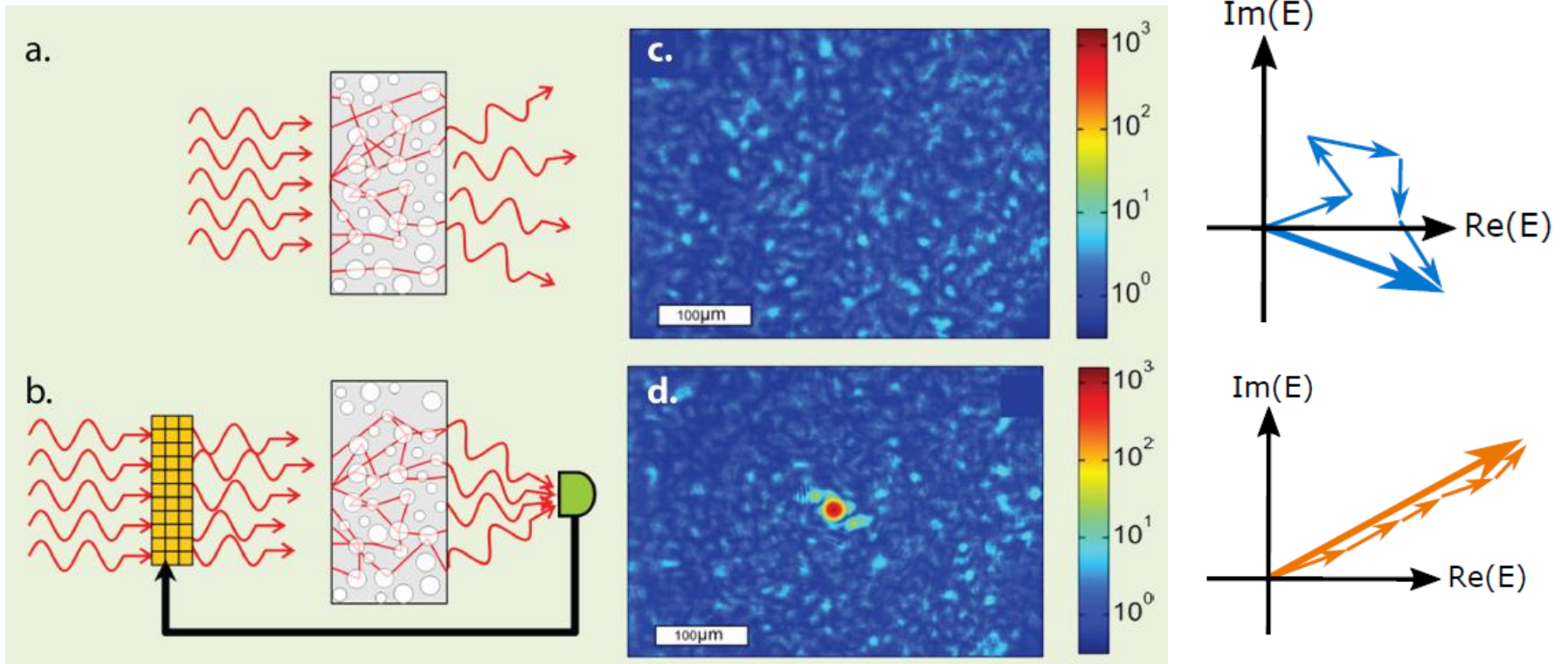
Optimization iterative process on N SLM pixels

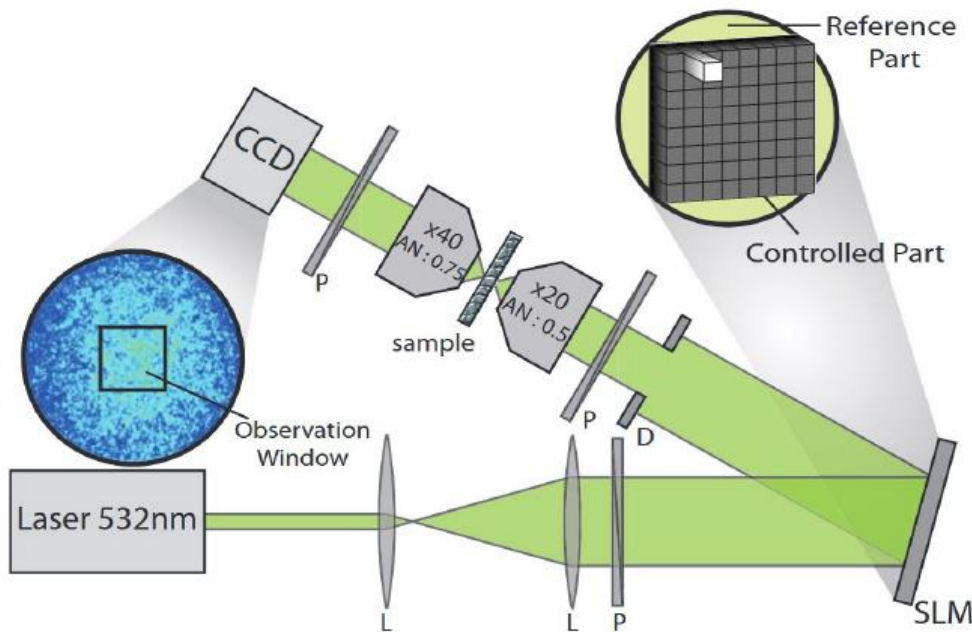# CW Wavefront Shaping by transmission matrix inversion (TM)
Popoff and Gigan, PRL 2010

E_{in}^+ E_{out}^+

E_{out}^- E_{in}^-

Scattering medium

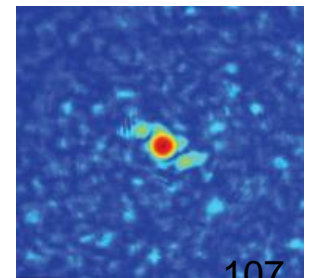$$E_m^{out} = \sum_{n=1}^{N} |t_{mn}| e^{i\theta_{mn}} E_n^{in}$$

CCD pixels
(measured by phase
step interferometry)

SLM pixels

Reference Part

Controlled Part

CCD

x40
AN:0.75

x20
AN:0.5

sample

P

P D

Observation
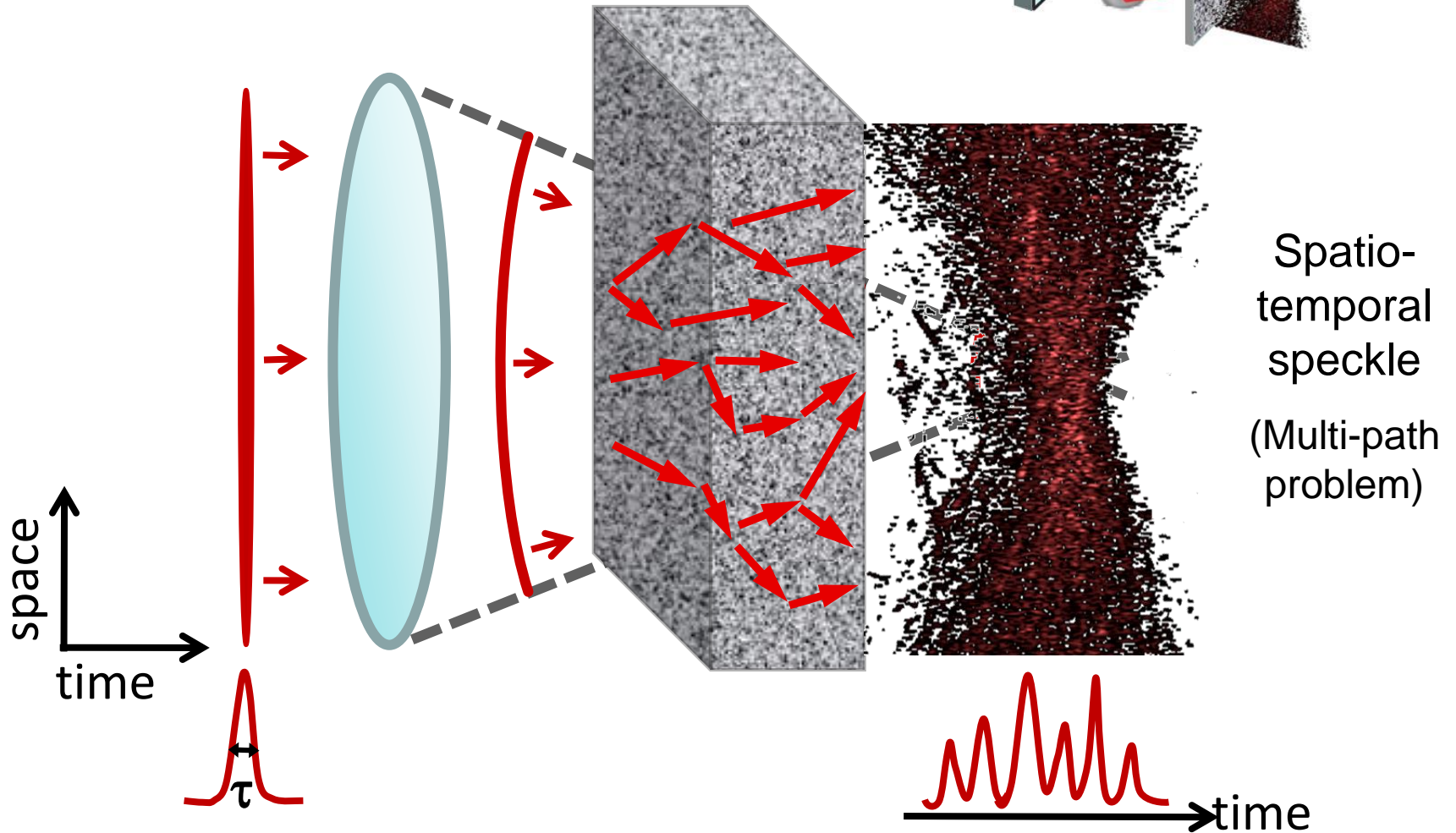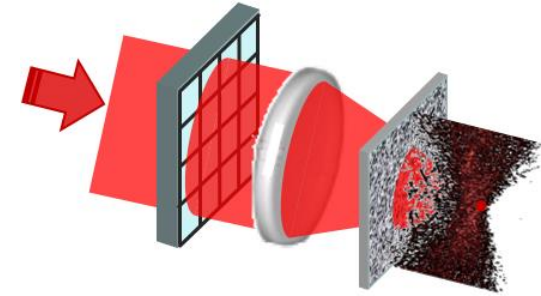Window

Laser 532nm

L L P SLM

Refocussing through a
scattering medium :

$$\tilde{E}^{in} = T^{\dagger} \tilde{E}^{target}$$
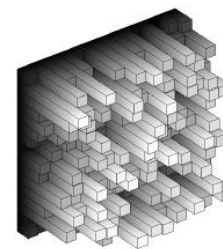
Ultrashort pulses in a scattering medium
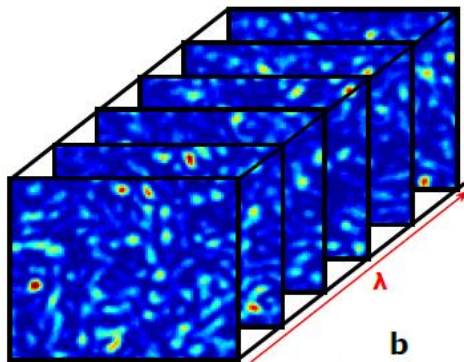
spatial + temporal distortions

space

time

τ

Spatio-
temporal
speckle

(Multi-path
problem)

time

Y. Silberberg

CW vs.short pulse propagation in scattering media
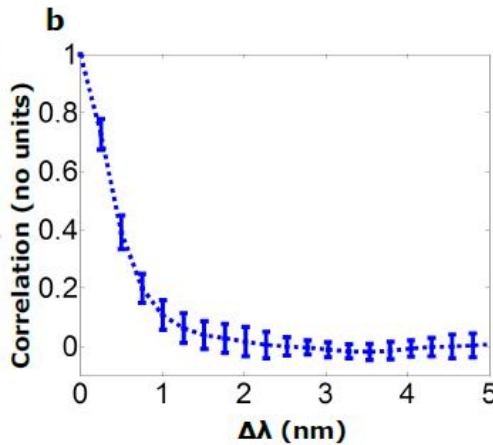

CW

fs

Y. Silberberg
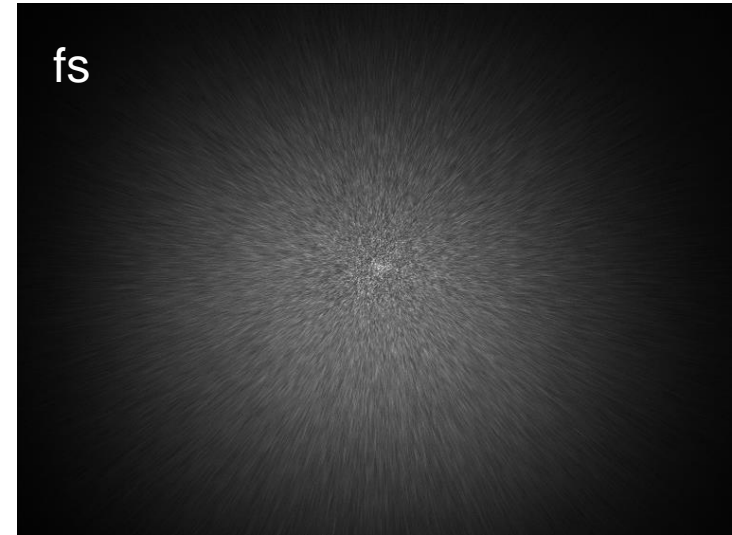
Short pulse propagation in scattering media

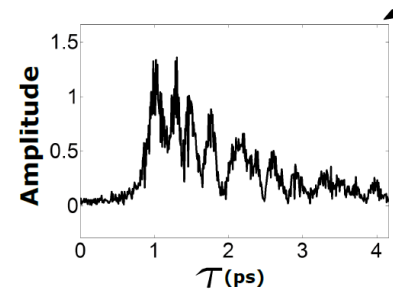## Medium spectral width $\delta\lambda_m$

(ZnO scattering thick sample)
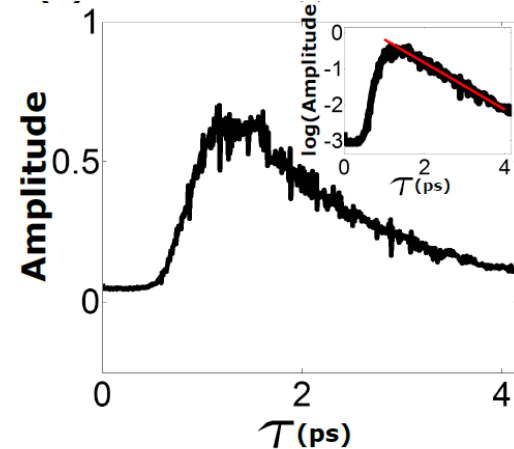
Autocorr.

Light confinement time τ_m

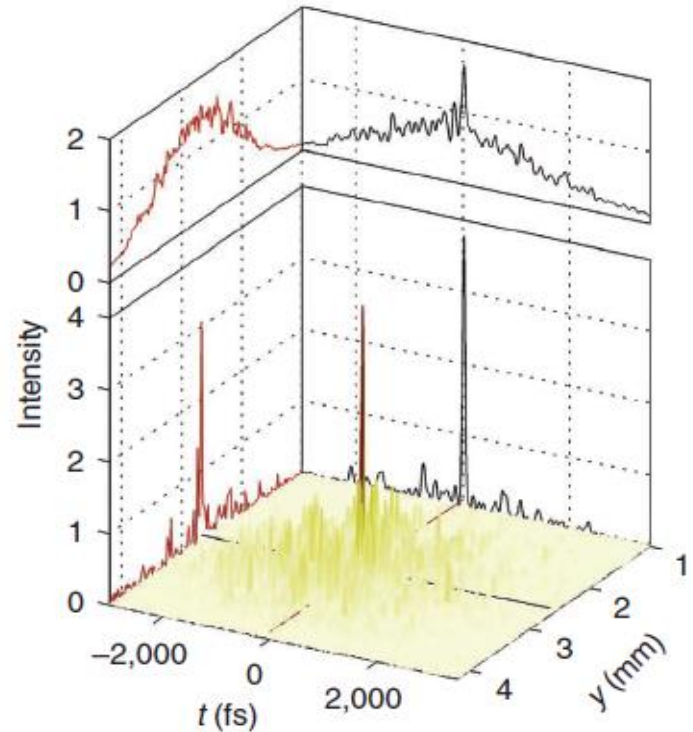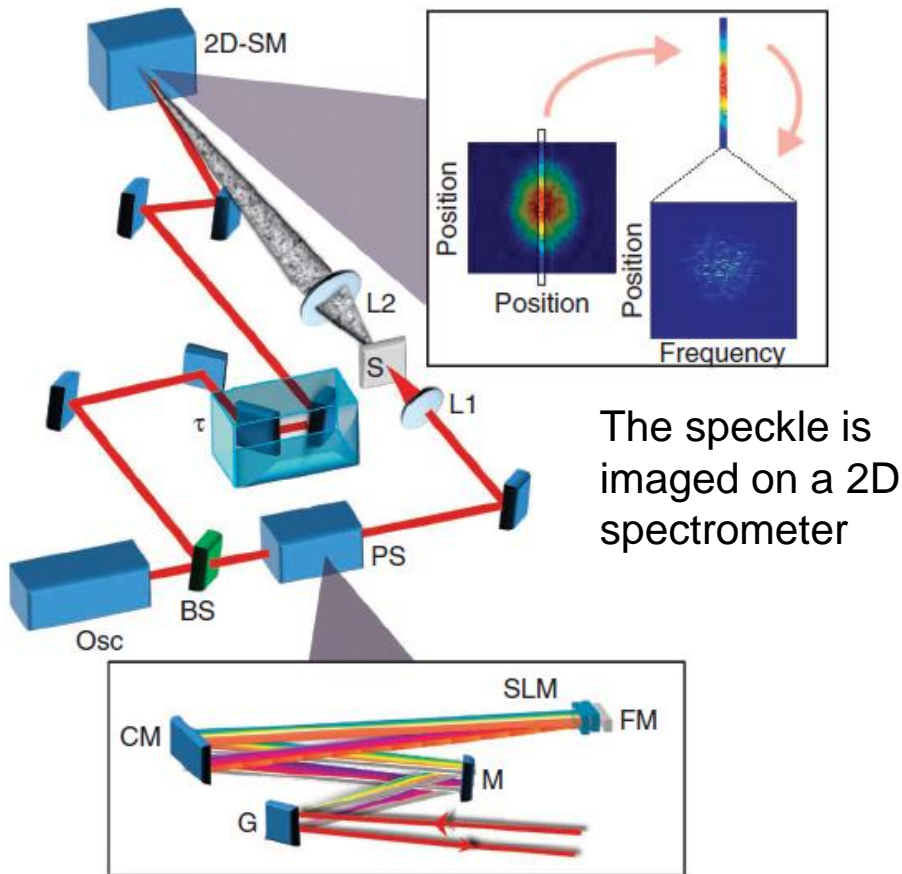Single speckle grain, interferom. Cross-corr.

Averaged 1000 speckle grains :

Number of spectral or temporal speckle grains (or modes) :

$$N_\lambda = \frac{\delta\lambda_L}{\delta\lambda_m} = \frac{\tau_m}{\delta\tau_L}$$

M. Mounaix PhD (2016)

Spatiotemporal focusing of an ultrafast pulse
by local pulse characterization
through a scattering medium

The speckle is imaged on a 2D spectrometer

After phase compensation at a precise location

Space and time are TL

D.J. McCabe, et al. Nat Comm (2011)
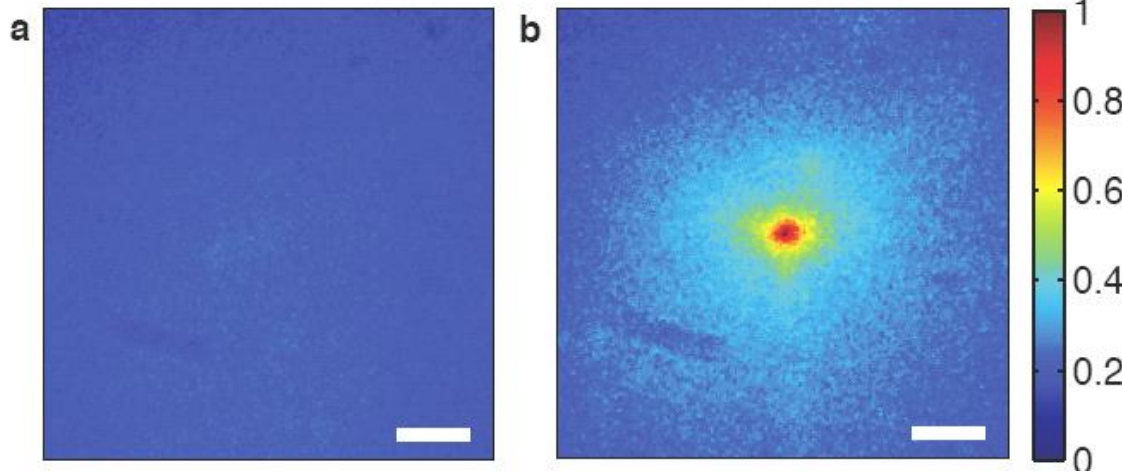
Spatiotemporal focusing by a spatial control

Optimization of
a 2PF signal
naturally optimizes
spatiotemporal focusing
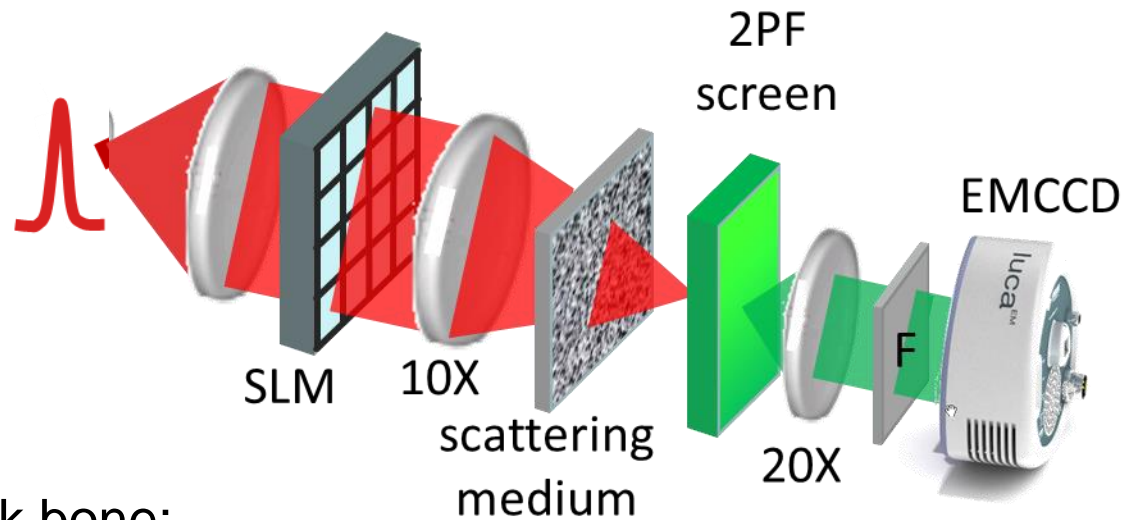
Through 500µm thick bone:

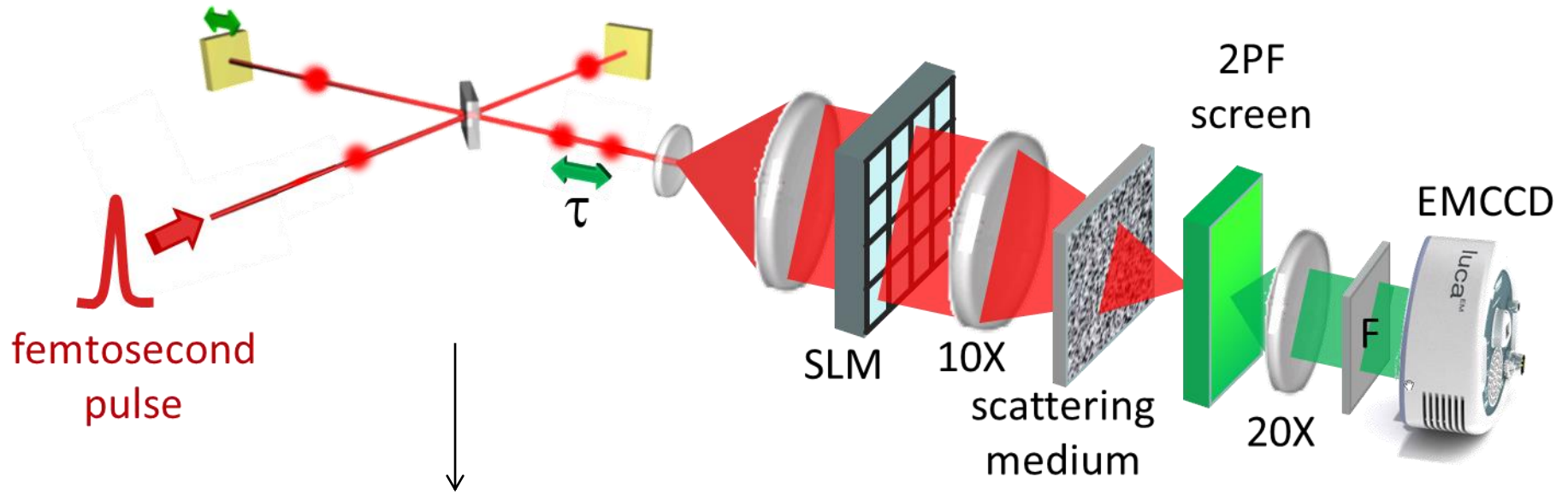Initial excitation   Optimized
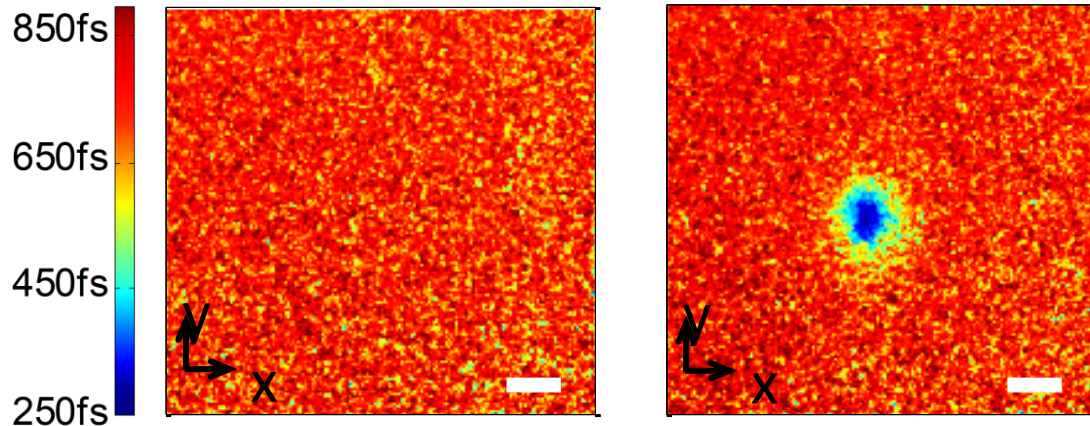

Katz et al. Nature Photonics **5** (2011)

Spatiotemporal focusing by a spatial control

Spatially resolved autocorrelation widths

Initial temporal width   Optimized

Temporal control is possible by spatial modulation

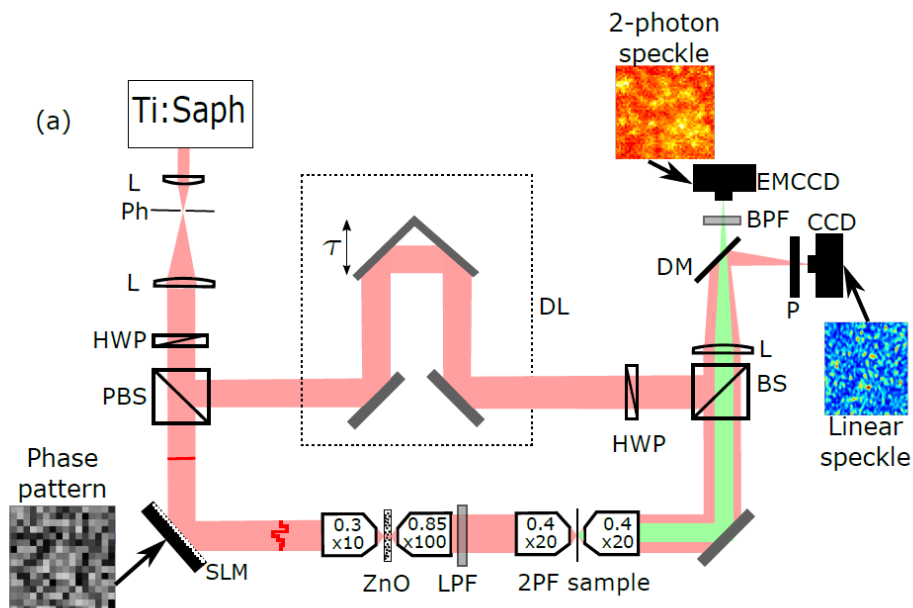Katz et al. Nature Photonics **5** (2011)

Coherent spectral control of the output pulse: Multi–Spectral Transmission Matrix

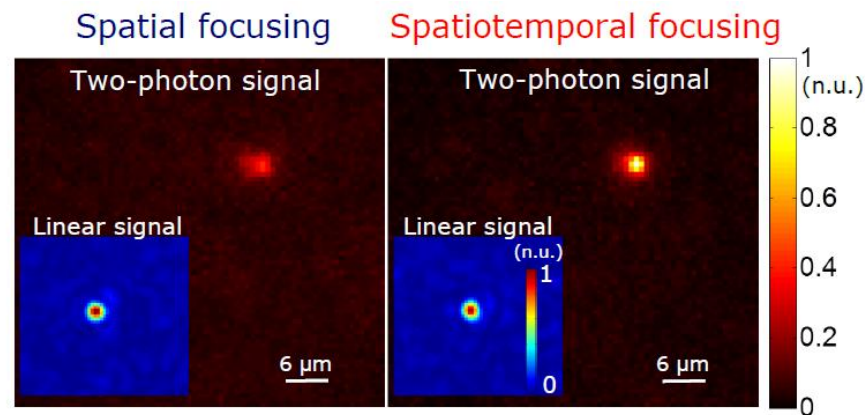TM measured for 21 wavelengths within a 13nm spectral window around 800nm

$$E_j^{\text{out}} = \sum_{m=1}^{N_{\text{SLM}}} \sum_{l=1}^{N_\omega} |h_{jml}| e^{i\varphi_{jl}} E_m^{\text{in}}(\lambda_l)$$

Both time and space can be controlled

$N_\lambda \times N_{\text{SLM}}$ measured spatio-spectral components of the TM
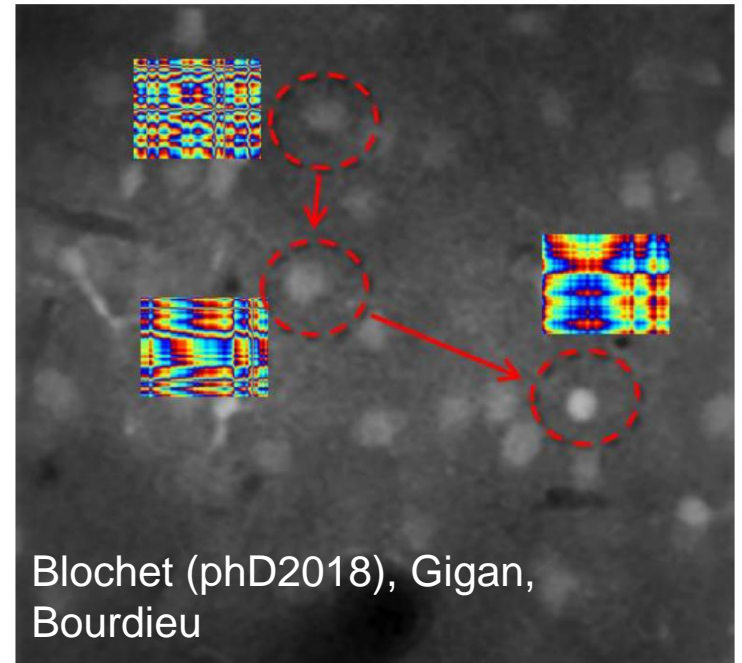

MSTM refocussing :

M. Mounaix, S. Gigan, PRL 2016

Conclusion

Efficient nonlinear microscopy imaging requires time, space and polarization control

Fundamental biological studies :
there is room for optimal optical schemes for in-depth real time imaging

Blochet (phD2018), Gigan, Bourdieu

Clinical applications : from nonlinear microscopy to endoscopy

Lensless endoscope

Rigneault et al. I. Fresnel
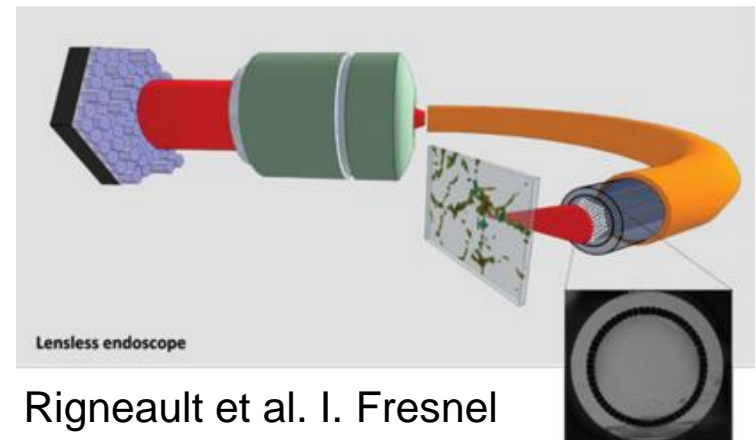
Thanks

H. Rigneault   J. Savatier   M. Mavrakis   H. De Aguiar

P. Gasecka   J. Duboisset   C. Cleff   M. Hofer   C. Valades

F.Z. Bioud   N. Balla   C. Rimoli   C. Rendon

Collaborators

F. Debarbieux
INT Marseille

S. Gigan
LKB Paris

R. Grange
ETH Zurich